Hyperbolic Prism, Poincaré Disc, and Foams

Alberto Tufaile[1], Adriana Pedrosa Biscaia Tufaile[1]

[1] Soft Matter Laboratory, Escola de Artes, Ciências e Humanidades, Universidade de São Paulo, São Paulo, Brazil
   (E-mail: tufaile@usp.br)

Abstract. The hyperbolic prism is a transparent optical element with spherical polished surfaces that refracts and reflects the light, acting as an optical element of foam. Using the hyperbolic prism we can face the question: is there any self-similarity in foams due to light scattering? In order to answer this question, we have constructed two optical elements: the hyperbolic kaleidoscope and the hyperbolic prism. The key feature of the light scattering in such elements is that this phenomenon is chaotic. The propagation of light in foams creates patterns which are generated due to the reflection and refraction of light. One of these patterns is observed by the formation of multiple mirror images inside liquid bridges in a layer of bubbles in a Hele-Shaw cell. We have observed the existence of these patterns in foams and their relation with hyperbolic geometry using the Poincaré disc model. The images obtained from the experiment in foams are compared to the case of hyperbolic optical elements, and there is a fractal dimension associated with the light scattering which creates self-similar patterns

Keywords: Hyperbolic Prism, Poincaré Disc, Foams, Kaleidoscope.

1 Introduction

Physically based visualization of foams improves our knowledge of optical systems. As long as the light transport mechanisms for light scattering in foams are understood, some interesting patterns observed can be connected with some concepts involving hyperbolic geometry, and this study involves mainly the classical scattering of light in foams and geometrical optics. This scattering system is an open system, in which the trajectories of light are not confined to a bound region [1]. The trajectories can leave the foam and eventually escape to infinity, as it is shown in Figure 1.

The physical system constituted by light interacting with foams can give hints for the understanding of collision processes, chaotic dynamics, the scatterers for wireless communications, and the construction of light traps, just to cite a few areas of the interest. Besides these scientific and technological applications, the enthrallment of the interaction of light, mirrors and curved surfaces can be found in many art works of great painters and writers from medieval to modern times, such as the Van Eyck's *Arnolfini Marriage*, *La Reproduction Interdite* by René Magritte, *Soap Bubbles* by Chardin, many

works of the Dutch graphic artist M. C. Escher, Lewis Carroll or Jorge Luis Borges.

A light ray entering in a foam can reflect and refract chaotically, because of the geometry of the interface of bubbles. In this study we present some patterns involving self-similarity and hyperbolic geometry.
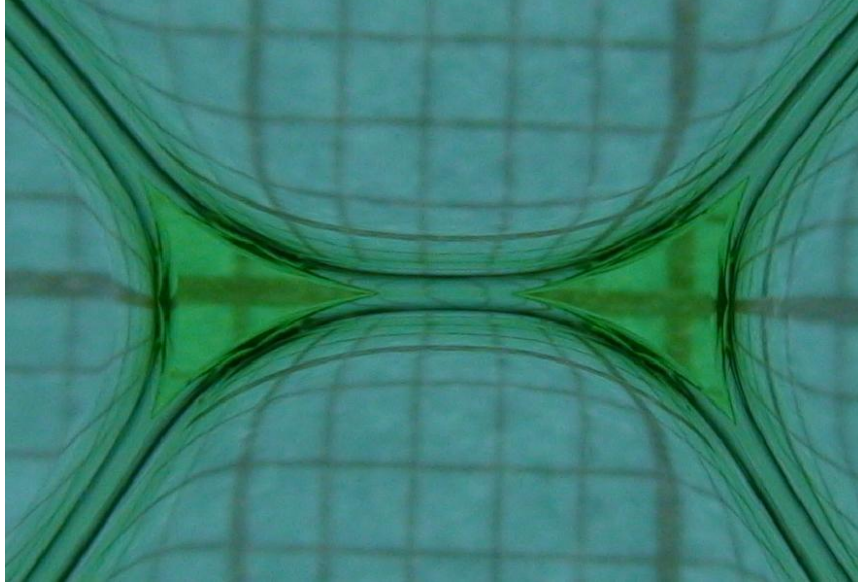

Fig. 1. Some transformations of the image a square grid behind a foam. The triangles are elements of foams known as Plateau borders. We can observe some contractions and transformations showing that the foam can act as a refractive system.

2 Kaleidoscopes

The branch of optics related to the geometry, the geometric optics, is based on the laws of ray reflection and refraction that are very simple:

$$\theta_i = \theta_r,$$
$$n_i \sin \theta_i = n_t \sin \theta_t,$$

(1)

In which θ_i is the angle of the incident ray in the interface of the foam, θ_r is the reflected ray, θ_t is the angle of the refracted ray, n_i and n_t are the refractive indices of the air and the liquid respectively. However the boundary conditions are very difficult to be determined precisely due to the bubble geometry and the paraxial approximation cannot be used for every scattered light ray.

Because of this aspect, we explore first some features of the pure reflective systems, obtaining some main features that can be compared with the concepts of geometry, and after that we can apply these concepts to explain some observed patterns.
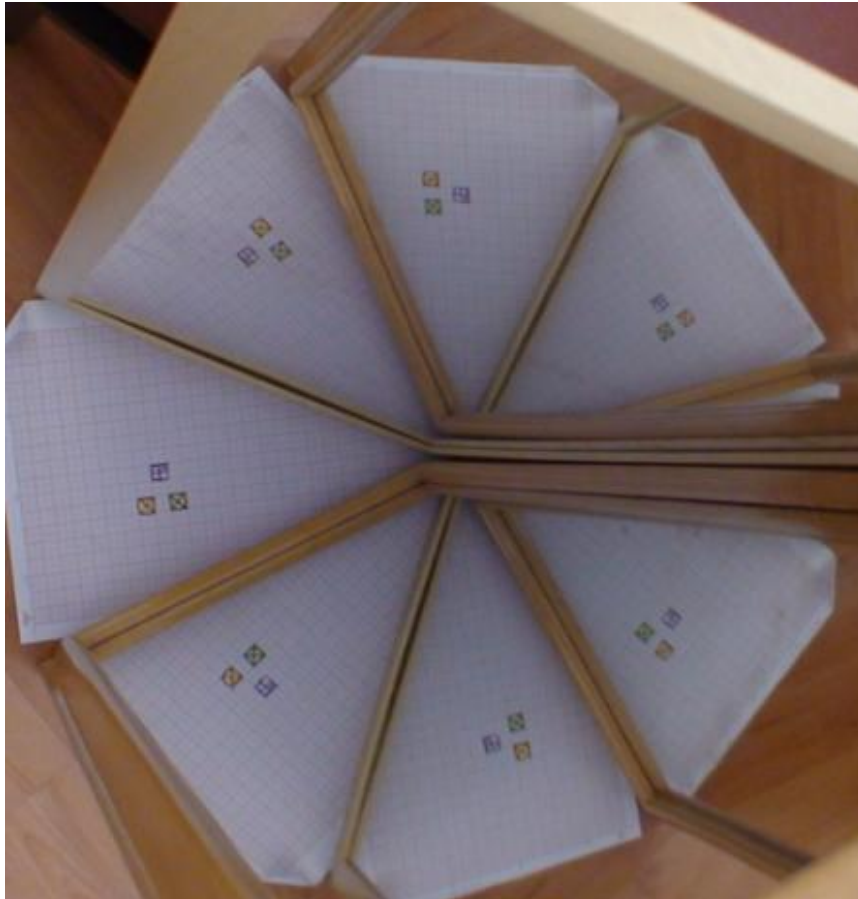
Fig. 2. A kaleidoscope can be obtained with two plain mirrors showing some Möbius transformations.

A kaleidoscope is a physical object made with two or more mirrors side by side, operating in the principle of multiple reflection, as it is shown in Figure 2. In general, the mathematics of kaleidoscopes in N dimensions is the study of finite groups of orthogonal N x N matrices that are generated by reflection matrices. We can observe transformations such inversions, translations and rotations. For certain angles of incidence, bubbles reflect the light, and we have done some experiments using Christmas balls as reflective spheres in order to understand the geometry of light scattering in curved surfaces. In Figure 3, there is an image of curved kaleidoscope using three Christmas balls. We can obtain more complex reflections increasing the number of spheres, which resembles some properties of fractal systems, as it is shown in Figure 4. These three mirrored spheres could be an analogy to a stereographic

projection of a regular kaleidoscope. Such stereographic projection is related to the Poincaré hyperbolic disc illustrated in Figure 5(e).

Fig. 3. Image of a curved kaleidoscope using three Christmas balls. We have used two different colors in order to provide the observation of the sequence of reflections.
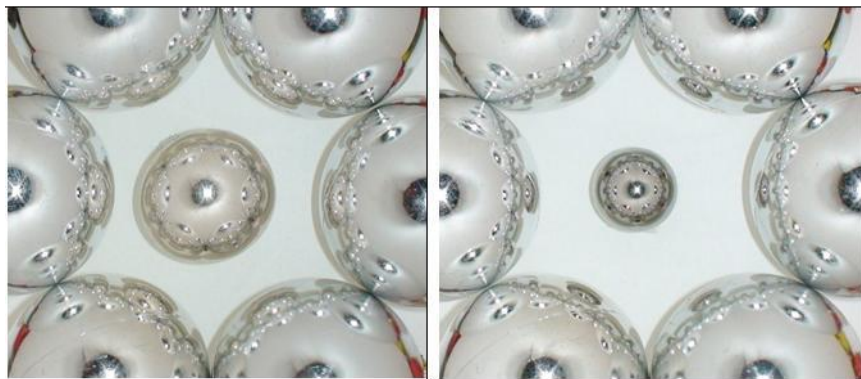

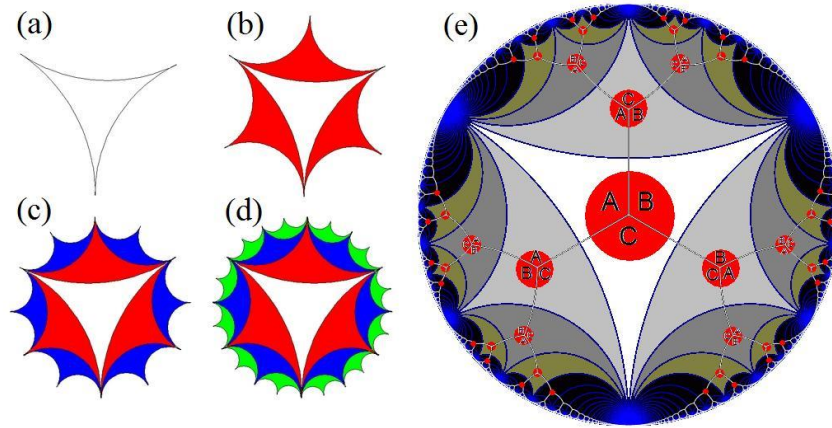Fig. 4. Image of a curved kaleidoscopes using multiple Christmas balls.

Fig. 5. How to construct the Poincaré hyperbolic disc? From (a) to (d) we present four steps to obtain some reflections and the multiple reflections of an object at the center of the disc.

3 The Poincaré Hyperbolic Disc

According to Needham[2], the Poincaré Disc model is a model for hyperbolic geometry in which a line is represented as an arc of a circle whose ends are perpendicular to disc boundary. What is the definition of parallel rays in this disc? Two arcs which do not meet correspond to parallel rays. In that geometry arcs which meet orthogonally correspond to perpendicular lines, and arcs which meet on the boundary are a pair of limit rays.

The Poincaré disc is a conformal map of the hyperbolic plane constructed by Beltrami in 1868 and rediscovered fourteen years later by Poincaré, which is now universally known as the Poincaré disc.

Using kaleidoscopes, we can see the reflections of the kaleidoscopes with plane mirrors of Figure 6(a) and (b) in the realm of the Euclidean geometry, while the kaleidoscope with reflective spheres in the realm of hyperbolic geometry, with the reflections representing Möbius transformations. Considering the red disc at the center of the Poincaré disc in Fig. 6(c), we can follow its respective reflections and understand the concept of a new kind of reflective system, known as hyperbolic kaleidoscope, similar to the kaleidoscopes of Figure 3 and Figure 4.

The complex pattern observed in the Poincaré disc represents a self-similar pattern, in which there is a fine structure at the border of the disc. This fractal pattern can be observed in the simulation of Figure 7(a) and in the image of the experiment of a hyperbolic kaleidoscope in Figure 7(b), in which a small sphere is placed at the center of the hyperbolic kaleidoscope. In this way, many physical properties of this system can be elucidated by the analysis of its geometry, using our sensory experience to guide us in more abstract concepts, such as symmetry groups or the tilling properties.
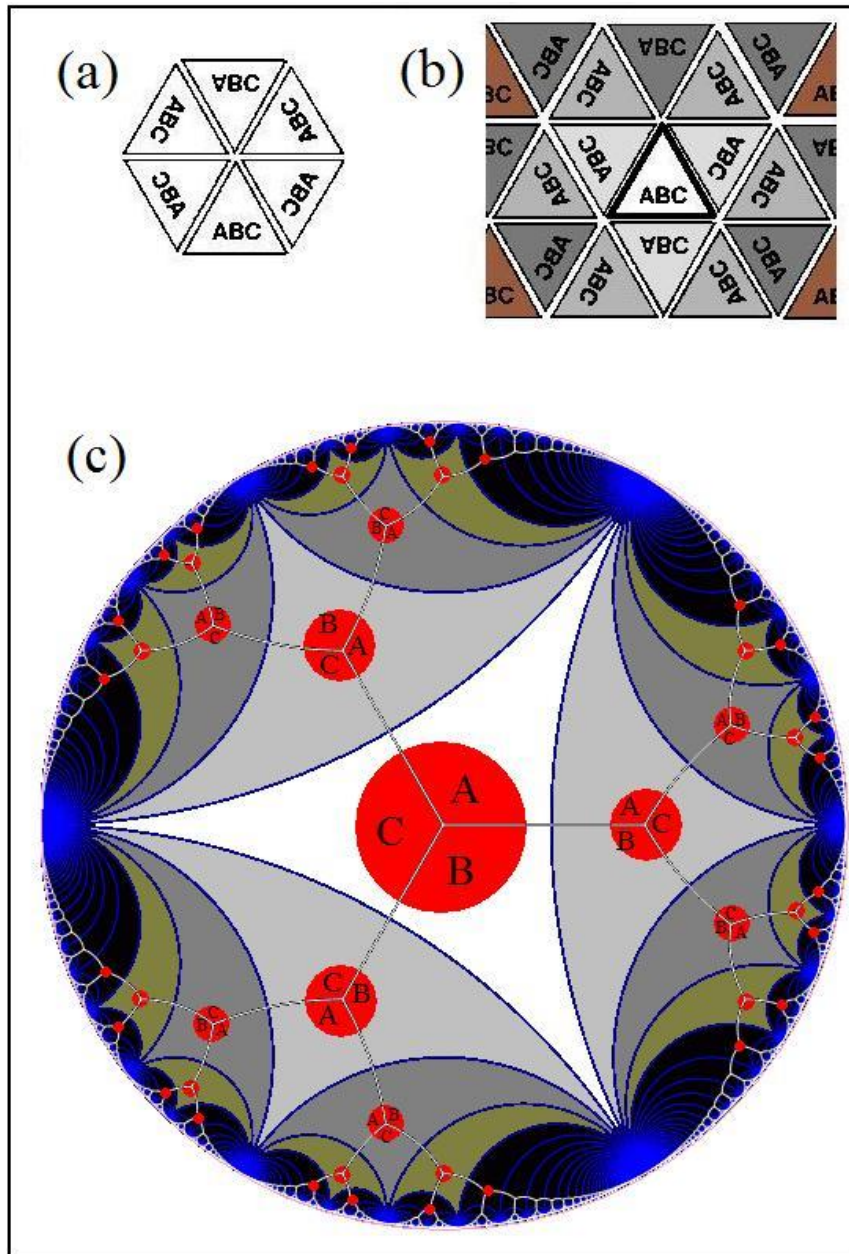
Fig. 6. Comparison between a kaleidoscope with three plane mirrors and the Poincaré disc model.

Besides the connection between geometry and physics, from the point of view of tilling, we can explore the association of the hyperbolic geometry

with some features of architecture. For example, Kaplan[3] applied the concepts of non-euclidean geometry to understand and create ornaments. In this study, patterns with the same properties of the hyperbolic kaleidoscopes are related to polyhedral models, and he presents a geometry-agnostic construction technique to be applied seamlessly to produce Islamic star patterns in the Euclidean plane, hyperbolic plane, and on the sphere.
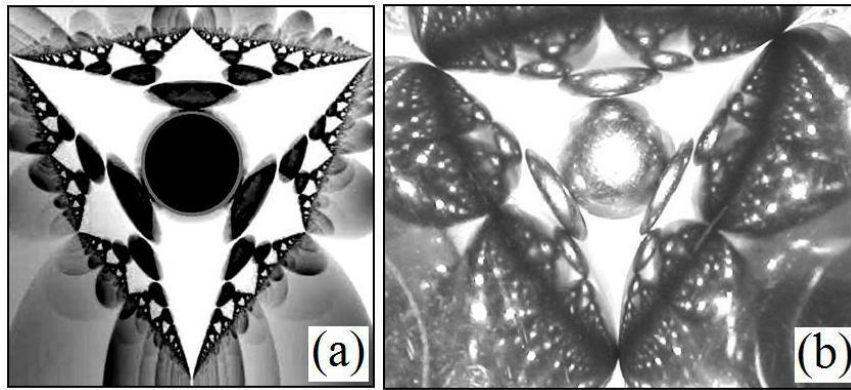

Fig. 7. In (a) the simulation of a hyperbolic kaleidoscope. In (b) there is an image of the hyperbolic kaleidoscope.
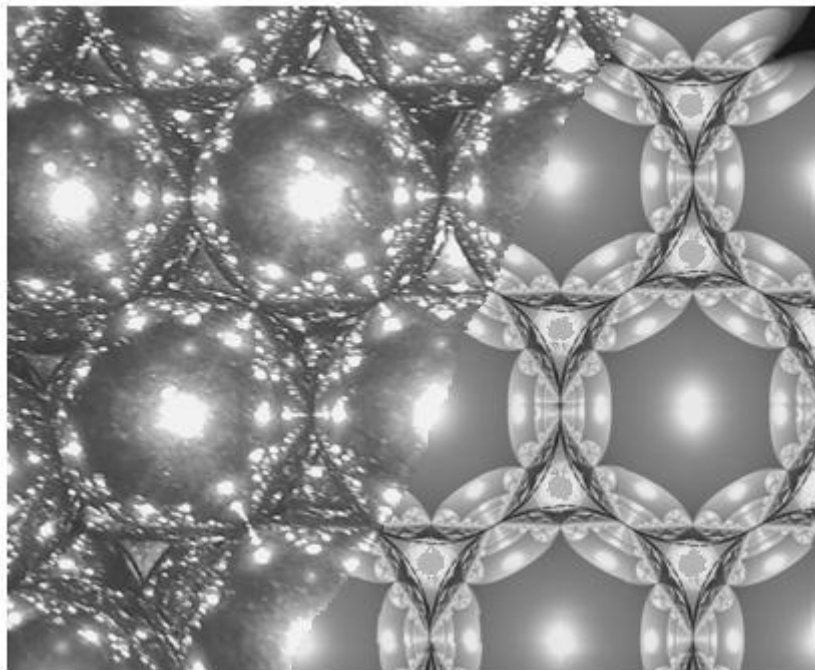

Fig. 8. Experiment and simulation of light scattering of an array of spheres.
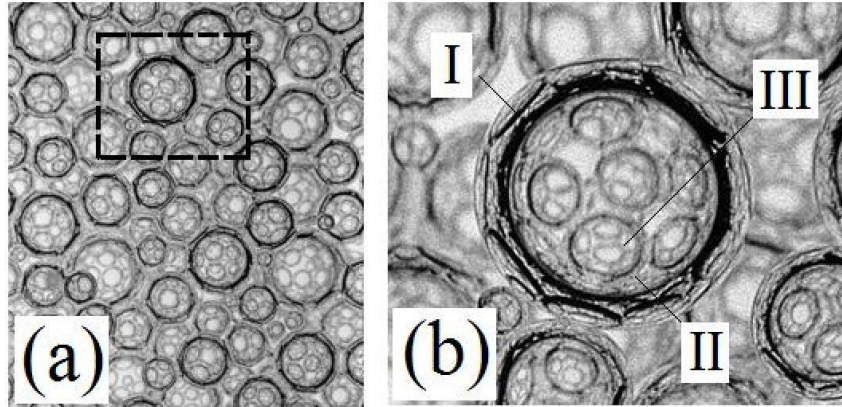
Fig. 9. Image of a foam showing some properties resembling self-similarity.

The array of spheres of Figure 8 is made with opaque objects. What happen if we use transparent objects like bubbles in a foam? The pattern can be observed in Figure 9(a). The zoom of Figure 9(b) shows the multiple reflections and refractions creating a more complex pattern than the case of the pure reflective spheres, with the first image of bubble represented by I, and inside this bubble we can see the image of other bubbles in II. The process is recurrent, and we can observe the image of three small bubbles in III, in which each bubble acts as a diverging lens and the bubble layers recursively image the optical patterns generated by the bubbles underneath, creating fractal-like patterns. Additional images and computational simulations of this phenomenon can be found in the paper of van der Net *et al.*[4], in which are presented some beautiful fractal-like patterns of bubble layers arranged a crystal ordering.

4 Chaotic scattering

The introduction of the study of chaotic systems in different areas of knowledge represented a paradigm shift, with the change in the perception of events which were already known. In this way, even though the scattering of light in foams is in the realm of classical optics, the approach using dynamical systems revealed some interesting features. For example, we can find the evidence of the butterfly effect in the light scattering in foams, with the sensitivity of initial conditions in the scattering of light in the interface of bubbles for reflection and refraction (for example, see Figure 13 of the paper of van der Net *et al.*[4]. In Figure 10, we present a simulation of the geometrical optics in the Plateau border, with the illustration of some incident light rays (R1) with their refractions (R2) and reflections (R3 and R4). The Plateau border is one of the structures found in foams, and this optical element can present some features observed in chaotic systems because this optical element shares some common features of the

hyperbolic kaleidoscopes. In Figure 11, we present an image of light scattering of a red laser beam in two bubbles in water.
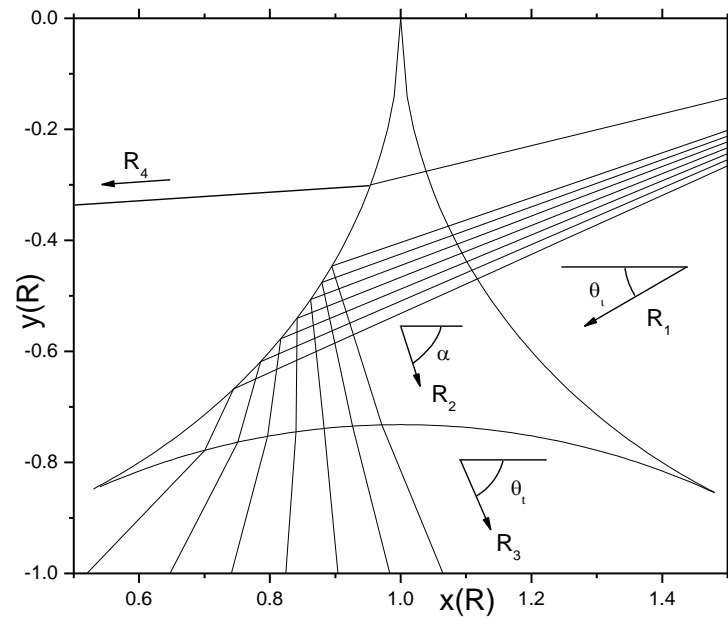
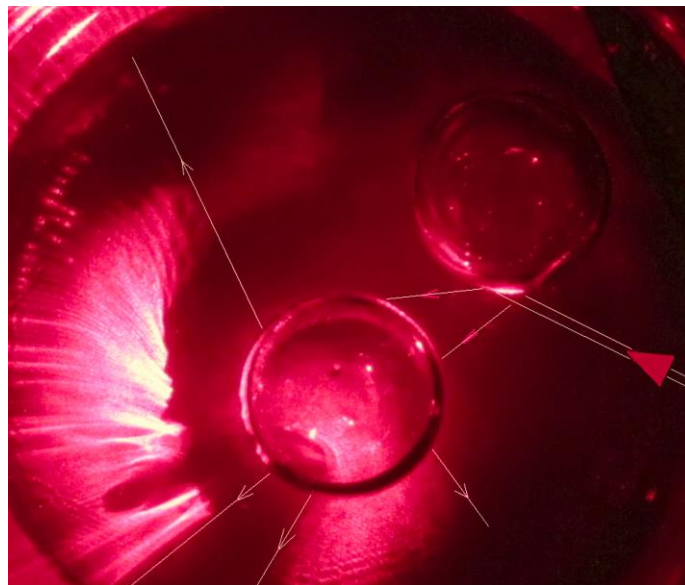

Figure 10. Light scattering in a plateau border.

Figure 11. The butterfly effect in the light scattering with two bubbles.

In this system with just two bubbles, the light scattering presents more possibilities to diverge due to the presence of reflection and refraction at same time, changing the power of light scattering. In this situation a light ray can split in two distinct rays: a reflected one and a refracted one, affecting the sensitivity to initial conditions. Analyzing the chaotization mechanisms of light in foams retains some properties of pure reflective systems, but the dynamics of rays passing from one medium to another can acquire unusual properties. According to Baryakhtar[5], the law of ray motion itself becomes deterministically chaotic.

Based in these assumptions, we have looked for the answer of the following question: how to quantify the chaos of light scattering in foams? To answer this question, we have used the concept of Komolgorov-Sinai entropy, which is related to the sum of the positive Lyapunov exponents of the system[1]. The Lyapunov exponent quantifies the separation of infinitesimally close trajectories of light rays. We have obtained an empirical formula for the light scattering in foams for the values of Komolgorov-Sinai entropy in reference Tufaile *et al.* [1]. According to our computations, for the case of pure reflective systems the Komolgorov-Sinai entropy is 1.98, and for the case of foams, the Komolgorov-Sinai entropy is 1.82. These values indicate that the both systems have the same degree of chaotization.
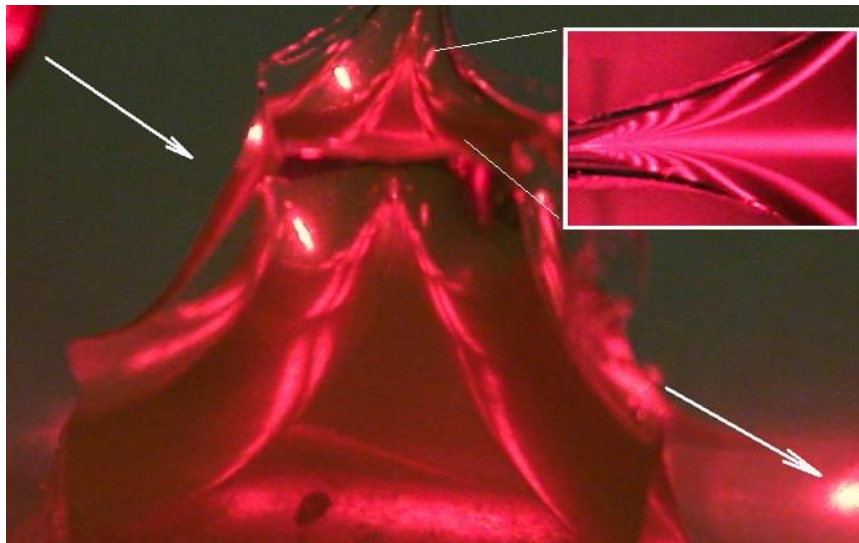
Fig. 12. The cavity hyperbolic prism reflecting the light following the pattern of the Poincaré disc. The inset is the observation of a fractal tree[6].

In order to represent the conection between the light scattering in foams and the Poincaré disc, we have made a hyperbolic prism and obtained some images with the features of self-similar systems related to the Poincaré disc. In Figure 12, we are presenting the cavity of the hyperbolic prism [6, 7] with some self-similar structures related to the Poincaré disc.

Conclusions

The observation of light scattering in foams suggested the existence of some dynamics represented by hyperbolic geometry. Motivated by this representation, due to refraction and reflection at the interfaces, the direction of the rays leaving the interfaces between bubbles can considerably vary for the same incident angle and a small positional offset. A close look at some configurations of the liquid bridges reveals the existence of some triangular patterns surrounded by a complex structure, which bear a resemblance to those observed in some systems involving chaotic scattering and multiple light reflections between spheres. Provided the optical and geometrical properties of the bubbles or spheres surfaces are chosen appropriately, self-similarity is a consequence of multiple scattering of light rays in these cavities. Inspired by the observation of light scattering in foams, we have constructed a hyperbolic prism. The cavity acts as a hyperbolic prism multiplying the scattering of light rays generating patterns related to Poincaré discs.

Acknowledgements

References

1. A. P. B. Tufaile, A. Tufaile, and G. Liger-Belair. Hyperbolic kaleidoscopes and chaos in foams in a Hele-Shaw cell. Journal of Physics: Conference Series 285, 012006, 2011.
2. T. Needham. Visual Complex Analysis, Claredon Press, Oxford, 1997.
3. C. S. Kaplan. Computer Graphics and Geometric Ornamental Design. Dissertation of Doctor Phylosophy, University of Washington, 2002.
4. A. van der Net, L. Blondel, A. Saugey , W. Drenckhan, Simulation and interpretation of images of foams with computational ray tracing techniques, Colloids and Surfaces A 309, 159, 2007.
5. V. G. Baryakhtar, V. V. Yanovsky, S. V. Naydenov, and A. V. Kurilo, Chaos in composite billiards, Journal of the experimental and theoretical physics, 2, 292-301, 2006.
6. A. Tufaile and A. P. B. Tufaile, Hyperbolic prisms and foams in Hele-Shaw cells, Physics Letters A 375, 3693-3698, 2011.
7. A. Tufaile, M. V. Freire, A. P. B. Tufaile, Some aspects of image processing using foams, Physics Letters A 378, 3111-3117, 2014.

Parhelic-like Circle and Chaotic Light Scattering

Adriana Pedrosa Biscaia Tufaile[1], Alberto Tufaile[1]

[1] Soft Matter Lab, School of Arts, Sciences and Humanities, University of São Paulo, São Paulo, Brazil
 (E-mail: atufaile@usp.br)

Abstract. The propagation of light in foams creates patterns which are explained by the Geometrical Theory of Diffraction, and some of these patterns are known as Parhelic-like circle or Parlaseric circle. We also present the analogy between the atmospheric phenomena known as Parhelic circle, Sun dogs and Sun pillars and the patterns obtained from light scattering in foams.
Keywords: Parlaseric circle, Parhelic circle, Plateau borders, Geometrical Theory of Diffraction.

1 Introduction

Scattering problems are at very heart of Physics, from Celestial to Quantum Mechanics, with particles or waves, we are always looking for a target. In our experiment, we are observing the light scattering in foams, and the results can be applied in Acoustics, Optics and Spectroscopy. Light through foams presents a complex behavior, for example, though the laws of ray reflection and refraction are simple, the boundary conditions for the light scattering are very difficult to be determined precisely due to many awkward technical aspects, such as nonlinearities, or if the thickness of the liquid films is sufficiently close to the wave length of visible light, there is light interference and thus produce the iridescent colors of soap bubbles.

In this paper we discuss the chaotic scattering, diffusion and some aspects of the interface between wave and geometric optics. We have observed that the light scattering dynamics in foams can present two main process: a diffusive one related to Gaussian process and another one related to chaotic dynamics, similar to those observed in chaotic saddles, with some rays of light bouncing back and forth for a certain time, and leaving it through one of several exits. In addition to those behaviors, between geometrics and wave optics, we also have observed the phenomena of the theory of geometrical refraction, with the parlaseric circle.

2 The experimental apparatus

This experiment involves light scattering in foam. The foam is obtained by shaking a liquid inside a transparent box consisting of two parallel Plexiglas

plates separated by a gap (19.0 x 19.0 x 2.0 cm^3). We can inspect the profiles of light scattered inside the foam and we have used a photographic camera to detect the resulting light patterns. The box contains air and an amount of dishwashing liquid diluted in water (V = 115 cm^3). The surfactant is Lynear Alkylbenzene Sulfonate (LAS), with surface tension around 25 dyne/cm and refractive indices equal to 1.333 for the liquid and 1.0 for the air. The light sources used when photographing the light scattered by the foam were laser diodes with colors red (635 nm), green (532 nm), and blue (405 nm).
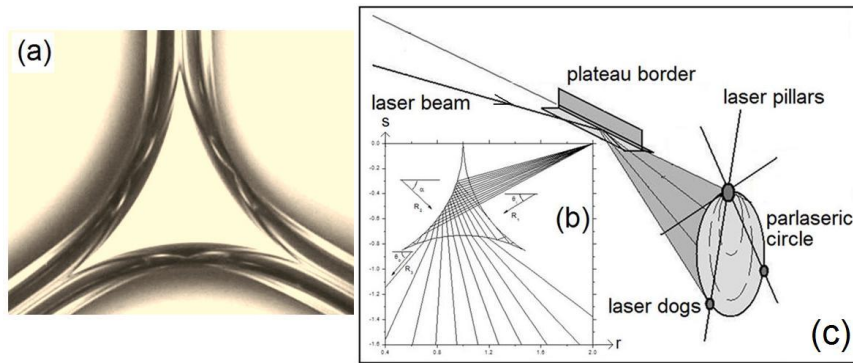

Fig.1. In (a) is shown the cross section of a Plateau border. The example of ray tracing in a Plateau border (b). The diagram of the experiment is shown in (c).
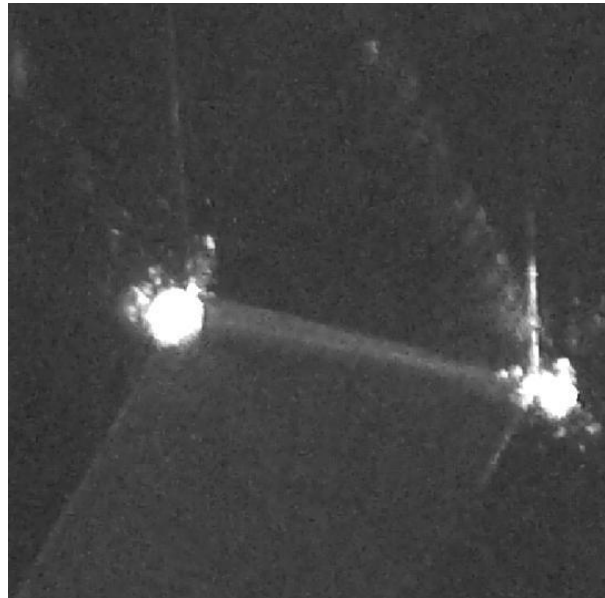
Fig. 2. Image of the laser beam in a Plateau border.

856

We use foams composed of bubbles in a network of surfactant solution and some single structures of foams known as Plateau borders and vertex. The Plateau border is an edge of foam in a junction of three soap films, while the vertex is a place where four Plateau borders meet.

3 Diffusion and Chaotic scattering

Using experiments involving the transport of light in foams, we have observed two main processes of light transport [1]: a diffusive one related to a Gaussian function, and another one related to a chaotic dynamics, similar to those observed in chaotic saddles, in which a ray of light bounces back and forth for a certain time in the scattering region, and leaves it through one of several exits, as it is shown in Figure 3 which represents a slice of the profile of light scattering. In this figure, we present the result obtained from the experiment involving light scattering in foams, in which a laser beam is injected in liquid foam inside a box.
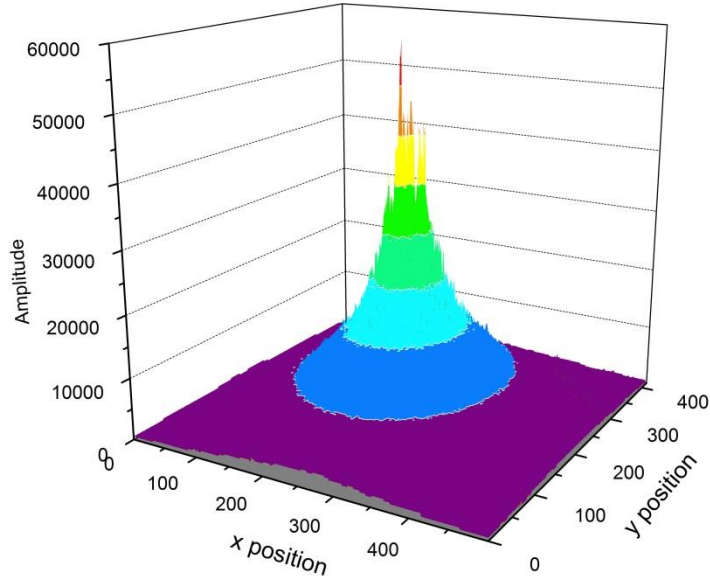
Fig. 3. Light intensity plot of the light scattering in foam.

The scattering process spreads the light and limits the depth of light penetration, creating a center glow located just above the interface of the box and the foam. We can represent the overall behavior of the light scattering $g(x,y)$ in foams with the following model:

857

$$g(x, y) = \frac{1}{2\pi\sigma^2} e^{-\frac{x^2+y^2}{2\sigma^2}} + f(x, y), \quad (1)$$

in which the first term represent the diffusive process present in all places, while the effects of the chaotic dynamics $f(x,y)$ are present mainly at the center of the foam, around the laser beam direction.
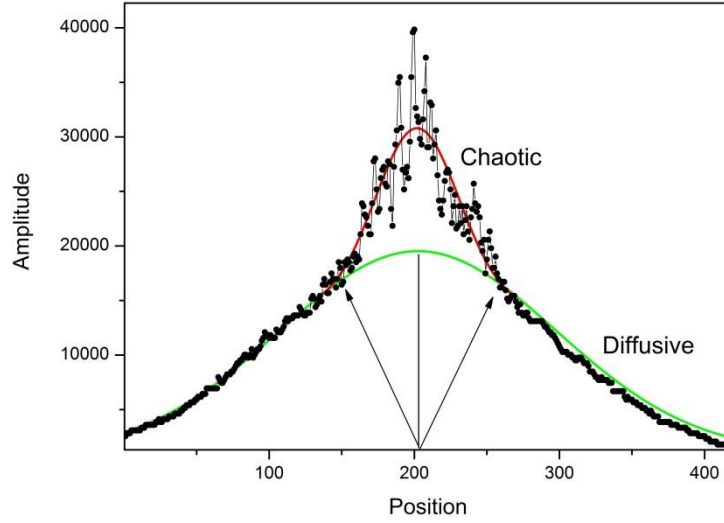
Fig. 4. Chaotic and diffusive light scattering.

4 The Parlaseric Circle

Besides these phenomena, we also observed the formation of some caustics. One of these caustics is the light pattern involving the parlaseric circle [2], explained by the Theory of Geometrical Diffraction [3].

The parlaseric circle is a luminous ring generated by light scattering in foams or soap bubbles. In analogy to the atmospheric phenomena known as parhelic circle, sun dogs, and sun pillars, we have named the features of the patterns observed as parlaseric circle, laser dogs, and laser pillars. The triangular symmetry of the Plateau borders is analogous to the hexagonal symmetry of ice crystals which produce these atmospheric phenomena. Working with one Plateau border at a time, we have observed wave optics phenomena that are not used in the explanation of the atmospheric phenomena, such as diffraction and interference.
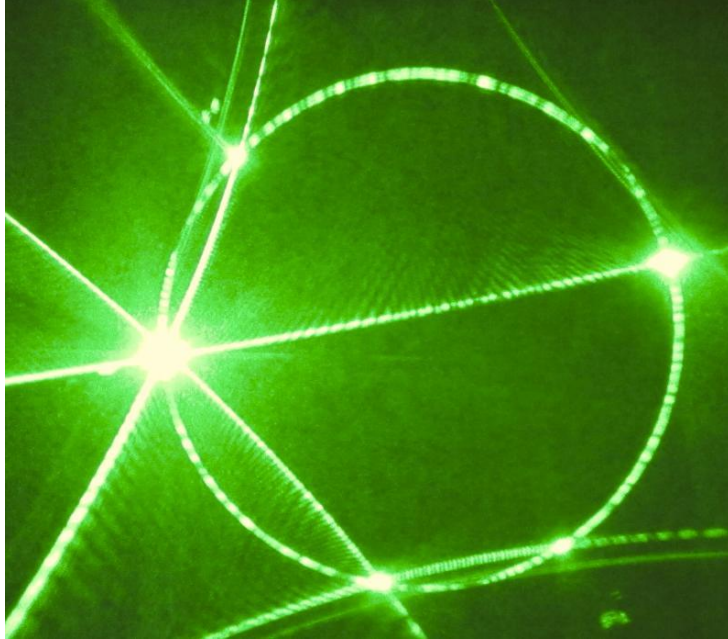
Fig. 5. The parlaseric circle, laser dogs and laser pillars obtained with green light.

Fig. 6. The parlaseric circle, two laser dogs and laser pillars obtained with blue light.

The main features of these patterns are the following: the laser spot and the laser dogs are always inscribed at the circumference of the parlaseric circle, and they are explained by the laws of geometrical optics. The lines crossing the laser spot are explained by the wave optics, and they represent the typical Fraunhofer diffraction of a triangle. The parlaseric circle is explained by the Theory of Geometrical Diffraction [3].

According to the Geometrical Theory of Diffraction suggested by Keller [3], when a light beam hits a straight edge obliquely, there is a cone of diffracted rays u_e and the cross section of this cone is a circle given by:

$$u_e = Du_i r^{-1/2} e^{ikr},$$ (2)

where D is a diffraction coefficient, u_i is the incident field, r is the distance between the edge and the screen, and $k=2\pi/\lambda$ is the wave number of the incident field with wavelength λ. This is the case when a laser light hits some structures of foams known as Plateau border, as previously observed by Tufaile and Tufaile [4].
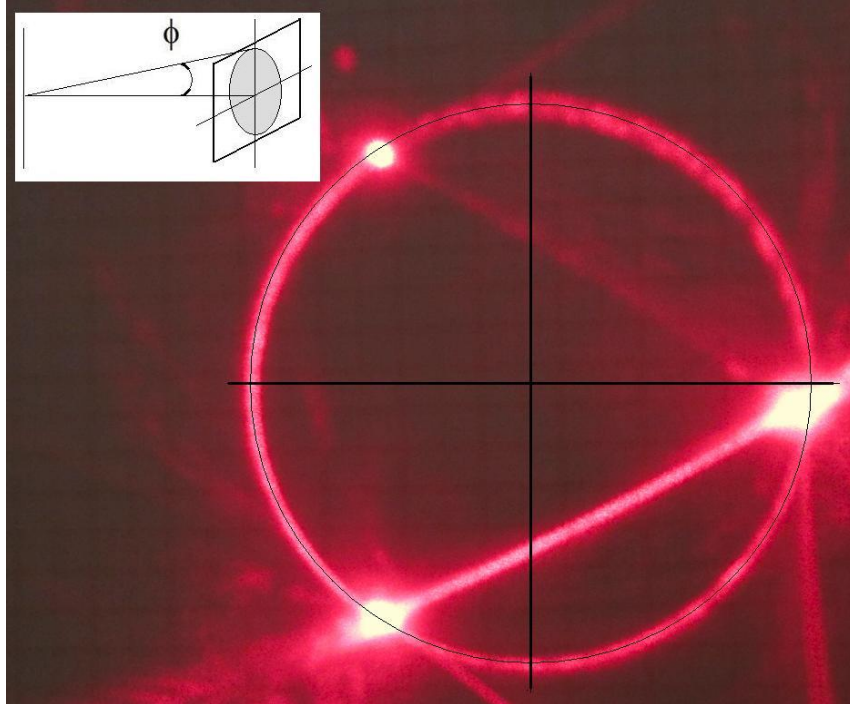
Fig. 7. According to the Geometrical Theory of Diffraction, when a light beam hits a straight edge obliquely, there is a cone of diffracted rays. ϕ is the semi angle of the diffraction cone that is equal to the incident angle measured from the laser beam direction.

The diagram of Figure 8 shows some important aspects of the parlaseric circle pattern, in which *LS* represent the laser spot, *LD1* and *LD2* are the laser dogs and the laser pillars are represented by the lines of diffraction and interference η_1, η_2 and η_3. Depending on the angle of incidence of light we can observe two or four laser dogs.

Laser Pillars and The Parlaseric Circle

The Plateau border has three sharp edges, and therefore the resulting point spread function produces a six pointed star.
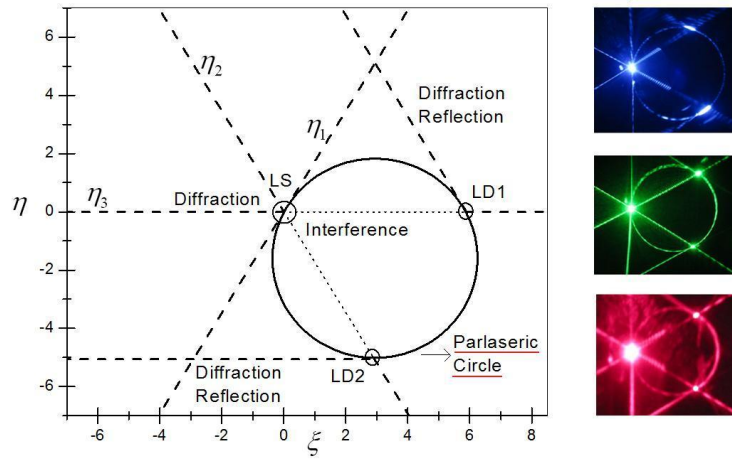
Fraunhofer diffraction of a regular triangle:

$$U(\xi,\eta) \propto \iint u(r,s)e^{-\frac{2\pi i}{\lambda z}(r\xi + s\eta)}drds \Rightarrow \eta_1(\xi) = \xi\sqrt{3}, \eta_2(\xi) = -\xi\sqrt{3}, \eta_3(\xi) = 0$$

Fig. 8. Laser pillars and the parhelic circle pattern diagram. LS is the laser spot, LDs are the laser dogs, η_n are the laser pillars.

5 Vertex Diffraction

In addition to the previous case, we have inspected the case known as vertex diffracted ray, when light hits a vertex formed by a junction of four Plateau borders, in which the corresponding diffracted waves are spherical with vertex at their center. Keller suggested that the field on the diffracted ray for this case is given by:

$$u = Cu_i \left(\frac{e^{ikr}}{r} \right). \tag{3}$$

The images in Figure 9 and Figure 10 obtained in our experiment show concentric fringes, could be the vertex diffraction, and in this case the amplitude varies as r^{-1} since the cross sectional area of a tube of diffracted rays is proportional to r^2, according to Keller.

| Fig. 9. Vertex diffraction with concentric circles. | Fig. 10. Vertex diffraction with concentric circles in a lager incident angle. |
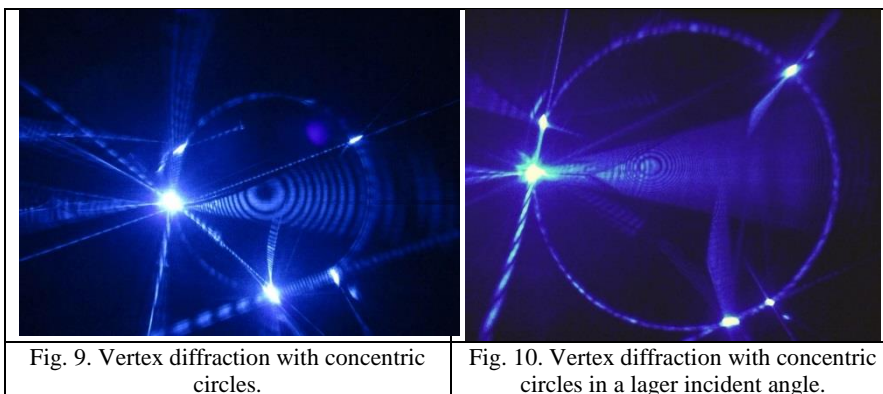
However, when we have moved the screen where the images were obtained, the interference pattern remained the same and the width of the fringes change, indicating that this is spherical wave of diffraction, resembling the interference patterns observed in the case of Newton rings or some patterns obtained in the Michelson interferometer. Increasing the angle of laser beam incidence and the axis of the Plateau border, the size of the fringes decrease.
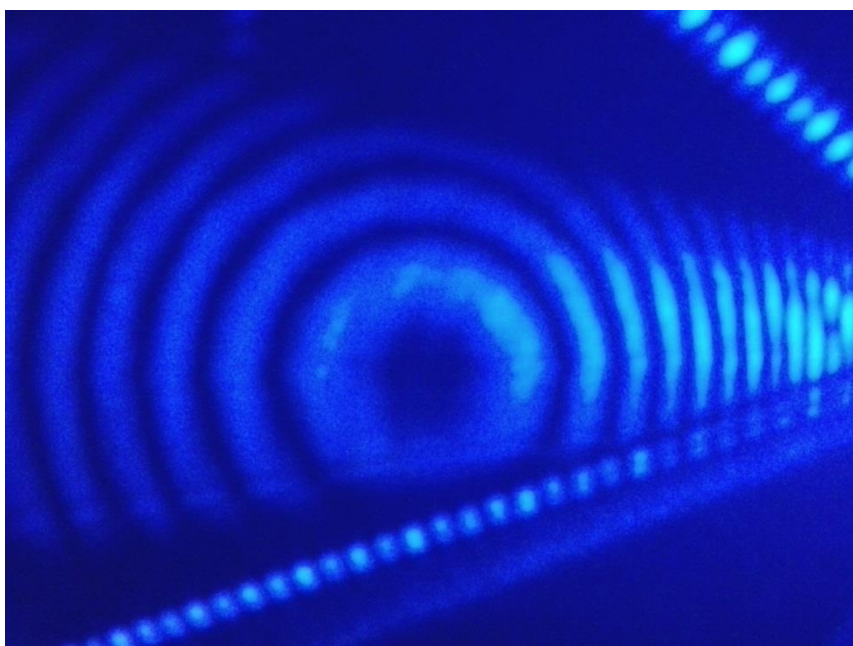
Fig. 11. Another image of the circular fringes at the center of the parlaseric circle.

By inspection of the patterns like those in Figures 9, 10 and 11, we are exploring the aspects of thin-film interference which occurs in a curved thin liquid film and, trying to associate with the case of Pohl interferometer, that is a device based in the amplitude splitting interference [5].

Conclusions

We are proposing the combination of two main processes of the light transport in foams: a diffusive one related to Gaussian function, and another one related to chaotic dynamics. Just considering the aspects of the geometrical optics, the curvature of soap film structures cause incident light to be scattered in different directions, because the direction of the rays leaving the soap film boundaries can vary greatly for the same incident angle with a small positional offset. Besides this, we have obtained some interesting patterns of light diffraction and compared them with the theory of geometrical diffraction suggested by Keller.

The classification of the optical phenomena somehow involves the scale of the scatterer, and the Plateau border is not just a regular prism. The pattern of the parlaseric circle present some features of the geometrical optics, wave optics and the theory of geometrical diffraction. All these phenomena are related to the nonlinear effects of light transport in foams, with applications in image processing, construction of new optical elements to generate halos or spherical waves, and with the possibility of improvements in the studies of atmospheric optics. Because all these phenomena can be observed with a table top experiment, they can be performed in order to get a better understanding of some concepts of optics, such as the Huygens principle.

Acknowledgements

References

1. A. Tufaile, M.V. Freire and A.P.B. Tufaile. Some aspects of image processing in foams. Physics Letters A **378**, 3111-3117, 2014.
2. E. Conover. Researchers create 'laser dogs' with soap bubbles. Science Magazine, 2015.
http://news.sciencemag.org/physics/2015/02/researchers-create-laser-dogs-soap-bubbles
3. J. Keller. Geometrical theory of diffraction. J. Op. Soc. Am. **52**, 116-130, 1962.
4. A. Tufaile and A.P.B. Tufaile, Parhelic-like circle from light scattering in Plateau borders. Physics letters A **379**, 529-534, 2015.
5. E. Hecht, Optics, Addison Wesley Longman, England, 1998.

Control of a Simple Chaotic Flow having a Line Equilibrium by means of a Single Passive Controller

Yılmaz Uyaroğlu [1], and Uğur Erkin Kocamaz [2]

[1] Department of Electrical & Electronics Engineering, Faculty of Engineering, Sakarya University, 54187 Serdivan, Sakarya, Turkey
E-mail: uyaroglu@sakarya.edu.tr
[2] Department of Computer Technologies, Vocational School of Karacabey, Uludağ University, 16700 Karacabey, Bursa, Turkey
E-mail: ugurkocamaz@gmail.com

Abstract. Recently, Jafari and Sprott (2013) have found nine simple chaotic flows with quadratic nonlinearities which include the unusual feature of having a line equilibrium. This study investigates the control of a simple chaotic system having a line equilibrium by means of the passive control method. Lyapunov function is used to realize that the passive controller ensures the global asymptotic stability of the system. In order to validate all the theoretical analyses, numerical simulations are demonstrated. Owing to the single passive controller, the chaotic flow stabilizes towards its line equilibrium in the state space effectively.
Keywords: Simple Chaotic Flow, Line Equilibrium, Passive Control, Chaos Control.

1 Introduction

Lorenz introduced the first chaotic attractor in 1963 [1]. It is an interesting nonlinear phenomenon, therefore chaos generation has received a great deal of attention from researchers. Rössler proposed a simple three-dimensional chaotic system in 1976 [2]. A double-scroll attractor was shown from Chua's circuit in 1984 [3]. Sprott focused on simpler chaotic systems in 1994 and uncovered 19 distinct chaotic flows which have either five terms and two nonlinearities or six terms and one nonlinearity [4]. In 1999, Chen and Ueta found a novel chaotic attractor called Chen chaotic system [5]. Lü et al. developed a new chaotic system, which represents the transition between the Lorenz and Chen systems in 2002 [6]. Then, Lü et al. proposed a generalized form of the Lorenz, Chen and Lü systems called unified chaotic system in 2002 [7]. In recent years, several new chaotic attractors have been revealed [8–10], and many more will be discovered on account of their potential applications especially in cryptology and secure communication [11, 12]. Recently, Jafari and Sprott have focused on the chaotic systems that have a line equilibrium and found nine simple chaotic flows [13]. They are three-dimensional continuous autonomous chaotic attractors and consist of six terms and two parameters [13].

In addition to searching for new chaotic systems, chaos control has become an important task. Its goal is to eliminate the chaotic trajectories and stabilize towards an equilibrium point of the system. At first, it was believed that controlling chaos cannot be done because chaotic systems are very sensitive to initial conditions. However, Ott, Grebogi, and Yorke applied the control of a chaotic system successfully in 1990 [14]. Afterwards, the chaos control has also received extensive attention. Many effective control methods such as linear feedback control [15], nonlinear feedback control [16], adaptive control [17], sliding mode control [18], passive control [19-25], impulsive control [26], and backstepping design [27] have been proposed for the control of chaos. Among them, the passive control method has been gaining significance due to using only one state controller which provides considerable benefits in reducing the complexity and cost. In this method, the main idea is to keep the system internally stable by using a controller which renders the closed loop system passive upon the properties of the system. In recent years, the passive control method has been applied for the control of Lorenz [19], Chen [20], unified [21], Rabinovich [22], Rucklidge [23] and some other chaotic systems [24, 25].

According to the literature review, the control of a chaotic system having a line equilibrium has not been investigated. Motivated by the chaos control studies, in this paper, the control of a chaotic flow having a line equilibrium has been implemented with a single state passive controller. The rest of this paper is organized as follows. In Section 2, a chaotic system which has a line equilibrium is described. In Section 3, a single passive controller is designed for the control. In Section 4, numerical simulations are demonstrated to validate the control. Finally, concluding remarks are given in Section 5.

2 A Simple Chaotic Flow having a Line Equilibrium

Jafari and Sprott [13] were inspired by the structure of the conservative Sprott case A system:

$$
\begin{aligned}
\dot{x} &= y, \\
\dot{y} &= -x + yz, \\
\dot{z} &= 1 - y^2,
\end{aligned}
\tag{1}
$$

and they searched for chaotic flows with a line equilibrium. They considered a general parametric form of Eq. (1) with quadratic nonlinearities of the form

$$
\begin{aligned}
\dot{x} &= y, \\
\dot{y} &= a_1 x + a_2 yz, \\
\dot{z} &= a_3 x + a_4 y + a_5 x^2 + a_6 y^2 + a_7 xy + a_8 xz + a_9 yz,
\end{aligned}
\tag{2}
$$

where the system has a line equilibrium in $(0, 0, z)$ with no other equilibria. An exhaustive computer search has been done and nine simple cases are found

which have only six terms. The ninth chaotic flow is given in the following equation:

$$\dot{x} = z,$$
$$\dot{y} = -ay - xz,$$
$$\dot{z} = z - bz^2 + xy,$$

(3)

where a and b are the system parameters [13, 28]. When they are selected as $a = 1.62$ and $b = 0.2$, the Lyapunov exponents become 0.0642, 0, and -0.6842 [13]. Thus, system (3) is chaotic for these parameters. Its Kaplan–Yorke dimension is 2.0939 [13].
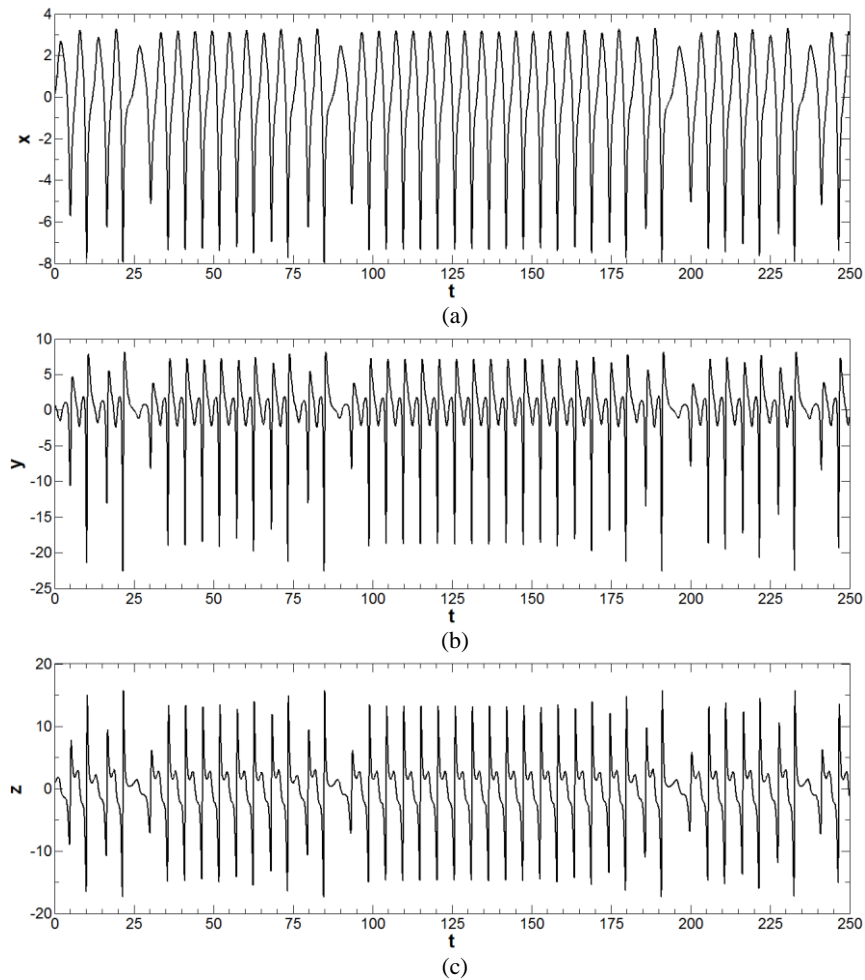
Fig. 1. Time series of the chaotic system having a line equilibrium for (a) x signals, (b) y signals, and (c) z signals.

The equilibria of the chaotic system (3) can be found by getting $\dot{x} = 0$, $\dot{y} = 0$, and $\dot{z} = 0$ as follows:

$$z = 0,$$
$$-ay - xz = 0, \tag{4}$$
$$z - bz^2 + xy = 0,$$

Hence, the chaotic system (3) has a line equilibrium point: $(x, 0, 0)$. Under the initial conditions $x(0) = 0$, $y(0) = 1$, and $z(0) = 0.8$, the time series, the 2D phase plots, and the 3D phase plane of chaotic system (3) are demonstrated in Fig. 1, Fig. 2, and Fig. 3, respectively.

(a)

(b)

(c)
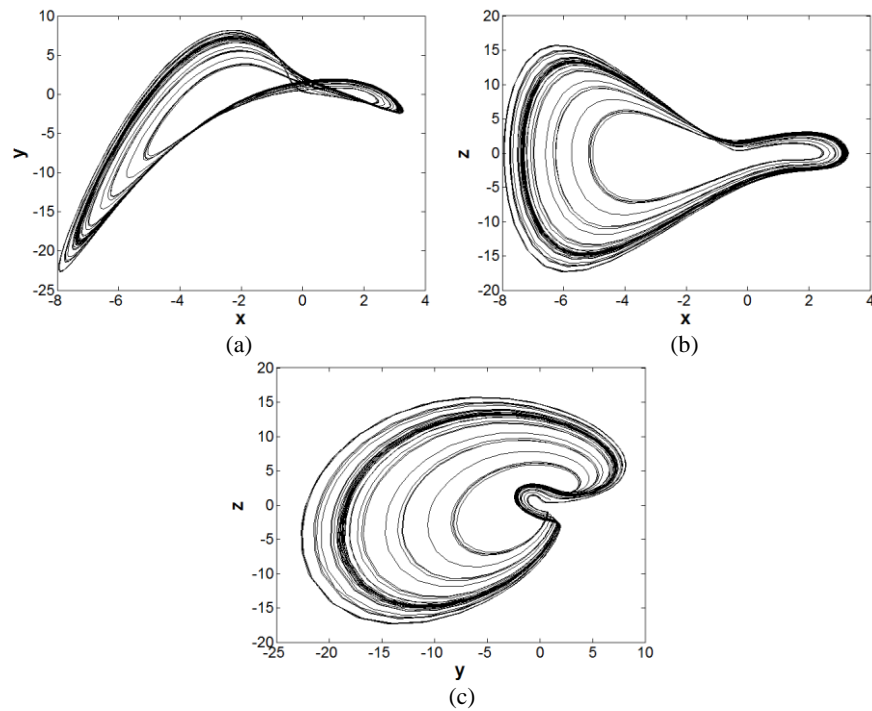
Fig. 2. Phase plots of the chaotic system having a line equilibrium for (a) x–y phase plot, (b) x–z phase plot, and (c) y–z phase plot.
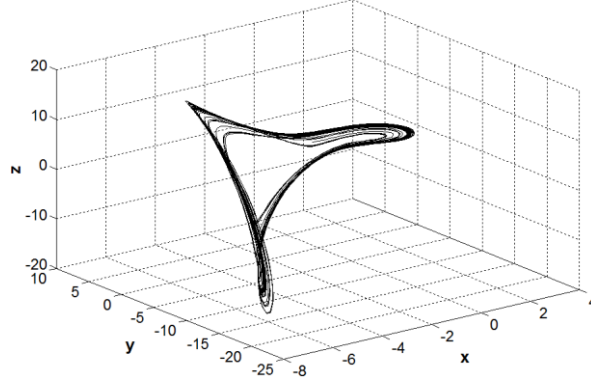
Fig. 3. Phase plane of the chaotic system having a line equilibrium.

3 Control with a Passive Controller

The passive control method is applied to system (3) in order to control the chaotic system having a line equilibrium to its equilibrium point. The controlled system is considered as follows:

$$
\begin{aligned}
\dot{x} &= z, \\
\dot{y} &= -ay - xz, \\
\dot{z} &= z - bz^2 + xy + u,
\end{aligned}
\tag{5}
$$

where u is the passive controller to be designed. By assuming that the state variable z is the output of the system and supposing that $z_1 = x$, $z_2 = y$, $Y = z$, and $Z = [z_1 \ z_2]^{\mathrm{T}}$, the system (5) can be denoted by normal form:

$$
\begin{aligned}
\dot{z}_1 &= Y, \\
\dot{z}_2 &= -az_2 - z_1 Y, \\
\dot{Y} &= Y - bY^2 + z_1 z_2 + u.
\end{aligned}
\tag{6}
$$

The passive control theory has the following generalized form

$$
\begin{aligned}
\dot{Z} &= f_0(Z) + p(Z, Y)Y, \\
\dot{Y} &= b(Z, Y) + a(Z, Y)u,
\end{aligned}
\tag{7}
$$

and according to system (6),

$$
f_0(Z) = \begin{bmatrix} 0 \\ -az_2 \end{bmatrix},
\tag{8}
$$

869

$$p(Z,Y) = \begin{bmatrix} 1 \\ -z_1 \end{bmatrix}, \tag{9}$$

$$b(Z,Y) = Y - bY^2 + z_1 z_2, \tag{10}$$

$$a(Z,Y) = 1. \tag{11}$$

The storage function is chosen as

$$V(Z,Y) = W(Z) + \frac{1}{2}(Y^2) \tag{12}$$

where

$$W(Z) = \frac{1}{2}(z_1^{\ 2} + z_2^{\ 2}) \tag{13}$$

is the Lyapunov function of $f_0(Z)$ with $W(0) = 0$. According to the Eq. (8), the derivative of $W(Z)$ is

$$\dot{W}(Z) = \frac{\partial W(Z)}{\partial Z} f_0(Z) = [z_1 \quad z_2] \begin{bmatrix} 0 \\ -az_2 \end{bmatrix} = -az_2^{\ 2} \le 0. \tag{14}$$

Since $W(Z) \ge 0$ and $\dot{W}(Z) \le 0$, it can be concluded that $W(Z)$ is the Lyapunov function of $f_0(Z)$ and that $f_0(Z)$ is globally asymptotically stable [21].

According to the passivity definition, the controlled system can be equivalent to a passive system and globally asymptotically stabilized at its zero equilibrium by the following controller [19]:

$$u = a(Z,Y)^{-1} \left[-b^T(Z,Y) - \frac{\partial W(Z)}{\partial Z} p(Z,Y) - \alpha Y + v \right]. \tag{15}$$

From the Eq. (15), the passive control function is

$$u = -Y + bY^2 - z_1 z_2 - z_1 + z_1 z_2 - \alpha Y + v, \tag{16}$$

where α is a positive constant and v is an external input signal. By taking back $z_1 = x$, $z_2 = y$, and $Y = z$ conversions, the passive controller u becomes

$$u = -z + bz^2 - xy - x + xy - \alpha z + v. \tag{17}$$

Substituting the Eq. (17) into system (3) yields

$$\dot{x} = z,$$
$$\dot{y} = -ay - xz, \tag{18}$$
$$\dot{z} = -x + xy - \alpha z + v.$$

The equivalent system (18) is a passive system of the chaotic system (3) which has a line equilibrium.

The passive controlled system can stabilize towards its any equilibrium point $(\bar{x}, \bar{y}, \bar{z})$. Let $\dot{x} = 0$, $\dot{y} = 0$, $\dot{z} = 0$ and then system (18) yields

$$0 = \bar{z},$$
$$0 = -a\bar{y} - \bar{x}\bar{z}, \tag{19}$$
$$0 = -\bar{x} + \bar{x}\bar{y} - \alpha\bar{z} + v.$$

This implies

$$\bar{z} = 0,$$
$$\bar{y} = 0, \tag{20}$$
$$v = \bar{x}.$$

The conditions in Eq. (20) maintain the global asymptotical stability of chaotic system (5) towards its $E(x, 0, 0)$ equilibrium point.

4 Numerical Simulations

The third-order Runge-Kutta method with variable time step is used in all numerical simulations of controlling the chaotic system having a line equilibrium. The same parameter values and initial conditions mentioned in Section 2 are considered to ensure the chaotic behaviour of the system. The controller is activated at $t = 50$ in all simulations. The passive control gain is taken as $\alpha = 1$. Simulation results for the control of this chaotic system towards (1, 0, 0), (0, 0, 0), and (-1, 0, 0) equilibrium points with a passive controller by setting $v = 1$, $v = 0$, and $v = -1$ are shown in Fig. 4, Fig. 5, and Fig. 6, respectively.
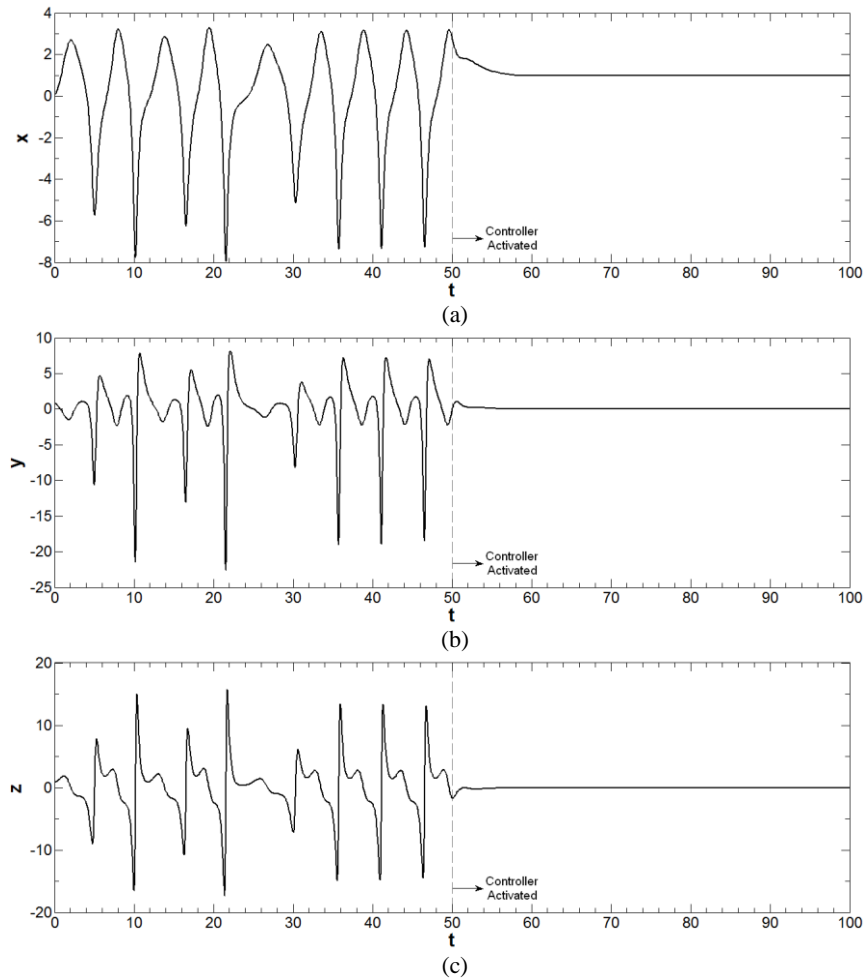
Fig. 4. Time responses of controlled chaotic system having a line equilibrium to (1, 0, 0) equilibrium point when the passive controller is activated at $t = 50$ for (a) x signals, (b) y signals, and (c) z signals.
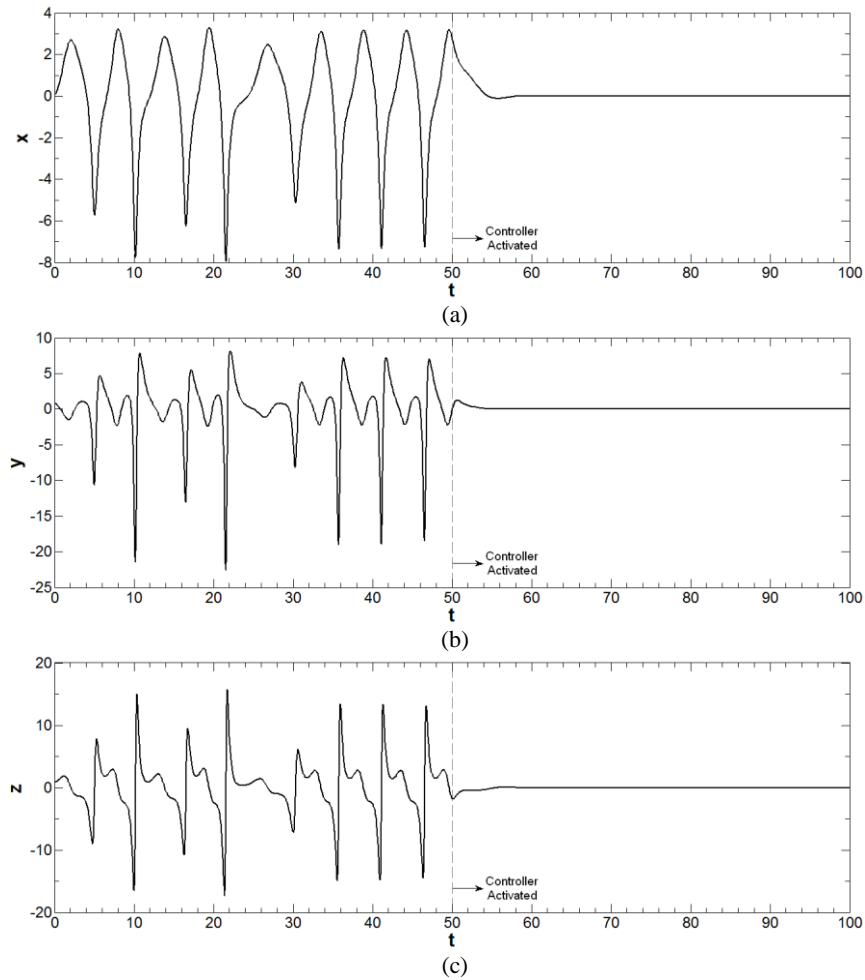
Fig. 5. Time responses of controlled chaotic system having a line equilibrium to (0, 0, 0) equilibrium point when the passive controller is activated at $t = 50$ for (a) x signals, (b) y signals, and (c) z signals.
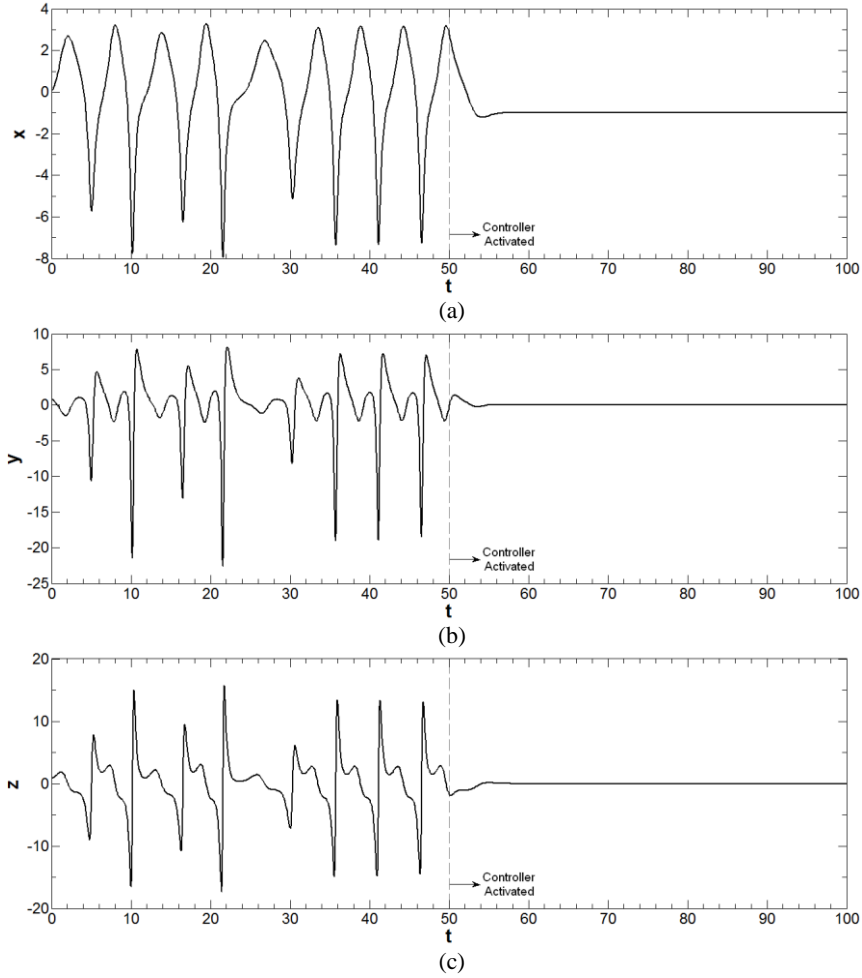
Fig. 6. Time responses of controlled chaotic system having a line equilibrium to (-1, 0, 0) equilibrium point when the passive controller is activated at $t = 50$ for (a) x signals, (b) y signals, and (c) z signals.

As seen in Figs. 4–6, the outputs of chaotic system converge to the (1, 0, 0), (0, 0, 0), and (-1, 0, 0) equilibrium points after the passive controller is activated. Therefore, the simulation results validate all the theoretical analyses. As seen in Fig. 4, when the passive controller is activated at $t = 50$, the control is provided at $t \geq 58$. Also, the control is observed after 8 time period in Fig. 5 and Fig. 6. Hence, the simulation results confirm the effectiveness of proposed passive control method.

5 Conclusions

In this paper, the control of a chaotic system having a line equilibrium is applied with a single state passive controller. The conditions of the asymptotic stability of the steady states of the controlled system are ensured with a Lyapunov function. Numerical simulations show that this three-dimensional continues time chaotic system can be controlled to its line equilibrium point in an appropriate amount of time with a passive controller. Hence, computer simulations have validated the effectiveness of passive control method in the control of the chaotic system having a line equilibrium.

References

1. E.N. Lorenz. Deterministic nonperiodic flow. Journal of Atmospheric Sciences, 20(2), 130-141, 1963.
2. O.E. Rössler. An equation for continuous chaos. Physics Letters A, 57(5), 397-398 1976.
3. T. Matsumoto. A chaotic attractor from Chua's circuit. IEEE Transactions on Circuits and Systems, CAS-31(12), 1055-1058, 1984.
4. J.C. Sprott. Some simple chaotic flows. Physical Review E, 50(2), 647-650, 1994.
5. G.R. Chen and T. Ueta. Yet another chaotic attractor. International Journal of Bifurcation and Chaos, 9(7), 1465-1466, 1999.
6. J.H. Lü, G.R. Chen and S.C. Zhang. The compound structure of a new chaotic attractor. Chaos, Solitons & Fractals, 14(5), 669-672, 2002.
7. J.H. Lü, G.R. Chen, D.Z. Cheng and S. Celikovsky. Bridge the gap between the Lorenz system and the Chen system. International Journal of Bifurcation and Chaos, 12(12), 2917–2926, 2002.
8. X.Y. Zhou. A novel chaotic system and its circuit simulation. Acta Physica Sinica, 61(3), Article Number: 030504, 2012.
9. B.J. Zhang and H.X. Li. A new four-dimensional autonomous hyperchaotic system and the synchronization of different chaotic systems by using fast terminal sliding mode control. Mathematical Problems in Engineering, 2013, Article Number: 179428, 2013.
10. V.T. Pham, C. Volos, S. Jafari, Z.C. Wei and X. Wang. Constructing a novel no-equilibrium chaotic system. International Journal of Bifurcation and Chaos, 24(5), Article Number: 1450073, 2014.
11. X.J. Wu, C.X. Bai and H.B. Kan. A new color image cryptosystem via hyperchaos synchronization. Communications in Nonlinear Science and Numerical Simulation, 19(6), 1884-1897, 2014.
12. C.C. Cheng, Y.S. Lin and S.W. Wu. Design of adaptive sliding mode tracking controllers for chaotic synchronization and application to secure communications. Journal of the Franklin Institute - Engineering and Applied Mathematics, 349(8), 2626-2649, 2012.
13. S. Jafari and J.C. Sprott. Simple chaotic flows with a line equilibrium. Chaos, Solitons & Fractals, 57, 79-84, 2013.
14. E. Ott, C. Grebogi and J.A. Yorke. Controlling chaos. Physical Review Letters, 64(11), 1196-1199, 1990.

15. G. Gambino, M.C. Lombardo and M. Sammartino. Global linear feedback control for the generalized Lorenz system. Chaos, Solitons & Fractals, 29(4), 829-837, 2006.

16. W.N. Zhou, L. Pan, Z. Li and W.A. Halang. Non-linear feedback control of a novel chaotic system. International Journal of Control, Automation and Systems, 7(6), 939-944, 2009.

17. Y.M. Zeng and S.N. Singh. Adaptive control of chaos in Lorenz system. Dynamics and Control, 7(2), 143-154, 1997.

18. M.J. Jang, C.L. Chen and C.K. Chen. Sliding mode control of chaos in the cubic Chua's circuit system. International Journal of Bifurcation and Chaos, 12(6), 1437–1449, 2002.

19. W. Yu. Passive equivalence of chaos in Lorenz system. IEEE Transaction on Circuits and Systems-I: Fundamental Theory and Applications, 46(7), 876-878, 1999.

20. D. Qi, G. Zhao and Y. Song. Passive control of Chen chaotic system. In: Proceedings of the 5th World Congress on Intelligent Control and Automation, Hangzhou, China, 1284–1286, 15–19 June 2004.

21. X. Chen and C. Liu. Passive control on a unified chaotic system. Nonlinear Analysis: Real World Applications, 11, 683–687, 2010.

22. S. Emiroglu and Y. Uyaroglu. Control of Rabinovich chaotic system based on passive control. Scientific Research and Essays, 5(21), 3298–3305, 2010.

23. U.E. Kocamaz and Y. Uyaroglu. Controlling Rucklidge chaotic system with a single controller using linear feedback and passive control methods. Nonlinear Dynamics, 75(1-2), 63–72, 2014.

24. G.M. Mahmoud, E.E. Mahmoud and A.A. Arafa. Passive control of n-dimensional chaotic complex nonlinear systems. Journal of Vibration and Control, 19(7), 1061–1071, 2013.

25. D.Q. Wei and Y.H. Qin. Controlling chaos in single-machine-infinite bus power system by adaptive passive method. Fourth International Workshop on Chaos-Fractals Theories and Applications, IWCFTA, Hangzhou, China, 295–297, 2011.

26. X. He, C.D. Li, X.M. Pan and M. Peng. Impulsive control and Hopf bifurcation of a three-dimensional chaotic system. Journal of Vibration and Control, 20(9), 1361-1368, 2014.

27. J.H. Lu and S.C. Zhang. Controlling Chen's chaotic attractor using backstepping design based on parameters identification. Physics Letters A, 286(2-3), 148-152, 2001.

28. U.E. Kocamaz and Y. Uyaroglu. Comments on "Simple chaotic flows with a line equilibrium" [Chaos, solitons & fractals 57 (2013) 79-84]. Chaos, Solitons & Fractals, 77, 340, 2015.

Inversive generator of the second order for the sequence of PRN's

Sergey Varbanets

Department of Computer Algebra and Discrete Mathematics, I.I. Mechnikov Odessa National University, str. Dvoryanskaya 2, 65026 Odessa, Ukraine
(E-mail: `varb@sana.od.ua`)

Abstract. The new inversive congruential method for generating uniform pseudorandom numbers is a particularly attractive alternative to linear congruential generators which have many undesirable regularities. In the present paper, a new inversive congruential generator of the second order for the sequence of PRN's is introduced. Exponential sums on inversive congruential pseudorandom numbers are estimated. The results show that these inversive congruential pseudorandom numbers pass the s-dimensional serial tests for the statistical independency.
Keywords: inversive congruential pseudorandom numbers, exponential sum, discrepancy.

1 Introduction

The uniform pseudorandom numbers (abbrev., PRN's) in the interval $[0, 1]$ are basic ingredients of any stochastic simulation. Its quality is of fundamental importance for the success of the simulation, since the typical stochastic simulation essentially depends on the structural and statistical properties of the producing pseudorandom number generators. In the cryptographical applications of pseudorandom numbers the significant importance is of the availability of property of the unpredictability to generated sequence of pseudorandom numbers. The classical and most frequently used method for generation of PRN's still is the linear congruential method. Unfortunately, its simple linear nature implies several undesirable regularities. Therefore, a variety of nonlinear methods for the generation of PRN's have been introduced as alternatives to linear methods. It is particularly interesting the nonlinear generators for producing the uniform PRN's, such as the inversive generators and its generalizations. Such generators were introduced and studied in [2], [6], [7]. These generators have several attractive properties such as an uniformity, unpredictability (statistical independence), pretty large period and simple calculative complexity. The most common types of the inversive generators define by the following congruential recursions.

Let $\mathbb{F}_q$ be a finite field with q elements and let y_0, a, b belong $\mathbb{F}_q$. Put

$$y^{-1} = \begin{cases} 0 \ if \ y = 0, \\ \text{multiplicative inverse to } y \text{ in } \mathbb{F}_q^* \text{ if } y \neq 0. \end{cases}$$

Then the recursion

$$y_{n+1} = ay_n^{-1} + b, \ n = 0, 1, 2, \ldots. \tag{1}$$

produces the inversive congruential generator over $\mathbb{F}_q$.
The generator (1) was introduced in [2], [?], [7], [11].

Other inversive generators consider over the ring $\mathbb{Z}_{p^m}$.

Let p be a prime number, $m > 1$ be a positive integer. Consider the following recursion

$$y_{n+1} \equiv a\overline{y}_n + b \pmod{p^m}, (a, b \in \mathbb{Z}), \tag{2}$$

where $\overline{y}_n$ is a multiplicative inversive modulo p^m for y_n if $(y_n, p) = 1$. The parameters a, b, y_0 we called the multiplier, shift and initial value, respectively.

In the works of Eichenauer, Lehn, Topuzoğlu[3]; Niederreiter, Shparlin-ski[10]; Eichenauer, Grothe[5] etc. were proved that the inversive congruential generator (2) produces the sequence $\{x_n\}$, $x_n = \frac{y_n}{p^m}$, $n = 0, 1, 2, \ldots$, which passes s-dimensional serial tests on equidistribution and statistical independence for $s = 1, 2, 3, 4$ if the defined conditions on relative parameters a, b, y_0 are accomplishable.

It was proved that this generator is extremely useful for Quasi-Monte Carlo type application (see, [9],[12]). The sequences of PRN's can be used for the cryptographic applications. Now the initial value y_0 and the constants a and b are assumed to be secret key, and then we use the output of the generator (2) as a stream cipher. At the last time it has been shown that we must be careful in the time of using the generator (2).

We call the generator (2) the inversive generator with constant shift.

In [14] we have given two generalization for the generator (2). The first generalization connects with the recurrence relation

$$y_{n+1} \equiv a\overline{y}_n + b + cF(n+1)y_0 \pmod{p^m} \tag{3}$$

under conditions

$$(a, p) = (y_0, p) = 1, \ b \equiv c \equiv 0 \pmod{p}, \ F(u) \text{ is a polynomial over } \mathbb{Z}[u].$$

We call the generator (3) the inversive congruential generator with a variable shift $b + cF(n+1)y_0$. The computational complexity of generator (3) is the same as for the generator (2), but the reconstruction of parameters a, b, c, y_0, n and polynomial $F(n)$ is a tricky problem even if the several consecutive values $y_n, y_{n+1}, \ldots, y_{n+N}$ will be revealed (for example, even the reconstruction of three-term polynomial $F(u)$ of large unknown degree is a very hard problem). Thus the generator (3) can be used in the cryptographical applications. Notice that the conditions $(a, p) = (y_0, p) = 1$, $b \equiv c \equiv 0 \pmod{p}$ guarantee that the

recursion (3) produces the infinite sequence $\{y_n\}$.

The second congruential recursion has the form

$$y_{n+1} \equiv a\bar{y}_n + b + cy_n \pmod{p^m} \tag{4}$$

with $(a, p) = 1$, $b \equiv c \equiv 0 \pmod{p}$.

We call the generator (4) the linear-inversive congruential generator.

We must notice that the conditions $a \equiv b \equiv 0 \pmod{p}$, $(y_0, p) = (c, p) = 1$ also give to generate the sequence of PRN's with appropriate properties for PRN's $\{x_n\}$. However, the conditions $a \equiv c \equiv 0 \pmod{p}$, $(y_0, p) > (b, p) = 1$ don't permit to construct the required sequence of PRN's.

For the case $p = 2$, Kato, Wu, Yanagihara[7] studied the generator (4). These authors proved that the appropriate sequence of PRN's $\{x_n\}$ has a period $\tau = 2^{m-1}$ if and only if $a + c \equiv 1 \pmod 4$ and $b \equiv 3 \pmod 4$.

The present paper deals with the congruential inversive generator of second order determined by the recursion

$$y_{n+1} \equiv a(y_{n-1}y_n)^{-1} + b \pmod{p^m}, \tag{5}$$

where $(a, p) = 1$, $b \equiv 0 \pmod{p}$, $(y_0, p) = (y_1, p) = 1$.

Notice that the superimposed requirements on a, b, y_0, y_1 permit to define every value y_n, $n = 2, 3, \ldots$.

Our purpose in this work is to show passing the test on equidistribution and statistical independence for the sequence $\{x_n\}$, $x_n = \frac{y_n}{p^m}$, and hence, the main point to be shown is the possibility for such sequences to be used in the problem of real processes modeling and in the cryptography.

In the sequel we will use the following notation.

2 Notation and auxiliary results

Variables of summation automatically range over all integers satisfying the condition indicated. The letter p denotes a prime number, $p \geq 3$. For $m \in \mathbb{N}$ the notation $\mathbb{Z}_{p^m}$ (respectively, $\mathbb{Z}_{p^m}^*$) denotes the complete (respectively, reduced) system of residues modulo p^m. For $z \in \mathbb{Z}$, $(z, p) = 1$ let z^{-1} be the multiplicative inverse of z modulo p^m. We write $\nu_p(A) = \alpha$ if $p^\alpha | A$, $p^{\alpha+1} \nmid A$. For integer t, the abbreviation $e_m(t) = e^{\frac{2\pi i t}{p^m}}$ is used.

We need the following simple statements.

Let $f(x)$ be a periodic function with a period τ. For any $N \in \mathbb{N}$, $1 \leq N \leq \tau$, we denote

$$S_N(f) := \sum_{x=1}^{N} e^{2\pi i f(x)}$$

Lemma 1. *The following estimate*

$$|S_N(f)| \leq \max_{1 \leq n \leq \tau} \left| \sum_{x=1}^{\tau} e^{2\pi i \left(f(x) + \frac{nx}{\tau} \right)} \right| \log \tau$$

holds.

879

This statement is well-known lemma about an estimate of uncomplete exponential sum by means of the complete exponential sum.

Lemma 2. *Let h_1, h_2, k, ℓ be positive integers and let $\nu_p(h_1 + h_2) = \alpha$, $\nu_p(h_1 k + h_2 \ell) = \beta$, $\delta - \min(\alpha, \beta)$. Then for every $j = 2, 3, \ldots$ we have*

$$\nu_p(h_1 k^{j-1} + h_2 \ell^{j-1}) \geq \delta.$$

Proof. By the equality

$$h_1 k^j + h_2 \ell^j = (h_1 k^{j-1} + h_2 \ell^{j-1})(k + \ell) - k\ell(h k^{j-2} + h_2 \ell^{j-2}),$$

applying the method of mathematical induction, we obtain at once $\nu_p(h_1 k^j + h_2 \ell^j) \geq \delta$, $j = 2, 3, \ldots$ $\square$

Lemma 3. *Let $p > 2$ be a prime number, $f(x)$, $g(x)$ be polynomials over $\mathbb{Z}$*

$$f(x) = A_1 x + A_2 x^2 + \cdots, \quad g(x) = B_1 x + B_2 x^2 + \cdots,$$

$$\nu_p(A_j) = \lambda_j, \quad \nu_p(B_j) = \mu_j, \quad j = 1, 2, 3, \ldots$$

and, moreover, $\alpha = \lambda_2 \leq \lambda_3 \leq \cdots$, $0 = \mu_1 < \mu_2 \leq \mu_3 \leq \cdots$.
Then for $m \geq 2$ the following bounds occur

$$\left| \sum_{x \in \mathbb{Z}_{p^m}} e_m(f(x)) \right| \leq \begin{cases} 2p^{\frac{m+\alpha}{2}} & if \ \nu_p(A_1) \geq \alpha, \\ 0 & if \ \nu_p(A_1) < \alpha; \end{cases}$$

$$\left| \sum_{x \in \mathbb{Z}_{p^m}^*} e_m(f(x) + g(x^{-1})) \right| \leq I(p^m) p^{\frac{m}{2}}$$

where $I(p^m)$ is a solution of the congruence

$$f'(y) \equiv g(y^{-1}) \cdot y^{-1} \pmod{p^{m-m_0}}.$$

Proof. Putting $x = y(1 + p^{m_0} z)$, $y \in \mathbb{Z}_{p^{m_0}}^*$, $z \in \mathbb{Z}_{p^{m-m_0}}$, we have modulo p^m

$$x^k = y^k + kp^{m_0} y^k z, \quad (x^{-1})^k = y^k - kp^{m_0} y^k z.$$

And then we obtain modulo p^m

$$f(x) + g(x^{-1}) = f(y) + g(y) + p^{m_0}(f'(y) - y^{-1} g'(y^{-1})) z.$$

Hence,

$$\sum_{x \in \mathbb{Z}_{p^m}^*} e_m(f(x) + g(x^{-1})) =$$

$$= \sum_{y \in \mathbb{Z}_{p^{m_0}}^*} e_m(f(y) + g(y^{-1})) \sum_{z \in \mathbb{Z}_{p^{m-m_0}}} e_m((f'(y) - y^{-1} g'(y^{-1})) z) =$$

$$= p^{m-m_0} \sum_{\substack{y \in \mathbb{Z}_{p^{m_0}}^* \\ f'(y) \equiv y^{-1} g'(y^{-1}) \pmod{p^{m-m_0}}}} e_m(f(y) + g(y^{-1})).$$

Now, if $m = 2m_0$, we obtain

$$\left| \sum_{x \in \mathbb{Z}_{p^m}^*} e_m(f(x) + g(x^{-1})) \right| = p^{\frac{m}{2}} I(p^m).$$

For $m = 2m_0 + 1$ we put $y = y_j + p^{m-m_0}t$, $t \in \mathbb{Z}_p$, y_j runs all solutions of the congruence $f'(y) \equiv y^{-1}g'(y^{-1}) \pmod{p^{m-m_0}}$ over $\mathbb{Z}_{p^{m-m_0}}^*$. Then setting $y = y_j(1 + pt)$, $t \in \mathbb{Z}_p$, we obtain

$$\sum_{\substack{y \in \mathbb{Z}_{p^{m_0}}^* \\ f'(y) \equiv y^{-1}g'(y^{-1}) \pmod{p^{m-m_0}}}} e_m(f(y) + g(y^{-1})) =$$

$$= \sum_{j=1}^{I(p^m)} e_m(f(y_j) + g(y_j^{-1})) \sum_{t \in \mathbb{Z}_p} e_{m-2m_0} \left(\frac{f'(y_j) - y_j^{-1}g'(y_j^{-1})}{p^{m_0}}t + B_1 y_j^{-2}t^2 \right).$$

The inner sum in right side of last equality is the Gaussian sum. Consequently, we finally have

$$\left| \sum_{x \in \mathbb{Z}_{p^m}^*} e_m(f(x)g(x^{-1})) \right| \le p^{\frac{m}{2}} \cdot I(p^m).$$

$\square$

For N arbitrary points $\mathfrak{t}_0, \mathfrak{t}_1, \ldots, \mathfrak{t}_{N-1} \in [0,1)^d$, the discrepancy is defined by

$$D(\mathfrak{t}_0, \mathfrak{t}_1, \ldots, \mathfrak{t}_{N-1}) = \sup_I \left| \frac{A_N(I)}{N} - |I| \right|, \tag{5.1}$$

where the supremum is extended over all subintervals I of $[0,1)^d$, $A_N(I)$ is the number of points among $\mathfrak{t}_0, \mathfrak{t}_1, \ldots, \mathfrak{t}_{N-1}$ falling into I, and $|I|$ denotes the d-dimensional volume I.

For study the discrepancy of points usually use the following lemmas.

For integers $q \ge 2$ and $d \ge 1$, let $C_q(d)$ denote the set of all nonzero lattice points $(h_1, \ldots, h_d) \in \mathbb{Z}^d$ with $-\frac{q}{2} < h_j \le \frac{q}{2}$, $1 \le j \le d$. We define

$$r(h, q) = \begin{cases} q \sin \frac{\pi|h|}{q} & if \ h \in C_1(q), \\ 1 & if \ h = 0 \end{cases}$$

and

$$r(\mathfrak{h}, q) = \prod_{j=1}^{d} r(h_j, q) \ \ for \ \mathfrak{h} = (h_1, \ldots, h_q) \in C_d(q).$$

Lemma 4 (Niederreiter,[9]). *Let $N \ge 1$ and $q \ge 2$ be integers. For N arbitrary points $\mathfrak{t}_0, \mathfrak{t}_1, \ldots, \mathfrak{t}_{N-1} \in [0,1)^d$, the discrepancy $D(\mathfrak{t}_0, \mathfrak{t}_1, \ldots, \mathfrak{t}_{N-1})$ satisfies*

$$D_N(\mathfrak{t}_0, \mathfrak{t}_1, \ldots, \mathfrak{t}_{N-1}) \le \frac{d}{q} + \frac{1}{N} \sum_{\mathfrak{h} \in C_d(q)} \frac{1}{r(\mathfrak{h}, q)} \left| \sum_{n=0}^{N-1} e(\mathfrak{h} \cdot \mathfrak{t}_n) \right|.$$

Lemma 5. *Let $\{\mathfrak{y}_k\}$, $\mathfrak{y}_k \in \{0, 1, \ldots, q-1\}^d$, is a purely periodic sequence with a period τ. Then for the discrepancy of the points $\mathfrak{t}_k = \frac{\mathfrak{y}_k}{q} \in [0,1)^d$, $k = 0, 1, \ldots, N-1$; $N \leq \tau$, the following estimate*

$$D_N(\mathfrak{t}_0, \mathfrak{t}_1, \ldots, \mathfrak{t}_{N-1}) \leq \frac{d}{q} + \frac{1}{N} \sum_{\mathfrak{h} \in C_d(q)} \sum_{h_0 \in \left(-\frac{\tau}{2}, \frac{\tau}{2}\right]} r^{-1}(\mathfrak{h}, q) r^{-1}(h_0, \tau) \cdot |\mathfrak{S}|$$

holds,

where $\mathfrak{S} := \sum\limits_{k=0}^{\tau-1} e(\mathfrak{h} \cdot \mathfrak{t}_k + \frac{k h_0}{\tau})$.

This assertion follows from Lemma 4 and from an estimate of uncomplete exponential sum through complete exponential sum (see, Lemma 1).

3 Preparations

We will obtain the representation of y_n in the form of rational function on y_0.

Denote $\nu_p(b) = \nu_0$. A straightforward computation by recursion (5) shows that modulo $p^{3\nu_0}$ we have

$$y_2 = \frac{a + b y_0 y_1}{y_0 y_1}, \quad y_3 = \frac{a y_0 + ab + b^2 y_0 y_1}{a y_0 y_1 + ab y_0 + ab^2}, \quad y_4 = \frac{a y_0 y_1 + ab y_0 + ab^2}{a y_0 + ab + b^2 y_0 y_1},$$

$$y_5 = \frac{2a^2 b + a^2 y_0 + 3ab^2 y_0 y_1}{a^2 + 2ab y_0 y_1 + ab^2 y_0}, \quad y_6 = \frac{2a^2 b + a^2 y_0 + 3ab^2 y_0 y_1}{a^2 + 2ab y_0 y_1 + ab^2 y_0}.$$

These relations give rise to proposal that representation of y_n will be found in the form of

$$y_n = \frac{A_0^{(n)} + A_1^{(n)} y_0 + A_2^{(n)} y_0 y_1}{B_0^{(n)} + B_1^{(n)} y_0 + B_2^{(n)} y_0 y_1}, \tag{6}$$

where $A_j^{(n)}$, $B_j^{(n)}$ are the polynomials from $\mathbb{Z}[n]$. From the above, for y_n we involve

$$y_{n+2} = \frac{(aB_0^{(n)} + bA_0^{(n+1)}) + (aB_1^{(n)} + bA_1^{(n+1)}) y_0 + (aB_2^{(n)} + bA_2^{(n+1)}) y_0 y_0}{A_0^{(n+1)} + A_1^{(n+1)} y_0 + A_2^{(n+1)} y_0 y_1} \tag{7}$$

Now, a straightforward computation suggest that modulo $p^{3\nu_0}$ we have

$$\begin{cases} A_0^{(3k-1)} \equiv a^k, \ A_1^{(3k-1)} \equiv (k^2 - 3k + 3) a^{k-1} b^2, \\ A_2^{(3k-1)} \equiv k a^{k-1} b + 6(k-3) a^{k-2} b^2; \\ B_0^{(3k-1)} = \frac{k(k-1)}{2} a^{k-1} b^2, \ B_1^{(3k-1)} = (3k-1) - 2(k-2) a^{k-1} b, \\ B_2^{(3k-1)} = a^{k-1} + 6a^{k-2} b; \end{cases} \tag{8}$$

$$\begin{cases} A_0^{(3k)} \equiv k a^k b, \ A_1^{(3k)} \equiv 2a^k; A_2^{(3k)} \equiv \frac{k(k+1)}{2} a^{k-1} b^2; \\ B_0^{(3k)} \equiv a^k, \ B_1^{(3k)} \equiv (k^2 - 3k + 3) a^{k-1} b^2; \\ B_2^{(3k)} \equiv k a^{k-1} b + 6(k-3) a^{k-1} b^2; \end{cases} \tag{9}$$

882

$$\begin{cases} A_0^{(3k+1)} = a^{k+1} + ka^k b^2, \ A_1^{(3k+1)} = (k^2 - 3k + 3)a^k b^2 + 2a^k b; \\ A_2^{(3k+1)} = ka^k b + 6(k-3)a^{k-1}b^2; \\ B_0^{(3k+1)} = ka^2 b, \ B_1^{(3k+1)} = 2a^k; \ B_2^{(3k+1)} = a^{k-1}b^2. \end{cases} \tag{10}$$

The validity of the formulas (8), (9) is not difficult establishes by the method of mathematical induction. The formula (10) follows by recursion (5). Other summands of A_j^n, $j = 0, 1, 2$; $n = \{3k - 1 \text{ or } 3k \text{ or } 3k + 1\}$, which modulo $p^{3\nu_0}$ are equal to 0, be represented the polynomials from $\mathbb{Z}[n]$ (it comes from formula (7)). So, we may write

$$A_0^{(3k-1)} = a^k + p^{3\nu_0} F_0(k), \ldots, B_2^{3k-1} = a^{k-1} + 6(k-3)a^{k-2}b^2 + p^{3\nu_0} G_2(k).$$

The number summands in any $F_j(k)$ or $G_j(k)$, $j = 0, 1, 2$ be less than $4m_0$, where $m_0 = \left[\frac{m+1}{\nu_0}\right]$ by virtue when passing from k to $k+2$ "old" coefficients gets multiplier divisible to $a \cdot b$. Therefore, appearance of the polynomials $F_j(k)$, $G_j(k)$ rallies, moreover, all summands in the polynomials $F_j(k)$, $G_j(k)$ contains factor a^ℓ, $k - m_0 \le \ell \le k$.

The relation (6) shows that for every $k = 0, 1, 2, \ldots$ the numerator and denominator contain a summand that is coprime to p, and every such summand contains the factor a^k. Multiply out numerator and denominator on multiplicative inverse modp^m to the respective summand of denominator and applying the expanding $(1 + pu)^{-1} = 1 - pu + p^2 u^2 - \cdots + (-1)^{m-1}(pu)^{m-1} \pmod{p^m}$, we obtain the representation of y_k power expansion of k with coefficients which depend only on y_0, y_1 and $(a^{-1})^j$, $0 \le j \le m$, where $a \cdot a^{-1} \equiv 1 \pmod{p^m}$.

So, after simple calculations we deduce modulo p^m

$$y_{3k-1} = y_0^{-1} y_1^{-1} \cdot S_1 \cdot S_2$$

where

$$S_1 = \Big[a + (k^2 - 3k + 3)b^2 y_0 +$$

$$+ (b + 6(k-3)a^{-1}b^2)y_0 y_1 + p^{3\nu_0} G(k, y_0, y_1)\Big]$$

$$S_2 = \Big[1 - 6a^{-1}by_0 y_1 - \frac{k(k-1)}{2}b^2 - (2k-4)b^2 -$$

$$- (2k-4)by_0 + 36a^{-2}b^2(y_0 y_1)^2 + (2k-4)^2 b^2 y_0^2 +$$

$$+ 12(2k-4)a^{-1}b^2 y_0^2 y_1 + p^{3\nu_0} F(k, y_0, y_1)\Big]$$

From where we have

$$y_{3k-1} = y_0^{-1} y_1^{-1} \left\{ (a + bc_0) + kb(1 - 2ay_1^{-1}) + \right.$$

$$\left. + k^2 b^2 (y_0 - \frac{1}{2}ay_1^{-1} + 4ay_1^{-1}) + b^3 H(k, y_0, y_1) \right\} \tag{11}$$

where $c_0 = -6a^{-1}by_0y_1 + b^2(3y_0 + 8a + 36a^{-1}(y_0y_1)^2 + 16ay_0^2 - 48y_0^2y_1) + 4by_0a$.

Next, by analogy, we infer

$$y_{3k} = [2y_0 - 3a^{-1}b^2y_0(1 - ba^{-1}y_1)] + kb(1 + bh(k)) +$$
$$+ k^2b^2(-\frac{1}{2}a^{-1}y_0y_1 - 2a^{-1}y_0^2) + p^{3\nu_0}L(k, y_0, y_1), \tag{12}$$

where $h(k) = 6a^{-1}by_0^2 - 12a^{-1}by_0^2y_1$,

$$y_{3k+1} = 2^{-1}y_0^{-1}[a + 2by_0 + 3b^2y_0(1 - 6a^{-1}y_1)] +$$
$$+ kb(y_0y_1 - 2^{-1}ay_0^{-1} + p^{3\nu_0}b(-3y_0)) + \tag{13}$$
$$+ k^2b^2(y_0 + 2^{-1}ay_0^{-2} - 2^{-2}y_0^{-1} - 2^{-1}y_1^{-1}) + p^{3\nu_0}M(k, y_0, y_1)y_0^{-1}.$$

From (11)-(13) we infer the following statement.

Proposition 1. *Let the sequence $\{y_n\}$ be produced by the recursion (5) with $(a, p) = (y_0, p) = (y_1, p) = 1$, $\nu_p(b) = \nu_0 > 0$. There exist the polynomials $F_{-1}(x), F_0(x), F_1(x) \in \mathbb{Z}[x]$ with the coefficient depending on y_0, y_1, such that*

$$y_{3k-1} = y_0^{-1}y_1^{-1}((a + b(-6a^{-1}y_0y_1) + b^2B_0(y_0, y_1)) +$$
$$+ kb(1 - 2ay_1^{-1} + bB_1(y_0, y_1)) + \tag{14}$$
$$+ k^2b^2(y_0 - \frac{7}{2}ay_1^{-1} + bB_2(y_0, y_1))) + p^{3\nu_0}F_{-1}(k)$$

$$y_{3k} = (2y_0 + b^2C_0(y_0, y_1)) + kb(1 + bC_1(y_0, y_1)) +$$
$$+ k^2b^2(-\frac{1}{2}a^{-1}y_0y_1 - 2a^{-1}y_0^2) + p^{3\nu_0}F_0(k) \tag{15}$$

$$y_{3k+1} = 2^{-1}y_0^{-1}(a + 2by_0 + 3b^2y_0(1 - ba^{-1}y_1)) + kb(y_0y_1 - 2^{-1}ay_0^{-1}) +$$
$$+ k^2b^2(y_0 + 2^{-1}ay_0^{-2} - (2^{-1})^2y_0^{-1} - 2^{-1}y_1^{-1}) + p^{3\nu_0}F_1(k). \tag{16}$$

In process of proof the Proposition 1 we obtain also the following corollaries.

Corollary 1. *For $k = 2, 3, \ldots$, we have*

$$y_{3k-1} = (a + kb + 8ab^2)y_0^{-1}y_1^{-1} + (-2akb + \frac{7}{2}ak^2b^2)y_0^{-1}y_1^{-2} +$$
$$+ (4ab + 3b^2 + k^2b^2)y_1^{-1} + 16ab^2y_0y_1^{-1} + \tag{17}$$
$$+ 48b^2y_0 - 6a^{-1}b + p^{3\nu_0}f_{-1}(y_0, y_1)$$

$$y_{3k} = kb + (2 - 3a^{-1}b^2)y_0 + (18a^{-2}b^2)y_0y_1 + (6a^{-1}b^2k - 2a^{-1}b^2k^2)y_0^2 -$$
$$- 12a^{-1}kb^2y_0y_1 + p^{3\nu_0}f_0(y_0, y_1) \tag{18}$$

$$y_{3k+1} = 2^{-1}ay_0^{-1} + (b + 2^{-1}k^2b + 3b^2) + (-3a^{-1}b^2 + kb)y_1 +$$
$$+ (-2^{-2}abk - 2^{-2}k^2b^2)y_0^{-2} + (-2^{-3}k^2b^2)y_0^{-3} - 2^{-2}y_0^{-1}y_1^{-1} + \tag{19}$$
$$+ p^{3\nu_0}f_1(y_0, y_1),$$

where f_{-1}, f_0, f_1 are homographic (rational) functions at y_0, y_1.

This Corollary at once follows from (11)-(13).

Corollary 2. *Let τ be a period length of the sequence $\{y_n\}$ generated by recursion (5); y_0, y_1 be initial values, and let $\nu_p(b) = \nu_0 > 0$. Then we have*

(A) $\tau = 3p^{m-\nu_0}$ *if only one congruence $4y_0^2 \equiv a \pmod p$*
$\qquad\qquad\qquad$ *or $y_1 \equiv 2 \pmod p$ violates;*
(B) $\tau = 3p^{m-\nu_0-\delta}$ *if $\min(\nu_p(4y_0^2 - a), \nu_p(y_1 - 2)) = \delta < m - \nu_0$;*
(C) $\tau \leq 3p^{m-\nu_0-\delta}$ *otherwise.*

Proof. Let $4y_0^2 \equiv a \pmod p$. Then, assuming $y_{3k} \equiv y_{3\ell+1} \pmod{p^m}$, we obtain $2y_0 \equiv 2^{-1}ay_0^{-1} \pmod p$. This gives a contradiction.

Similarly, from $y_{3k-1} \equiv y_{3\ell+1} \pmod{p^m}$ and $y_{3k} \equiv y_{3\ell+1} \pmod{p^m}$ we infer $y_0^{-1}y_1^{-1}a \equiv 2^{-1}ay_0^{-1} \pmod p$ and $2y_0 \equiv 2^{-1}ay_0^{-1} \pmod p$, i.e. $y_1 \equiv 2 \pmod p$ and $4y_0^2 \equiv a \pmod p$.

Let $n_1 \equiv n_2 \pmod 3$. Then from Corollary 1 we deduce that $y_{n_1} \equiv y_{n_2} \pmod{p^m}$ if and only if $n_1 \equiv n_2 \pmod{p^{m-\nu_0}}$. Hence, $\tau = 3p^{m-\nu_0}$. the second and third parts of Corollary 3 are also clear. $\qquad\square$

4 Exponential sums over the sequence of PRN's

In this section we prove the theorems 1-3 on the estimates of exponential sums on the sequence of pseudorandom numbers $\{y_n\}$ which are generated by recursion (5).

Let

$$\sigma_{k,\ell}(h_1, h_2; p^m) := \sum_{y_0 \in \mathbb{Z}_{p^m}^*} e\left(\frac{h_1 y_k + h_2 y_\ell}{p^m}\right), \ (h_1, h_2 \in \mathbb{Z}).$$

Here we consider y_k, y_ℓ as a functions of initial values y_0, y_1 generated by (5).

Theorem 1. *Let $(h_1, h_2, p) = 1$, $\nu_p(h_1 + h_2) = \mu_1$, $\nu_p(h_1k + h_2\ell) = \mu_2$, $k, \ell \in \mathbb{Z}_{\geq 0}$ and let $\{y_n\}$ produced by (5). The following estimates*

$$|\sigma_{k,\ell}(h_1, h_2; p^m)| \leq \begin{cases} 0 & if \ k \not\equiv \ell \pmod 3, \ \nu_p(h_2) > 0, \\ 4p^{m+\nu_0} & if \ \nu_p(h_2) = 0, \ k \not\equiv \ell \pmod 3, \\ 0 & if \ \mu_1 = 0, \ k \equiv \ell \pmod 3, \\ 4p^{m+\nu_0} & if \ \min(\mu_1, \mu_2) \geq \nu_0, \ k \equiv \ell \pmod 3. \end{cases}$$

hold.

Proof. Without restricting the generality it may be assumed that $(h_1, h_2, p) = 1$, $(h_1, p) = 1$. We considerate two cases:

(I) Let k and ℓ be nonnegative integers with $k \not\equiv \ell \pmod 3$, i.e. $k = 3k_1 \pm 1$, $\ell = 3\ell_1$ or $k = 3k_1 - 1$, $\ell = 3\ell_1 + 1$.
For $k = 3k_1$, $\ell = 3\ell_1 + 1$, by Corollary 1 we have

$$h_1 y_{3k_1} + h_2 y_{3\ell_1+1} = A_0 + A_1 y_0 + A_2 y_0^{-1} + bg_1(y_0^{-1}) + bB_1 y_1^{-1} + B_2 y_1^{-1} + bg_2(y_1^{-1}),$$

where modulo p^{ν_0}

$$A_1 = 2h_1, \ A_2 = 2^{-1}h_2, \ B_1 = h_2k, \ B_2 = -2^{-2}y_0^{-1}.$$

Thus, by Lemma 3, we easily infer

$$|\sigma_{3k_1-1,3\ell}(h_1, h_2)| \leq \begin{cases} 0 & if \ \nu_p(h_2) > 0, \\ 4p^{m+1} & if \ \nu_p(h_2) = 0. \end{cases}$$

Such result gives the case $k = 3k_1$, $\ell = 3\ell_1 + 1$ or $k = 3k_1 - 1$, $\ell = 3\ell_1 + 1$.

(II) Let $k \equiv \ell \pmod 3$. For definiteness we will consider only the case $k \equiv \ell \equiv 0 \pmod 3$. Then we have from Corollary 1

$$\begin{aligned} h_1 y_{3k} + h_2 y_{3\ell} =\ & (h_1 k + h_2 \ell)b + (h_1 + h_2)(2 - 3a^{-1}b^2)y_0 + \\ & + (h_1 + h_2)18a^{-2}b^2 y_0 y_1 + 6a^{-1}b^2(h_1 k + h_2 \ell) - \\ & - 2a^{-1}b^2(h_1 k^2 + e_2\ell^2)y_0^2 - 12a^{-1}b^2(h_1 k + h_2 \ell)y_0 y_1 + \\ & + p^{3\nu_0} \sum_{j=0}^{m_0} a_j(h_1 k^j + h_2 \ell^j)f_j(y_0, y_1). \end{aligned}$$

Again, by Lemmas 2 and 3, we obtain

$$|\sigma_{3k,3\ell}(h_1, h_2)| \leq \begin{cases} 0 & if \ \mu_1 = 0, \ k \equiv \ell \pmod 3, \\ 4p^{m+1} & if \ \min(\mu_1, \mu_2) \geq \nu_0, \ k \equiv \ell \pmod 3. \end{cases}$$

In the cases (I) and (II) we take into account that $I(p^m)$ (see, the notation in Lemma 3) are zero or 2. $\qquad \square$

Let the least length of period for $\{y_n\}$ is equal to τ.

Theorem 2. *Let the linear-inversive congruential sequence generated by the recursion (5) has the period τ, and let $\nu_p(b) = \nu_0$ and $4y_0^2 \not\equiv a \pmod p$ or $y_1 \not\equiv 2 \pmod p$. Then the following bounds*

$$|S_\tau(h, y_0)| \leq \begin{cases} O(m) & if & \delta > \nu_0, \ n_p(h) < m - 2\nu_0 - \delta, \\ 4p^{\frac{m+\nu_p(h)}{2}} & if & \delta \geq \nu_0, \ \nu_p(h) < m - 2\nu_0, \\ \tau & otherwise. \end{cases}$$

hold,
with the constant implied by the O-symbol is absolute.

Proof. Let we have the sequence produced by recursion (5). Without lose the generality, we cas assume that the sequence $\{y_n\}$ has a period $\tau = 3p^{m-\nu_0}$. By Corollary 2 we have

$$\begin{aligned} |S_\tau(h, y_0, y_1)| = \left| \sum_{n=0}^{\tau-1} e_m(hy_n) \right| = \left| \sum_{n=0}^{3p^{m-\nu}-1} e_m(hy_n) \right| \leq \\ \leq \left| \sum_{k=1}^{p^{m_1}} e_m(hy_{3k-1}) \right| = \left| \sum_{k=1}^{p^{m_1}} e_m(hy_{3k+1}) \right| + O(m), \end{aligned} \qquad (20)$$

886

where $m_1 = m - \nu_0$, and

$$y_{3k-1} = F_{-1}(k) := A_0 + A_1 k + A_2 k^2 + \cdots$$
$$y_{3k} = F_0(k) := B_0 + B_1 k + B_2 k^2 + \cdots$$
$$y_{3k+1} = F_1(k) := C_0 + C_1 k + C_2 k^2 + \cdots$$

with A_i, B_i, C_i defined by Proposition 1.

The summand $O(m)$ in (20) appears in virtue of the fact that the representation y_n as a polynomial on k holds only $k \geq 2m_0 + 1$.

Thus, by Lemma 3 we easily obtain

$$|S_\tau()| \leq \begin{cases} O(m) & \text{if } \delta < \nu_0, \ \nu_p(h) < m - \nu_0 - \delta, \\ 4p^{\frac{m+\nu_p(h)}{2}} & \text{if } \delta \geq \nu_0, \ \nu_p(h) < m - 2\nu_0, \\ \tau & \text{otherwise.} \end{cases}$$

with the constant implied by the O-symbol is absolute. $\qquad\square$

Theorem 3. *Let the sequence $\{y_n\}$ be produced by (5) with parameters a, b, y_0, y_1, $(a,p) = (y_0 y_1, p) = 1$, $\nu_p(b) = p^{\nu_0}$, $\nu_0 \geq 1$. Then for every $h \in \mathbb{Z}$, $(h, p^m) = \mu \leq m$, we have*

$$\overline{S}_N(h) = \frac{1}{(\varphi(p^m))^2} \sum_{y_0, y_1 \in \mathbb{Z}_{p^m}^*} |S_N(h, y_0, y_1)| \leq 12 N^{\frac{1}{2}} + 12 N p^{-\frac{m-\nu_0}{2}}.$$

Proof. Let $\nu_p(h) = 0$, i.e. $(h, p) = 1$. By the Cauchy-Schwarz inequality we get

$$\left|\overline{S}_N(h)\right|^2 = \frac{1}{(\varphi(p^m))^2} \left| \sum_{y_0, y_1 \in \mathbb{Z}_{p^m}^*} \sum_{n=0}^{N-1} e_m(h y_n) \right|^2 =$$

$$= \frac{1}{(\varphi(p^m))^2} \sum_{y_0, y_1 \in \mathbb{Z}_{p^m}^*} \sum_{k,\ell=0}^{N-1} e_m(h(y_k - y_\ell)) \leq$$

$$\leq \frac{1}{(\varphi(p^m))^2} \sum_{k,\ell=0}^{N-1} |\sigma_{k,\ell}(h, -h)| = \frac{1}{(\varphi(p^m))^2} \sum_{r=0}^{\infty} \sum_{\substack{k,\ell=0 \\ \nu_p(k-\ell)=r}}^{N-1} |\sigma_{k,\ell}(h, -h)| =$$

$$= \frac{1}{(\varphi(p^m))^2} \sum_{t=0}^{m-1} \sum_{\substack{k,\ell=0 \\ \nu_p(k-\ell)=t}}^{N-1} |\sigma_{k,\ell}(h, -h)| + \frac{1}{(\varphi(p^m))^2} \sum_{k=0}^{N-1} |\sigma_{k,k}(h, -h)| =$$

$$= N + \frac{1}{(\varphi(p^m))^2} \sum_{t=0}^{m-1} \sum_{\substack{k,\ell=0 \\ \nu_p(k-\ell)=t}}^{N-1} |\sigma_{k,\ell}(h, -h)|.$$

Using Theorem 1, we obtain

$$\left|\overline{S}_N(h)\right|^2 \leq N + \frac{1}{(\varphi(p^m))^2} \times$$

$$\times \sum_{r=0}^{m-1} \left(\sum_{\substack{k,\ell=0 \\ k\not\equiv\ell \pmod 3 \\ \nu_p(k-\ell)=r}}^{N-1} |\sigma_{k,\ell}(h,-h)| + \sum_{\substack{k,\ell=0 \\ k\equiv\ell \pmod 3 \\ \nu_p(k-\ell)=r}}^{N-1} |\sigma_{k,k}(h,-h)| \right) \le$$

$$\le N + \frac{1}{(\varphi(p^m))^2} \times$$

$$\times \left[4p^m \sum_{r=0}^{m-1} \frac{N^2}{p^r} + \left(\sum_{r<m-\nu_0} + \sum_{m-\nu_0 \le r \le m-1} \right) \sum_{\substack{k,\ell=0 \\ k\equiv\ell \pmod 3}}^{N-1} |\sigma_{k,\ell}(h,-h)| \right] \le$$

$$\le N + \frac{N}{(\varphi(p^{(m)}))^2} \times$$

$$\times \left(4Np^m + \sum_{r<m-\nu_0} \frac{N}{p^r} p^{m+\nu_0+r} + p^m \sum_{r\ge m-\nu_0} \frac{N}{p^r} \right) \le$$

$$\le N + N^2 p^{-m} \cdot 11 p^{\nu_0}(m-\nu_0).$$

Hence, for $(h,p)=1$ we obtain

$$\left| \overline{S}_N(h) \right| \le N^{\frac{1}{2}} + 12Np^{-\frac{m-\nu_0}{2}}.$$

$\square$

Theorems 1-3 and Lemmas 4-5 permit to obtain the following bound for discrepancy pf the sequence of point $\{\frac{y_n}{p^m}\} \in [0,1)$ and points $X_n^{(s)} \in [0,1)^s$, $X_n^{(s)} = \left(\frac{y_n}{p^m}, \frac{y_{n+1}}{p^m}, \ldots, \frac{y_{n+s-1}}{p^m} \right)$, where $\{y_n\}$ is generated by the recursion (5).

Theorem 4. *Let* $p > 2$ *be a prime number,* $y_0, y_1, a, b, m \in \mathbb{N}$, $m \ge 3$, $(ay_0y_1, p) = 1$, $\nu_p(b) = \nu_0 \ge 1$. *Then for the sequence* $\{x_n\}$, $x_n = \frac{y_n}{p^m}$, $n = 0, 1, \ldots$, *with the period* τ, *generated by recursion (5), we have for any* $1 \le N \le \tau$,

$$D_N(x_0, x_1, \ldots, x_{N-1}) \le \frac{1}{p^m} + 3N^{-1}p^{\frac{m-\nu_0}{2}} \left(\frac{1}{p} \left(\frac{2}{\pi} \log p^m + \frac{7}{5} \right)^2 + 1 \right).$$

Theorem 5. *Let the sequence* $\{X_n^{(s)}\}$ *with the period* $\tau = 3p^{m-\nu_0}$ *be produced by recursion (5). Then its discrepancy*

$$D_N^{(s)}(X_0^{(s)}, \ldots, X_{\tau-s}^{(s)}) \le 2p^{-\frac{m}{2}+\nu_0} \left(\frac{1}{\pi} \log p^{m-\nu_0} + \frac{3}{5} \right)^s + 2p^{-m+\nu_0}$$

for every $s = 1, 2, 3, 4$.

The assertions of Theorems 4 and 5 are the simple conclusions of Theorems 2 and 3 and Lemmas 4 and 5.

From Theorems 4 and 5 we conclude that the sequence of PRN's $\{y_n\}$ produced by generater (5) passes the s-dimensional serial test on the equidistribution and statistical independency.

References

1. W.-S. Chou. The period lengths of inversive congruential recursions. *Acta Arith*, 73(4), 325-341, 1995.
2. J. Eichenauer and J. Lehn. A non-linear congruential pseudorandom number generator. *Statist. Hefte*, 27, 315-326, 1986.
3. J. Eichenauer, J. Lehn and A. Topuzoğlu. A nonlinear congruential pseudorandom number generator with power of two modulus. *Math. Comp.*, 51,757-759, 1988.
4. J. Eichenauer-Herrmann and A. Topuzoğlu. On the period of congruential pseudorandom number sequences generated by inversions. *J. Comput. Appl. Math.*, 31, 87-96, 1990.
5. J. Eichenauer-Herrmann, H. Grothe. A New Inversive Congruential Pseudorandom Number Generator with Power of Two Modulus. *ACM Transactions of Modelling and Computer Simulation*, 2(1), 1-11, 1992.
6. T. Kato T., L.-M. Wu, N. Yanagihara. The serial test for a nonlinear PRN's generator. *Math. Comp.*, 63(214), 761-769, 1996.
7. T. Kato, L.-M. Wu, N. Yanagihara. On a nonlinear congruential pseudorandom number generator. *Math. of Comp.*, 65(213), 227-233, 1996.
8. H. Niederreiter. Some new exponential sums with applications to pseudorandom numbers. *Topics in Number Theory (Debrecen, 1974), Colloq. Math. Soc. Janos. Bolyai, vol.13, North-Holland, Amsterdam*, 209-232, 1976.
9. H. Niederreiter. *Random Number Generation and Quasi-Monte Carlo Methods. SIAM*, Philadelphia, Pa., 1992.
10. H. Niederreiter, I. Shparlinski. Exponential sums and the distribution of inversive congruential pseudorandom numbers with prime-power modulus. *Acta Arith*, 90(1), 89-98, 2000.
11. H. Niederreiter, I. Shparlinski. On the Distribution of Inversive Congruential Pseudorandom Numbers in Parts of the Period. *Math. of Comput.*, 70, 1569-1574, 2000.
12. H. Niederreiter and I. Shparlinski. Recent advances in the theory of nonlinear pseudorandom number generators. *Proc. Conf. on Monte Carlo and Quasi-Monte Carlo Methods, 2000, Springer-Verlag, Berlin*, 86-102, 2002.
13. P. Varbanets, S. Varbanets. Exponential sums on the sequences of inversive congruential pseudorandom numbers with prime-power modulus. *Voronoï's Impact on modern science, Proceedings of the 4th International Conference on Analytic Number Theory and Spatial Tessellations, Book 4, Volume 1, Kyiv, Ukraine, September 22-28*, 112-130, 2008.
14. S. Varbanets. Generalizations of Inversive Congruential Generator. *Analytic and Probabilistic Methods in Number Theory, Proceedings of the Fifth International Conference in Honour of J. Kubilius, Palanga, Lithuania, 4-10 Septembre 2011*, 265-282, 2012.

Sunspot in Endogenous Growth Two-Sector Models

Beatrice Venturi, Alessandro Pirisinu*

July 30, 2015

Abstract

In this paper we consider a class of endogenous growth two-sector models.The system possesses stochastic characteristics which arise from indeterminate equilibrium and cycles (Hopf cycles, closed to the steady state) (see Chiappori and Guesnerie, 1991, Benhabib, Nishimura, and Shigoka, 2006, Slobodyan 2009). As applications of our analysis, we compare the dynamical behaviour of the following well-known models: the Lucas Model, the Modified Romer Model, the natural resource model (see Bella 2010). For each of them, we show the existence of indeterminacy and sunspot equilibria close to a Hopf cycle. We show that the stochastic approach suggests a way out to the poverty enviroment trap only for the natural disposal resource model.

Keywords: multiple steady states, sunspots, indeterminacy, Hopf Bifurcations,

JEL classification: C61, C62, E32

1 Introduction

The problem of the indeterminacy and sunspot equilibrium in economic financial models has been analysed by many authors in recent times: among them, Nishimura, Shigoka, Yano (2006), and Benhabib, Nishimura, Shigoka (2008), Slobodyan (2009).

Many papers reported the occurrence of the stochastic behaviour (sunspots) also in presence of individual optimization, self-fulfilling expectations and compensations of competitive markets. We remember that a phenomenon is called sunspot when the fundamental characteristics of an economy are deterministic but the economic agents believe nevertheless that equilibrium dynamics is affected by random factors apparently irrelevant to the fundamental characteristics (Nishimura, Shigoka, Yano 2006).

In this paper, we consider the mechanism that leads to the existence of sunspots close to the indeterminate equilibrium (the Hopf orbit) in a class of

---

*Corresponding Author. Department of Economics and Business, University of Cagliari, Italy. Email: venturi@unica.it

---

endogenous growth two-sector-models with externality. Nishimura, and Shigoka (2006) consider the reduced form of the Lucas and Romer models, as a continous deterministic three-dimensional non linear differential system, with one pre-determined variable (a combination of the state variables) and two non-predetermined variables (related with the control variables). They constructed a stationary sunspot equilibrium near the stable Hopf cycle that emerges from the unique equilibrium point adding a Wiener variable to the non-predetermined variables, in their formulation, the cycle represents a compact solution of the stochastic process associated with the deterministic model.

Benhabib, Nishimura, Shigoka (2008) prove the existence of a sunspot equilibrium that comes from a Hopf cycle or a homoclinic orbit in a continuous time model of economic growth with positive externalities and with variable capacity utilization; the model has one only predetermined variable (the state variable) and one non-predetermined variable (the control variable). In their model, the positive externality produces the existence of multiple equilibria. Through dynamical analysis they show that the equilibrium is globally indeterminate in the periodic orbit; moreover, there exists a sunspot equilibrium with a support located in the bounded region enclosed by either a homoclinic orbit or a periodic orbit, such that each sample path does not converge to any specific point and continues to fluctuate without decaying asymptotically. As in the previous model, the stochastic formulation comes from adding a white noise to the non-predetermined variable.

Slobodyan (1999) treated the indeterminacy in a deterministic continuous-time model with infinitely lived agents, one predetermined variable (the state variable) and one non-predetermined variable (the control variable); the model is characterized by increasing social returns to scale due to externality in the production function of which the agents are assumed to be unaware. There are two steady states: one has zero capital and zero consumption (the origin), while the other is characterized by positive levels of both capital and consumption. For some parameter values, both steady states are indeterminate, and the whole state space is separated into two regions of attraction of the steady states. The region of attraction in the origin can be regarded as a development trap. Also in this case, the indeterminacy allows for the existence of sunspot equilibria related with the non-predetermined variable. Slobodyan (2009) studied the possibility of "rescuing" an economy from a development trap through sunspot-driven self-fulfilling expectations.

In this work, we construct sunspot equilibria in a deterministic general class of endogenous growth two sector models with externalities in the line of Mulligan and Sala-i-Martin (1993), Venturi (2014) and we compare the dynamical situations arising from the different applications: the Lucas model, the Romer model and a resource disposable endogenous growth two-sector model (Bella 2010).

Following Mulligan and Sala-i-Martin (1993), we put the endogeneous growth two-sector model in the reduced form; it means that we consider a three dimensional deterministic continous non linear differential system, whose solution is called a Balanced Growth Path (BGP) if it entails a set of functions of time

solving the optimal control problem, that is all variables grow at a constant rate.

Starting from a three-dimensional standard reduced deterministic model that admits stable cycles (with one predetermined variable and two non-predetermined variables), the model can be reformulated adding a stochastic term to the non-predetermined variables (as a white noise) and transforming it into a stochastic model that leads to indeterminacy, multiple steady stades and bifurcations. If for a given endogenous growth model, there exists a continuum of equilibria in a small neighborhood of a BGP that continues to stay in this neighborhood, it is said that equilibrium is locally indeterminate. If there exists a continuum of equilibria outside a small neighborhood of a BGP, it is said that equilibrium is globally indeterminate (i.e. Hopf cycle or homoclinic orbit; see Mattana, Nishimura, Shigoka 2008).

Following Slobodyan 2009, in our formulation, the stochastic approch suggests a way out from the cycle trap only for disposable resource application (the model has multiple equilibrium points); in the other examples (Lucas, Romer) the model has one only equilibrium point and we have no way out when the initial conditions start inside the stable bounded cycle: this is the so-called poverty development trap.

The paper is organized as follows. The second Section analyze the general economic model.and introduces stochastic dynamics related with the existence of sunspots in the economic model. The third Section compares Lucas, Romer and the Resource model (Bella 2010). In the last we show the results and the economic implications of existence of sunspot equilibrium in a natural resource system with externalities.

2 The Economic General Model

We consider the deterministic economic general model (Mulligan, Sala-i-Martin 1993, Venturi 2014) that deals with the maximization of an objective function

$$\underset{c(t),\; u(t)}{Max} \int_0^\infty U(c)e^{-\rho t}dt \tag{2.1}$$

$subject\ to\quad :$

$$\dot{k} = A((r(t)^{\alpha_h}u(t)^{\alpha_u})(\nu(t)^{\alpha_\nu}k(t)^{\alpha_k})\hat{r}(t)^{\alpha_{\hat{r}}}k(t)^{\alpha_{\hat{k}}} - \tau_k k(t) - c(t)$$

$$\dot{r} = B((r(t)^{\beta_r}(1-u(t)^{\beta_u}))((1-\nu(t)^{\beta_\nu}k(t)^{\beta_k})\hat{r}(t)^{\beta_{\hat{r}}}k(t)^{\beta_{\hat{k}}} - \tau_r r(t)$$

$$k(0) = k_0$$

$$r(0) = r_0$$

where

$$U(c) = \frac{c^{1-\sigma}-1}{1-\sigma} \tag{2.2}$$

is a standard utility function, c is per-capita consumption, ρ is a positive discount factor and σ is the inverse of the intertemporal elasticity of substitution.

The constraints are two equations related with the growth process of the analyzed economic system .

Notation is as follows c is per-capita consumption, k is a physical capital and r could be the human capital (see the Lucas model 1998), the knowledge (the Romer model, 199) or a natural resource (see Bella, 2010). Individuals have a fixed endowment of time, normalized to unity at each point in time, which is allocated to physical and to the other capital sector (respectively: human, knowledge or natural resource), α_k and α_r being the private share of physical and the other capital sector in the output sector, β_k and β_r being the corresponding shares share in the second sector, u and v are the fraction of aggrega other sector and physical capital used in the final output sector at instant t (and conversely, $(1 - u)$ and $(1 - v)$ are the fractions used in the second sector), A and B are the level of the technology in each sector, τ is a discount factor, $\alpha_{\hat{k}}$ is a positive externality parameter in the production of physical capital, $\alpha_{\hat{r}}$ is a positive externality parameter in the production of the second sector

The equalities $\alpha_k + \alpha_r = 1$ and $\beta_k + \beta_r = 1$ ensure that there are constant returns to scale at the private level. At the social level, however, there may be increasing, constant or decreasing returns depending on the signs of the externality parameters.

All other parameters $\pi = (\alpha_k,\, \alpha_{\hat{k}}, \alpha_r,\, \alpha_{\hat{r}}, \beta_k, \beta_{\hat{k}}, \beta_r, \beta_{\hat{r}},\, \sigma, \gamma, \delta, \rho)$ live inside the following set $\Pi \subset (0,\, 1) \times (0,\, 1) \times (0,\, 1) \times (0,1) \times (0,1) \times (0,1) \times (0,1) \times (0,\, 1) \times \mathrm{R}_+^4$.

The representative agent's problem (1.1)-(1.2) is solved by
defining the current value Hamiltonian.

$$
\begin{aligned}
H \;=\; & \frac{c^{1-\sigma} - 1}{1 - \sigma} + \lambda_1 (A((r(t)^{\alpha_r} u(t)^{\alpha_u})(\nu(t)^{\alpha_\nu} k(t)^{\alpha_k})\hat{r}(t)^{\alpha_{\hat{r}}} k(t)^{\alpha_{\hat{k}}} - \tau_k k(t) - c(t)) + \\
& + \lambda_2 (B((r(t)^{\beta_r}(1 - u(t)^{\beta_u}))((1 - \nu(t)^{\beta_\nu} k(t)^{\beta_k})\hat{r}(t)^{\beta_{\hat{r}}} k(t)^{\beta_{\hat{k}}} - \tau_r r(t)) \qquad (2.3)
\end{aligned}
$$

where λ_1 and λ_2 are co-state variables which can be interpreted as shadow prices of the accumulation. The solution candidate comes from the first-order necessary conditions (for an interior solution) obtained by means of the Pontryagin Maximum Principle with the usual transversality condition

$$
\lim_{t \to \infty} \left[e^{-\rho t} (\lambda_1 k + \lambda_2 r) \right] = 0 \qquad (2.4)
$$

We consider only the competitive equilibrium solution (as well known, it follows from the presence of the externality that the competitive solution differs from the planner's solution[1]).

---

[1] The planner's solution involves a choice of $k, r, c, u,$ and r_a which maximizes the control optimal model (2.1) and to $r = r_a$ for all t.

In the other hand the path for r coincides with the given path r_a in the competive solution then the system is in equilibrium (see Lucas 1990, Mattana and Venturi, 1999).

The equilibrium solution taking r_a as exogenously determined.

After eliminating $v(t)$ the rest of the first order conditions and accumulation constraints entail four first order non linear differential equations in four variables: two controls (c and u) and two states (k and r). The solution of this autonomous system is called a Balanced Growth Path (BGP) if it entails a set of functions of time solving the optimal control problem (2.1)-(2.4) such that k, r and c grow at a constant rate and u is constant.

With a change of variable. in standard way, (since k, r and c grow at a constant rate and u is a constant in the BGP), we transforme a system of four first orderordinary differential equations in c, u, k and r into a system of three first order ordinary differential equations with two non-predetermined variables (the control variables) and one predetermined (a linear combination of the state variables)

Setting $A = B = 1$ and

$$x_1 = kr^{\frac{\alpha_{\hat{r}}}{(\alpha_{\hat{r}}-1)}} \quad ; \quad x_2 = u; \quad x_3 = \frac{c}{k} \tag{2.5}$$

we get:

$$\begin{aligned}\dot{x}_1 &= \phi_1(x_1, x_2, x_3)\\ \dot{x}_2 &= \phi_2(x_1, x_2, x_3)\\ \dot{x}_3 &= \phi_3(x_1, x_2, x_3)\end{aligned} \tag{2.6}$$

in vectorial form

$$(\dot{x}_1, \dot{x}_2, \dot{x}_3)^T = \phi_i(x_1, x_2, x_3) \tag{2.7}$$

where the $\phi_i \in R^3$, are countinuos and derivable complicated nonlinear functions,which depend of the parameters $(\alpha_k, \alpha_{\hat{k}}, \alpha_r, \alpha_{\hat{r}}, \beta_k, \beta_{\hat{k}}, \beta_r, \beta_{\hat{r}}, \sigma, \gamma, \delta, \rho)$ of the model, and $\phi_i : U x R^3 \longrightarrow R^3$ with $U \subset R$, an open subset, and $i = 1, 2, 3$.

3   The Emergence of a Hopf Orbit in the general Model.

As well known a stationary (equilibrium) point of system (2.6) is any solution of

$$\begin{aligned}\dot{x}_1 &= \phi_1(x_1, x_2, x_3) = 0\\ \dot{x}_2 &= \phi_2(x_1, x_2, x_3) = 0\\ \dot{x}_3 &= \phi_3(x_1, x_2, x_3) = 0\end{aligned} \tag{3.1}$$

Assuming the existence, at least of one solution, at some point $P^*(x_1^*, x_2^*, x_3^*)$ the local dynamical properties of (2.6) are described in terms of the Jacobian (see P. Mattana, and B. Venturi (1999), U. Neri and B. Venturi (2007) matrix of (2.6), $J(P)$,with $J(P^*) = J^*$ for brevity.

Lemma 1 *Let $\pi \in \overset{\wedge}{\Pi} \subseteq \Pi$ be. In $\overset{\wedge}{\Pi}$ where is at least one value $\sigma = \sigma_c$, (σ is the bifurcation parameter[2]) such that the Jacobian matrix J^* has a pair of purely imaginary roots and a real root different from zero.*

Proof. By Routh-Hurvitz's criterion we can state that J^* can have one (real) eigenvalue $\lambda_1 = r$ and two complex conjugate roots $\lambda_{2/3} = p \pm qi$ whose real parts can be either positive or negative. The real part of the two complex conjugate roots is a countinous function (a four order polinomial) $G(\sigma)$:

$$G(\sigma) = -B(J^*)Tr(J^*) + Det(J^*) \tag{3.2}$$

that change sign *in $\overset{\wedge}{\Pi}$* when the parameter σ is varied. ∎

In fact, since the real parts of the complex conjugate roots vary continuously with respect to σ, there must exist at least one value $\sigma = \sigma_c$ such that $G(\sigma) = 0$. When this occurs, by Vieta's theorem, J^* has a simple pair of purely imaginary eigenvalues.

The solutions of characteristic polinomial
$-\lambda^3 + Tr(J^*)\lambda^2 - B(J^*)\lambda + Det(J^*) = 0.$
for $\sigma = \sigma_c$ became:
$\lambda_1 = Tr(J^*)$ and $\lambda_{2/3} = \pm\sqrt[2]{B(J)}i$
cvd.

Lemma 2 *If $\pi \in \overset{\wedge}{\Pi}$ the derivative of the real part of the complex conjugate eigenvalues with respect to σ, evaluated at $\sigma = \sigma_c$, is always different from zero.*

Proof. We have only to verify that the following derivative $\frac{d}{d\sigma}G(\sigma) \neq 0$ is different from zero in $\overset{\wedge}{\Pi}$. ∎

Theorem 1 *The system (2.6) undergoes at hopf bifurcations in $\overset{\wedge}{\Pi}$ for $\sigma = \sigma_c$.*
Proof. *It follows directly from lemma 1 and lemma 2 that the assumptions of Hopf Bifurcations Theorem are satisfied.* ∎

As well known the study of the stability of the emerging orbits on the center manifold[3], can be performed by calculating the sign of a coefficient q depending on second and third order derivatives of the non-linear part of the system written in normal form.

If $q > 0$ $(q < 0)$ then the closed orbits Hopf-bifurcating from the steady state $P_c^*(x_1^*, x_2^*, x_3^*)$ are attracting (super-critical) (repelling (sub-critical)) on the center manifold.

---

[2] The dynamical characteristic of the Jacobian matrix evalueted in the the steady state point suggest which bifurcation parameter choosen.

[3] It is a manifold associated with the complex conjugate roots with real part zero

4 Stochastic Dynamic

We build a stochastic system that has sunspot equilibria as solutions, the costruction is very similar to that reported in T. Shigoka (1994) and J. Benhabib, K. Nishimura, and T. Shigoka (2006), J. Benhabib, K. Nishimura and Y. Mitra, (2008).

Our system (2.7) includes one predetermined variable x_1 and two non-predetermined variables x_2 and x_3, in vectorial form :

$$(\dot{x}_1, \dot{x}_2, \dot{x}_3)^T = \phi_i \ (x_1, x_2, x_3) \tag{4.1}$$

with $\phi_i : U x R^3 \longrightarrow R^3$, $U \subset R$, $i = 1, 2, 3$.

If the deterministic dynamic given by (2.7) satisfies the hypothesis of the theorem 1, in other words the parameters set of the model belongs to $\overset{\wedge}{\Pi}$, then (2.7) has a period solution Γ [4].

The equilibrium is globally indeterminate in the interior of the bounded region enclosed by Γ.

We remember that a probability space is a triple $(\Omega, \ B_{R^3}, \ P_{R^3})$ where: Ω denotes the space of events, B is the set of possible outcomes of a random process; B is a family of subsets of Ω that, from a mathematical point of view, represents a σ-algebra [5].

The σ-algebra can be interpreted as information (on the properties of the events) [6].

We add a "noise" (a Wiener process) in the equations related with the control variables of the optimal choice problem.

Let $s_t(\omega) = (\omega, t)$ be a random variable irrelevant to fundamental characteristic of the optimal economy, it means that doesn't affect preferences , technology and endowment (i.e. sunspot). We assume that a set of sunspot variable $\{s_t(\omega)\}_{t \geq 0}$ is generated by a two-state continuous-time Markov process with stationary transition probabilities and that $s_t : \Omega \longrightarrow \{1, 2\}$ for each $t \geq 0$. Let $[\{s_t(\omega)\}_{t \geq 0}, (\Omega, \ B_{R^3}, \ P_{R^3})]$ be a continuous time stochastic process [7], where $\omega \in \Omega$, B_Ω is a σ-field in Ω, and P_Ω is a probability measure. The probability space is a complete measure space and the stochastic process is separable.

Let $(R^3_{+++}, \ B_{R^3_{+++}}, \ P_{R^3_{+++}})$ be a probability space on the open subset R^3_{+++} of R^3 where $B_{R^3_{+++}}$ denotes the Borel σ-field in R^3_{++}. Let (Φ, B, P) be the product probability space of $(R^3_{+++}, \ B_{R^3_{+++}}, \ P_{R^3_{+++}})$ and $(\Omega, \ B_\Omega, \ P_\Omega)$, that is $(R^3_{+++} \times \Omega, \ B_{R^3_{+++}} \times B_\Omega, \ P_{R^3_{+++}} \times P_\Omega)$. Let $(\Phi, \ B^*, \ P^*)$ be the completion of

---

[4] The Hopf cycle is an invariant set inside a two dimensional manifold: the center manifold.

[5] A σ - algebra differs from an algebra, for the property that the union of infinite elements of the family must belong to the set.

[6] The smallest σ- algebra that can be built with subsets of real numbers is represented by open intervals that are called Borel sets and indicated with B. So, it can be concluded that a probability space is a triple $(\Omega, \ F, \ Pr)$ where Ω denotes the space of events and F a family of subsets of Ω.

[7] A stochastic process is a family of random variables

(Φ, B, P). Let (x_0^1, x_0^2, x_0^3) be the value of our model at the time $t = 0$. We denote a point $(x_0^1, x_0^2, x_0^3, \omega)$ in Φ as φ: in other words, $\varphi = (x_0^1, x_0^2, x_0^3, \omega)$. Let $B_t = B(x_0^1, x_0^2, x_0^3, s_s, s \leq t)$ the smallest σ-field of φ respect to which (x_0^1, x_0^2, x_0^3) $s_s, s \leq t$ are measurable.

Let $B_t^* = B^*(x_0^1, x_0^2, x_0^3, s_s, s \leq t)$ be the σ-field of φ sets which are either B_t sets or which differ from B_t sets by sets of probability zero.

Let E_t the conditional expectation operator relative to B_t^*.

The following equation is a first order condition of some intertemporal optimization problem with market equilibrium conditions incorporated:

$$(\dot{x}_1, E_t(d\dot{x}_2/dt), E_t(d\dot{x}_3/dt) = \phi_i(x_1(\varphi), x_2(\varphi), x_3(\varphi)) \qquad (4.2)$$

where $(x_0^1(\varphi), x_0^2(\varphi), x_0^3(\varphi)) = (x_0^1, x_0^2, x_0^3)$ and $\frac{dx_{1t}}{dt}, \frac{dx_{2t}}{dt}, \frac{dx_{3t}}{dt}$ are defined as:

$$\frac{dx_t^i}{dt} = \lim_{h \to 0^+} \frac{(x_{t+h}^i - x_t^i)}{h} (i = 1, 2, 3)$$

if the limit exists.

Definition 2 *Suppose that $\{(x_{1t}(\varphi), x_{2t}(\varphi), x_{3t}(\varphi))\}_{t \geq 0}$ is a solution of the stochastic differential equation (4.2) with $(x_{1t}(\varphi), x_{2t}(\varphi), x_{3t}(\varphi)) \in R_{+++}^3$. If for any pair $(t > s \geq 0)$, $(x_{1t}(\varphi), x_{2t}(\varphi), x_{3t}(\varphi))$ is B_t^*-measurable but non B_s^*-measurable it constitutes a sunspot equilibrium.*

Theorem 3 *If the deterministic system (4.1) has a Hopf solution or a homoclinic orbit (a cycle), then a sunspot equilibrium (SE) is a solution of the stochastic process $\{(x_0^1(\varphi), x_0^2(\varphi), x_0^3(\varphi))\}_{t \geq 0}$ with a compact support.*
Proof. *It follows directly from the definition of sunspot and the construction of the stochastic system.* ∎

4.1 The Lucas Model

As an application of the general model we indicated above, we consider now the Lucas model. In the original optimal control model, the state variables are: k, the physical capital and $r = h$, the human capital; the control variables are: u, the non-leisure time and c, the consumption.

The deterministic reduced form of this model is given by:

$$
\begin{aligned}
\dot{x}_1 &= A x_1^\beta x_2^{1-\beta} + \frac{\delta(1-\beta+\gamma)}{\beta}(1-x_2)x_1 - x_3 x_1 \qquad (4.3) \\
\dot{x}_2 &= \frac{\delta(\beta-\gamma)}{\beta}x_2^2 + \frac{\delta(1-\beta+\gamma)}{\beta}x_2 - x_3 x_2 \\
\dot{x}_3 &= -\frac{\rho}{\sigma}x_3 + A\frac{\beta-\sigma}{\sigma}x_1^{\beta-1}x_2^{1-\beta}x_3 + x_3^2
\end{aligned}
$$

where: $x_1 = h^{\left(\frac{1-\beta+\gamma}{\beta-1}\right)}k$; $x_2 = u$; $x_3 = \frac{c}{k}$; $\gamma = \alpha_{\wedge}$. x_1 is a pre-determined variable (it is a combination of the state variables), while x_3 and x_2 are the non pre-determined variables.

The three dimensional deterministic system (4.3) undergoes a stable Hopf bifurcation in a parameter set (see Mattana Venturi 1999; Nishimura Shigoka Yano 2006). In line with Nishimura Shigoka Yano, we can re-write the model in the form of a stochastic system and we can apply the theorem 3. Then the system has a compact sunspot equilibrium as a solution of the stochastic process.

The model has one only equilibrium point and there is no way out when the initial conditions start inside the stable bounded cycle or very close to the boundary.

4.2 The Modified Romer Model

We consider now the modified Romer model. In the original optimal control model, the state variables are: k, the physical capital and $r = A$,where A is the level of knowledge currently available, the human capital (Romer 1990, Slobodyan 2007); the control variables are: H_Y, is the human capital, the skilled labour employed in the final sector; c, the consumption.

The deterministic reduced form of this model is given by:

$$\dot{x}_1 = x_1^\gamma x_2^\alpha - \frac{\zeta-\gamma}{1-\gamma}\delta(1-x_2)x_1 - x_3 x_1 \qquad (4.3)$$

$$\dot{x}_2 = \frac{\gamma(\zeta-\gamma)}{\zeta(1-\alpha)}x_1^{\gamma-1}x_2^{\alpha+1} + \frac{\delta(\zeta-\gamma-1)}{1-\alpha}x_2 - \frac{\delta}{1-\alpha}(1-\zeta+\gamma+\frac{\gamma}{\zeta\alpha}(\zeta-\gamma))x_2^2 - \frac{\gamma}{1-\alpha}x_2 x_3$$

$$\dot{x}_3 = x_3^2 + (\frac{\gamma^2}{\sigma\zeta}-1)x_1^{\gamma-1}x_2^\alpha x_3 - \frac{\rho}{\sigma}x_3$$

where:$x_1 = A^{\left(\frac{\alpha+\beta+\gamma}{\alpha+\beta}\right)}k$; $x_2 = H_Y$; $x_3 = \frac{c}{k}$; $\gamma = \alpha_\wedge\atop h$.

x_1 is a pre-determined variable (it is a combination of the state variables), while x_3 and x_2 are the non pre-determined variables; the parameters $\alpha+\beta+\gamma = 1$. and $\zeta \geq 1$ is a parameter that captures the degree of complementarity between the inputs (the case $\zeta = 1$ corresponds to non complementarity).

The three dimensional deterministic system (4.3) undergoes a stable Hopf bifurcation in a parameter set (see Mattana Venturi 1999; Nishimura Shigoka Yano 2006). In line with Nishimura Shigoka Yano, we can re-write the model in the form of a stochastic system and we can apply the theorem 3. Then the system has a compact sunspot equilibrium as a solution of the stochastic process.

The model has one only equilibrium point and there is no way out when the initial conditions start inside the stable bounded cycle or very close to the boundary.

4.3 The Natural Resource System

Our natural disposal resource system (5.3) includes two non-predetermined variables $x_1$and x_2 and one, predetermined variable x_3.:

$$\dot{x}_1 = (-\frac{\rho}{\sigma})x_1 + (\frac{\beta-\sigma}{\sigma})x_1 - x_1^2$$
$$\dot{x}_2 = (\frac{\gamma\delta}{\beta})(1 - x_2)x_2 + x_1 x_2 \qquad (4.4)$$
$$\dot{x}_3 = (\frac{\gamma\delta}{\beta})((1 - x_2)x_3 + (\beta - 1)x_3^2$$

where $x_1 = \frac{c}{k}; x_2 = nr; x_3 = \frac{y}{k}$.

We can build a stochastic process considering the following equation:

$$(E_t(d\dot{x}_1/dt), E_t(d\dot{x}_2/dt), \dot{x}_3) = \phi_i(x_1(\varphi), x_2(\varphi), x_3(\varphi)) \qquad (4.5)$$

where $(x_0^1(\varphi), x_0^2(\varphi), x_0^3(\varphi)) = (x_0^1, x_0^2, x_0^3)$ and $\frac{dx_{1t}}{dt}, \frac{dx_{2t}}{dt}, \frac{dx_{3t}}{dt}$ are defined as $\frac{dx_t^i}{dt} = \lim\limits_{h \to 0^+} \frac{(x_{t+h}^i - x_t^i)}{h}$ ($i = 1, 2, 3$) if the limit exists. It can be demonstrated that the theorem 3 applies also to this model

The deterministic equilibrium dynamic (5.3) has a family of periodic orbits Γ_{σ_c} emerging from one steady state , with Γ_{σ_c} in the center manifold (a two-dimensional invariant manifold in R_{+++}^3). For some set of parameters in the model (see Bella 2010), there exists a sunspot equilibrium whose support is located in the bounded region enclosed by the periodic orbit Γ_{σ_c} . Each sample path of the sunspot equilibrium does not converge to any specific point and continues to fluctuate without decaying asymptotically.

For some parameter value, due to pessimistic self-fulfilling expectations, sunspot equilibria exist in some neighbourhood of a steady-state. If the periodic orbit emerging from a steady state is super-critical , there is no way out (Slobodyan, 2007). If the periodic solution is repelling, then there is a possibility of a way out of the orbit (in fact the growth rate of economy μ becames positive for low level of the externality γ) and the optimal path can reach another steady state. Such situation can be understood as a poverty or development trap.

5   Conclusions

In the applicative examples here proposed, we analyzed different aspects.

In Lucas model, there are two main causes of endogeneous growth: the first is the accumulation of human capital: in other words, this endogeneous growth is due to the fact that the factors determining human capital accumulation remain unchanged; the second is the presence of the externality: it is not necessary to have endogenous growth but it works as an incentive to accumulate human capital and not to let it decrease as time passes by .

In his models, Romer (1986) describes capital that has decreasing returns to scale on the microeconomic level but increasing returns on the macroeconomic level, due to spillovers; so it predicts positive sustained per capita growth. On the other hand, Romer (1990) puts knowledge (and the technological change that is its fruit) at the heart of economic growth: it provides the incentive for capital accumulation and accounts for much of the increase in output per hour worked. In this line, authors like Sala-i-Martin (1997) have shown that the investment share is a robust variable in explaining economic growth.

In the model of natural resource, the endogeneous growth and the chance to escape the development trap are strictly bounded to the expectations: positive or negative outlook can crucially determinate the growth of the economic system.

This positive and statistically significant effect of investment on the growth rate of countries suggests that investment not only affects the stock of physical capital but also increases intangible capital (for example, knowledge) in a way such that the social return to investment is larger than the private return.

For real-world economies, it's important to underline that, in case of endogenous growth, the balanced growth rate crucially depends on the marginal product of physical capital, which varies positively with the stock of knowledge capital. Thus, when the level of knowledge capital plays its important role, economies with a large stock of knowledge may compensate for a large stock of physical capital. Consequently, the growth rate will be higher in those countries in which the stock of knowledge capital is relatively large: this fact can explain high growth rates of Germany and Japan after World War II, for example.

More generally, economies may be both globally and locally indeterminate. Global indeterminacy refers to the balanced growth rate that is obtained in the long run and states that the initial value of consumption crucially determines to which BGP the economy converges and, thus, the long-run balanced growth rate.

Moreover, local indeterminacy around the BGP with the lower growth rate, can be observed if the parameter constellation is such that the trace of the Jacobian matrix is smaller than zero, so that both eigenvalues have negative real parts. If in that situation a certain parameter is varied, two purely imaginary eigenvalues may be observed that generate a Hopf bifurcation, which leads to stable limit cycles.

Some other authors have studies both development and poverty traps: it is indicated that poverty traps and indeterminacy in macroeconomic models may be caused by the same set of reasons, like externalities or increasing returns to scale. Among many, Slobodyan (1999) tried to understand, in this framework, how important sunspot-driven fluctuations could be for the economy's escape from the poverty trap: for a chosen level of the noise intensity (approximately 14% SD of the log consumption), the probability of escaping the trap is not negligible, only when the initial condition is very close to the trap boundary. The set of those initial conditions is not very large and is restricted to initial level of consumption, within 85% of the level necessary to put the system right on the boundary between the poverty trap and the region of attraction of the positive steady state.

The probability of escape, as expected, increases as expectations become more optimistic: for very optimistic expectations (i.e., initial consumption very close to the boundary) absolute majority of escapes happens very fast. So the economy that starts with a very low initial capital and very pessimistic expectations of future interest rates and wages gets trapped. It will probably continue the downward spiral (the change from "pessimistic" level of consumption to the "optimistic" one may constitute hundreds and thousands percent of the

901

"pessimistic" level). The escape happens if it chosen a random variable with bounded support, as the sunspot variable. The sunspot variable has a natural interpretation of a change in perceived present discounted wealth.

References

[1] C. Azariadis (1981), "Self-fulfilling prophecies," Journal of Economic Theory 25, 380-396.

[2] G. Bella (2010), Periodic solutions in the dynamics of an optimal resource extraction model Environmental Economics, Volume 1, Issue 1, 49-58.

[3] J. Benhabib, K. Nishimura, T. Shigoka, (2008), "Bifurcation and sunspots in the continuous time equilibrium model with capacity utilization. International Journal of Economic Theory", 4(2), 337–355.

[4] J. Benhabib, and R. Perli (1994), "Uniqueness and indeterminacy: On the dynamics of endogenous growth," Journal of Economic Theory 63, 113-142.

[5] J. Benhabib, and A. Rustichini (1994), "Introduction to the symposium on growth, fluctuations, and sunspots: confronting the data," Journal of Economic Theory 63, 1-18.

[6] D. Cass, and K. Shell (1983), "Do sunspots matter?" Journal of Political Economy 91.

[7] P. A. Chiappori, and R. Guesnerie (1991), "Sunspot equilibria in sequential market models,"in: W. Hildenbrand, and H. Sonnenschein, Eds., Handbook of mathematical economics, Vol.4, North-Holland, Amsterdam, 1683-1762.

[8] J. L. Doob (1953), Stochastic processes, John Wiley, New York.

[9] J. P. Drugeon, and B. Wigniolle (1996), "Continuous-time sunspot equilibria and dynamics in a model of growth," Journal of Economic Theory 69, 24-52.

[10] R. E. A. Farmer, and M. Woodford (1997), "Self-fulfilling prophecies and the busyness cycle," Macroeconomic Dynamics 1, 740-769.

[11] J. M. Grandmont (1986), "Stabilizing competitive business cycles," Journal of Economic Theory 40, 57-76.

[12] J. Guckenheimer, and P. Holmes (1983), Nonlinear oscillations, dynamical systems, and bifurcations of vector fields, Springer-Verlag, New York.

[13] R. Guesnerie, and M. Woodford (1992), "Endogenous fluctuations," in: J. J. Laffont, Ed., Advances in economic theory, sixth world congress, Vol. 2, Cambridge University Press, New York, 289-412.

[14] R. E. Lucas (1988), "On the mechanics of economic development," Journal of Monetary Economics" 22, 3-42.

[15] P. Mattana (2004), The Uzawa-Lucas endogenous growth model, Ashgate Publishing Limited Gower House, Aldershot, England.

[16] P. Mattana, and B. Venturi (1999), "Existence and stability of periodic solutions in the dynamics of endogenous growth," International Review of Economics and Business 46, 259-284.

[17] K. Nishimura,, T. Shigoka, M. Yano, (2006), "Sunspots and Hopf bifurcations in continuous time endogenous growth models", *International Journal of Economic Theory*, *2*, 199–216.

[18] J. Peck (1988), "On the existence of sunspot equilibria in an overlapping generations model,"Journal of Economic Theory 44, 19-42.

[19] P. Romer (1990), "Endogenous technological change," Journal of Political Economy 98, S71-S102.

[20] K. Shell (1977), "Monnaie et Allocation Intertemporelle," mimeo. Seminarie d'Econometrie Roy-Malinvaud, Paris.

[21] T. Shigoka (1994), "A note on Woodford's conjecture: constructing stationary sunspot equilibria in a continuous time model," Journal of Economic Theory 64, 531-540.

[22] S. Slobodyan (2009), "Indeterminacy and Stability in a modified Romer Model: a General Case," Journal of Economic Theory 64, 531-540

[23] S. Slobodyan (2005), "Indeterminacy, Sunspots, and Development Traps." Journal of Economic Dynamics and Control, 29, pp. 159-185.

[24] S. E. Spear (1991), "Growth, externalities, and sunspots," Journal of Economic Theory 54, 215-223.

[25] B.Venturi (2014)"Chaotic Solutions in non Linear Economic - Financial models" Chaotic Modeling and Simulation (CMSIM) 3, 233-254.

6 Appendix

The application 3 (natural resource model)

1. The reduction form

$$x = \frac{c}{k}, q = nr, m = \frac{y}{k}$$

$\frac{\dot{k}}{k} = Ak^{\beta-1}(nr)^{1-\beta} r_a^{\gamma} - c$

$\frac{\dot{r}}{r} = \delta(1-n)$

$\frac{\dot{Y'}}{y} = \delta(1-n)$

$\frac{n'}{n} =$

$y = Ak^{\beta}(nr)^{1-\beta} r_a^{\gamma}$

$\frac{d}{dt}\log y = \frac{d}{dt}(\log Ak^{\beta}(nr)^{1-\beta} r_a^{\gamma}) =$

$= A\beta \frac{k^{\beta-1}(t)}{k^{\beta}(t)} k'(t) + (1-\beta)\frac{n^{1-\beta-1}(t)}{n^{1-\beta}} n'(t) + (1-\beta)\frac{r^{1-\beta-1}(t)}{r^{1-\beta}} r'(t) + \gamma \frac{r_a^{\gamma-1}(t)}{r_a^{\gamma}} r_a'(t) =$

$= A\beta \frac{k'(t)}{k(t)} + (1-\beta)\frac{n'(t)}{n(t)} + (1-\beta)\frac{r'(t)}{r(t)} + \gamma \frac{r_a'(t)}{r_a(t)}$

$\log m = \log \frac{y}{k} = \log y - \log k$

$\frac{d}{dt}(\log m) = \frac{d}{dt}(\log y - \log k) = \frac{y'(t)}{y(t)} - \frac{k'(t)}{k(t)}$

$\frac{d}{dt}\left(\frac{c(t)}{k(t)}\right) = \frac{c'(t)k(t)-c(t)k'(t)}{k(t)^2} = \frac{c'(t)k(t)-c(t)k'(t)}{k(t)} = \frac{c'(t)}{k(t)} - \frac{c(t)}{k(t)}\frac{k'(t)}{k(t)}$

$\frac{d}{dt}(nr) = n'(t)r(t) + n(t)r'(t) =$

$$\frac{d}{dt}\left(\frac{c(t)}{k(t)}\right) \quad = \quad \frac{c'(t)k(t)-c(t)k'(t)}{k(t)^2} = \frac{c'(t)k(t)-c(t)k'(t)}{k(t)^2} \tag{A.1}$$

$$= \quad \frac{c'(t)}{k(t)} - \frac{c(t)}{k(t)}\frac{k'(t)}{k(t)} = \frac{c(t)}{k(t)}\left[\frac{c'(t)}{c(t)} - \frac{k'(t)}{k(t)}\right] \tag{1}$$

$$\frac{d}{dt}\left(\frac{y(t)}{k(t)}\right) = \frac{y'(t)k(t)-y(t)k'(t)}{k(t)^2} = \frac{y'(t)k(t)-y(t)k'(t)}{k(t)} = \frac{y'(t)}{k(t)} - \frac{y(t)}{k(t)}\frac{k'(t)}{k(t)} \tag{A.2}$$

$G(\sigma) = -B(J^*)Tr(J^*) + Det(J^*)$

$\rho = 0.002 \ \delta = \ 0.04$

$\sigma^* = 0.66 \ \sigma^{**} = 0.975$

$\beta = 0.66$

$\gamma = 2$

$\sigma^* = \beta \ \sigma^* = \frac{\beta\gamma - \rho(1-\beta)}{\beta\gamma}$

$\mu = -\frac{\rho}{\sigma - \beta\gamma + \beta^2}.$

The Jacobian matrix associated with the system (4.4) is given by

$$J(P) = \begin{bmatrix} \frac{1}{\sigma}(-\rho + 2\sigma x_1 + (\beta - \sigma)x_3) & 0 & \frac{1}{\sigma}x_1(\beta - \sigma) \\ -x_2 & \frac{1}{\beta}(\gamma\delta(1-2x_2) + \beta x_1) & 0 \\ 0 & \frac{1}{\beta}\gamma\delta x_3 & \frac{1}{\beta}\gamma\delta(1-x_2) + 2(\beta-1)x_3 \end{bmatrix} \tag{A.3}$$

The invariant of the Jacobian matrix $J(P)$ a evaluated in $P^*(x_1^*, x_2^*. x_3^*)$: $J(P) = J^*$ are:

Let us consider the Jacobian matrix of the system (2.6) in steady states

Trace: $Tr(J) = x_1 - 3\frac{\gamma\delta}{\beta}x_2 + \left(\frac{\beta}{\sigma} + 2\beta - 3\right)x_3 + 2\frac{\gamma\delta}{\beta} - \frac{\rho}{\sigma}$;

Determinant
$$Det(J^*) = \left(-\frac{\rho}{\sigma} + \frac{\beta-\sigma}{\sigma}x_3 + 2x_1\right)\cdot\left(\frac{\gamma\delta}{\beta}(1-2x_2) - x_1\right)\cdot\left(2(\beta-1)x_3 + \frac{\gamma\delta}{\beta}(1-x_2)\right) +$$
$$x_2\left(\frac{\gamma\delta}{\beta}x_3 \cdot \frac{\beta-\sigma}{\sigma}x_1\left(-\frac{\rho}{\sigma} + \frac{\beta-\sigma}{\sigma}x_3 + 2x_1\right)\right);$$

The sum of the principals minors of $J(P)$.
$$B(J^*) = \left(\frac{\gamma\delta}{\beta}(1-2x_2) - x_1\right)\cdot\left[2(\beta-1)x_3 + \frac{\gamma\delta}{\beta}(1-x_2)\right] + \left(-\frac{\rho}{\sigma} + \frac{\beta-\sigma}{\sigma}x_3 + 2x_1\right)\left[2(\beta-1)x_3 + \frac{\gamma\delta}{\beta}(1-x_2)\right] -$$
$$\left(-\frac{\rho}{\sigma} + \frac{\beta-\sigma}{\sigma}x_3 + 2x_1\right)\cdot\left(\frac{\gamma\delta}{\beta}(1-2x_2) - x_1\right);$$

The expression of the characteristic polynomial of J^* in term of Jacobian invariants is given by:
$$-\lambda^3 + Tr(J)\lambda^2 - B(J)\lambda + Det(J) = 0.$$

A stationary (equilibrium) point of the system is any solution of

$$(\frac{\rho}{\sigma})x_1 + (\frac{\alpha-\sigma}{\sigma})x_1 - x_1^2 = 0$$
$$(\frac{\gamma\delta}{\sigma})(1 - x_2)x_2 + x_1 x_2 = 0 \qquad (A.4)$$
$$-(\frac{\gamma\delta}{\sigma})((1 - x_2)x_3 + (\alpha - 1)x_3^2 = 0$$

We found eight steady states values:
1)$P_1^*(0, 0, 0)$;
2)$P_2^*(0, 0, (\frac{\gamma\delta}{\beta(1-\beta)}))$;
3)$P_3^*(0, 1, 0)$ (It is a double solution);
4)$P_4^*(\frac{\rho}{\sigma}, 0, 0)$;
5)$P_5^*(\frac{1}{\sigma}[\rho - \frac{\gamma\delta(\beta-\sigma)}{\beta(1-\beta)}], 0, (\frac{\gamma\delta}{\beta(1-\beta)}))$;
6)$P_6^*(\frac{\rho}{\sigma}, 1 - \frac{(\beta\rho)}{\sigma\gamma\delta}, 0)$;
7)$P_7^*(\frac{\rho(1-\beta)}{\beta(1-\sigma)}, 1 - \frac{\rho(1-\beta)}{\gamma\delta(1-\sigma)}, \frac{\rho}{\beta(1-\sigma)})$.

It is well-known that many theoretical result relating to the system depend upon the eigenvalues of the Jacobian matrix evaluated at the stationary point P_i^* with $i = 1, 2, 3, 4, 5, 6, 7$ in some values of the parameters.

The local bifurcation analysis permits to determine the structurally unstable solution of the model.

6.1   Hopf Bifurcations

Theorem 4 **Lemma 3** *There is a parameter $\sigma = \sigma_c$ such that in the steady state P_7^* the Jacobian Matrix $J(P_7^*)$ possesses two complex conjugated roots with real part equal to zero and the real root different from zero.*
Proof. *We consider the function:*

$$G(\sigma) = -B(J_{P_7^*})Tr(J_{P_7^*}) + Det(J_{P_7^*}) \tag{A.5}$$

We evalute the invariant elements of the Jacobian and we get:
$Tr(J_{P_7^*}) = \frac{\rho(1-\beta)}{\beta(1-\sigma)} - \frac{\gamma\delta}{\beta};$
$B(J_{P_7^*}) = -\left(\frac{\rho(1-\beta)}{\beta(1-\sigma)}\right);$
$Det(J_{P_7^*}) = \frac{\rho^2\gamma\delta(1-\beta)}{\beta^2\sigma(1-\sigma)}\left(1 - \frac{\rho(1-\beta)}{\gamma\delta(1-\sigma)}\right);$
We determine two solutions in which the function $G(\sigma)$ vanishes: $\sigma_c^* = \beta$ and $\sigma_c^{**} = \frac{\gamma\delta-\rho(1-\beta)}{\gamma\delta}$. ■

Lemma 4 *The derivative of the real part of the complex conjugate eigenvalues of $(J_{P_7^*})$ evaluated at $\sigma = \sigma_c^*$ and $\sigma = \sigma_c^{**}$, is always different from zero.*

The proof follows from direct calculation.

Theorem 5 *A family of Hopf bifurcations emerges around the steady state P_7^* of the system (5.3), for $\sigma = \sigma_c^*$ and $\sigma = \sigma_c^{**}$.*
Proof. *It follows directly from the assumptions of the Hopf bifurcation Theorem. Q.E.D.* ■

We consider some numerical simulations: in particular, we consider the following two sets of parameters (Bella, 2010):
a)
$\rho = 0.002$
$\beta = 0.66$
$\gamma = 2$
$\delta = 0.04$
$\sigma_c^* = 0.66$
b)
$\rho = 0.002$
$\beta = 0.66$
$\gamma = 2$
$\delta = 0.04$
$\sigma_c^{**} = 0.975$
We evaluate the growth rate of an economy (appendix 1) and we get $\mu = -\frac{\rho}{\sigma-\beta\gamma+\beta^2}$.
In a first simulation, we fix $\gamma = 2$, $\beta = 0.66$.
We consider μ as a function of σ :

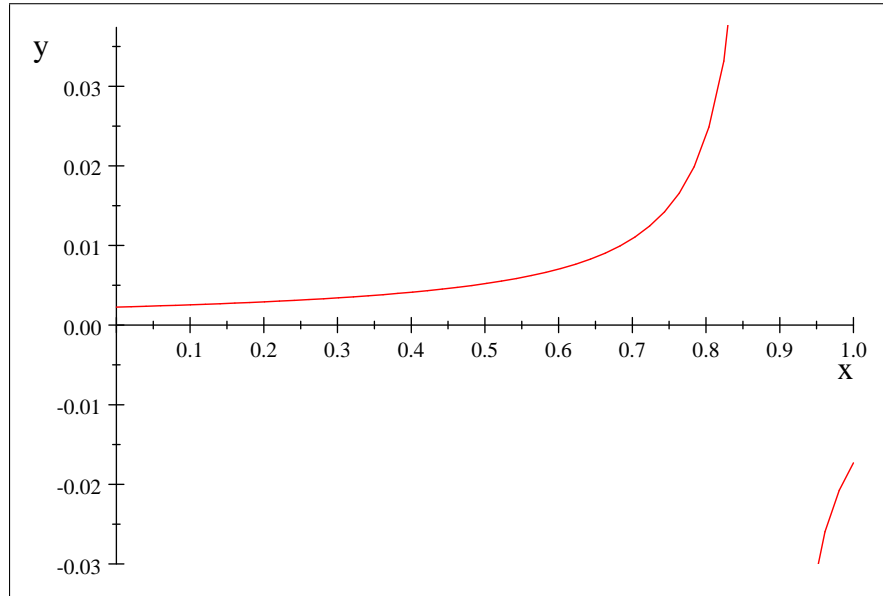$$\mu = f(\sigma) = -\frac{0.002}{\sigma - 2 \cdot 0.66 + 0.66^2}.$$

Figure 1. $\mu = f(\sigma)$

We find that the growth rate is positive for $\sigma < 0.8844$.

For the first set of parameters we have:

$\mu_c^* = 0.0089$

For the second set of parameters it is:

$\mu_c^{**} = -0.022$

In another simulation we consider μ^* as a function of β :fixing the value of $\sigma_c^* = 0.66$
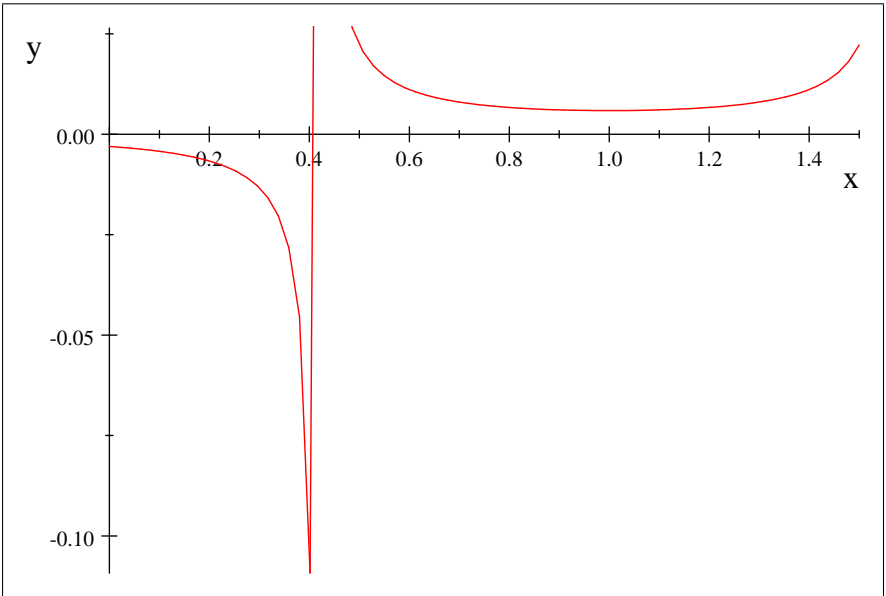
$$\mu = f(\beta) = -\frac{0.002}{0.66 - 2\beta + \beta^2}$$

Figure 2. $\mu = f(\beta)$ with $\sigma_c^* = 0.66$

This time, growth rate is positive for $0.41 < \beta < 1.58$.
A third simulation has been conducted fixing the value of $\sigma_c^{**} = 0.975$,

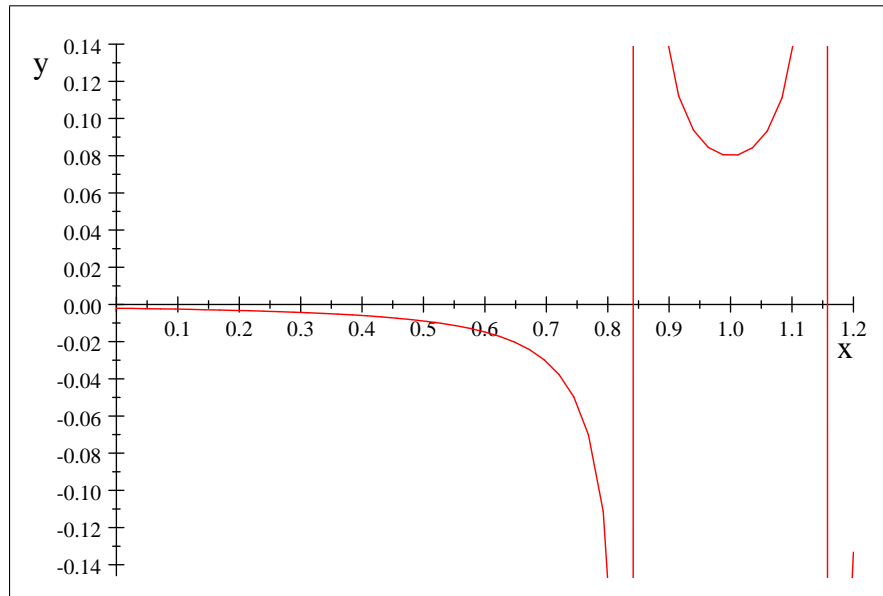$$\mu = f(\beta) = -\frac{0.002}{0.975 - 2\beta + \beta^2}$$

Figure 3. $\mu = f(\beta)$ with $\sigma_c^{**} = 0.975$

The growth rate is positive for $0.84 < \beta < 1.15$.

Another simulation shows the function of the growth rate as function of β and σ :

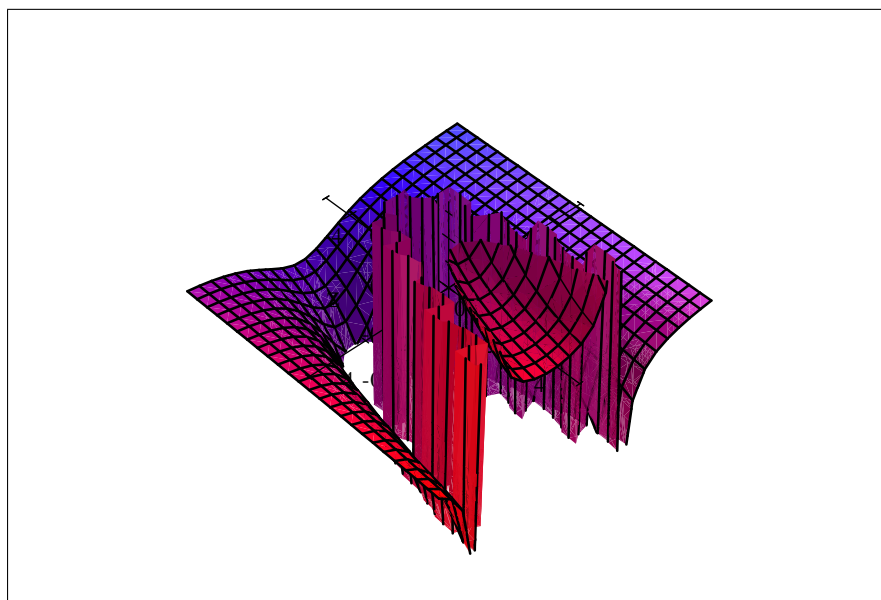$\mu = f(\sigma, \beta) = \frac{0.002}{2\beta - \beta^2 + \sigma}$; the graphic is:

Figure 4. $\mu = f(\sigma, \beta)$

The last simulation shows the function of the growth rate as function of γ and σ :

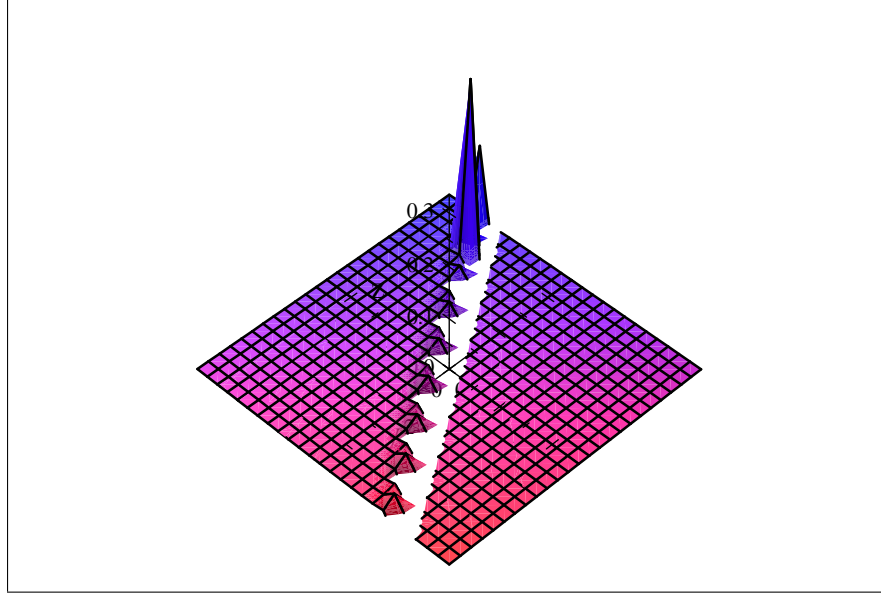$\mu = f(\sigma, \gamma) = \frac{0.002}{0.66\gamma - \sigma - 0.4356}$; the graphic is:

Figure 5. $\mu = f(\sigma, \gamma)$

The calculation of the stability coefficient q (Bella, 2010) gives some results for our parameter sets; for the set $a)$:

$\rho = 0.002$
$\beta = 0.66$
$\gamma = 2$
$\delta = 0.04$
$\sigma^* = 0.66$

we have $q = -2.40 \cdot 10^{12} < 0$; it means that bifurcation is super-critical, the steady state is unstable and the periodic orbits are attracting on the center manifold.

For the set $b)$:

$\rho = 0.002$
$\beta = 0.66$
$\gamma = 2$
$\delta = 0.04$
$\sigma^* = 0.975$

we have $q = 8.37 \cdot 10^{14} > 0$; it means that bifurcation is sub-critical and the periodic orbits start repelling.

The dynamics of Hamiltonians with non-integrable normal form

Ferdinand Verhulst

Mathematisch Instituut, University of Utrecht, The Netherlands
(E-mail: f.verhulst@uu.nl)

Abstract. In general Hamiltonian systems are non-integrable but their dynamics varies considerably depending on the question whether the corresponding normal form is integrable or not. We will explore this issue for two and three degrees of freedom systems; additional remarks on Hamiltonian chains can be found in [9]. A special device, the quadratic part of the Hamiltonian $H_2(p,q)$ is used to illustrate the results.
Keywords: Hamiltonian Chaos, normal forms, Hamiltonian time series.

1 Integrability versus non-integrability

We will consider time-independent Hamiltonian systems, Hamiltonian $H(p,q)$, $p, q \in \mathbb{R}^n$ with $n \geq 2$ degrees of freedom (DOF). A more detailed study is found in [9]. Regarding mechanics, or more generally dynamical systems, Hamiltonian systems are non-generic.
In addition we have that the existence of an extra independent integral besides the energy for two or more degrees of freedom is again non-generic for Hamiltonian systems (shown by Poincaré in 1892, [4] vol. 1).
So the following question is relevant: why would we bother about the integrability of Hamiltonian systems?
We give a few reasons, leaving out the esthetic arguments:

- Symmetries play a large part in mathematical physics models. Symmetries may sometimes induce integrability but more often integrability of the normal forms. An example is discrete (or mirror) symmetry.
- Near-integrability plays a part in many models of mathematical physics where the integrability, although degenerate , can be a good starting point to analyze the dynamics. Integrals of normal forms may help.
- Non-integrability is too crude a category, it takes many different forms. A first crude characterization is to distinguish non-integrable Hamiltonian systems with integrable or non-integrable normal form.

2 How to pinpoint (non-)integrability?

Looking for a smoking gun indicating integrability there are a few approaches:

1. Poincaré [4] vol. 1:
   A periodic solution of a time-independent Hamiltonian system has two characteristic exponents zero. A second integral adds two characteristic exponents zero except in singular cases. This can be observed (for an explicit Hamiltonian system) as a continuous family of periodic solutions on the energy manifold. Finding such a continuous family can be either a special degeneration of the system or a sign of the existence of an extra integral.
2. Symmetries of course; strong symmetries like spherical or axial symmetry induce extra integrals. Weaker symmetries may or may not induce an integral. An example is studied in [6] where discrete symmetry is explored in two degrees of freedom systems. It is shown for instance that the spring-pendulum displays many degenerations depending on the resonance studied.
3. Degenerations in variational equations or bifurcations are degenerations that often suggest the presence of integrals.

3 Normal forms

There are many papers and books on normalization. A rather complete introduction is [5]. One considers k-jets of Hamiltonians:

$$H(p, q) = H_2 + H_3 + \ldots + H_k,$$

usually in the neighbourhood of stable equilibrium $(p, q) = (0, 0)$. The H_m are homogeneous polynomials in the p, q variables.

An important feature is that $H_2(p, q)(t)$ is an independent normal form integral, see [5]; its physical interpretation is that H_2 is the energy of the linearized equations of motion. The implication of the existence of this integral is that near stable equilibrium, for two DOF, the normal form is for all resonance ratios integrable so that chaos has for two DOF near stable equilibrium generally a smaller than algebraic measure. This explains a lot of analytic and numerical results in the literature (see again [5]).

In general, for more than two DOF, integrability of the normal form can not be expected without additional assumptions. If we find integrability, it restricts the amount of chaos and also of Arnold diffusion.

Example: Braun's parameter family
Two DOF normal forms are integrable but it is still instructive to consider them. An exampe is Braun's family of Hamiltonians:

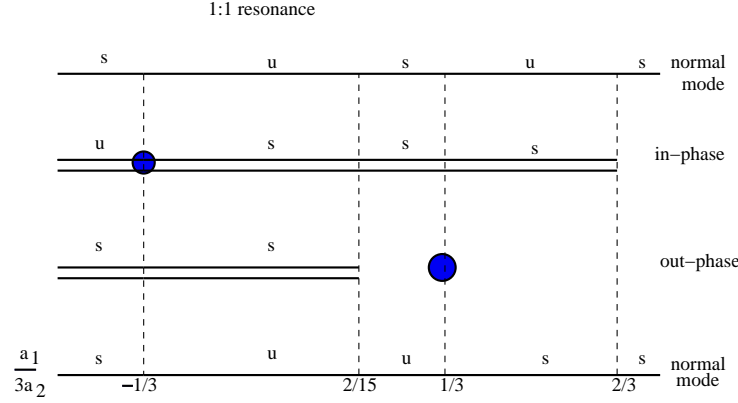$$H(p, q) = \frac{1}{2}(p_1^2 + p_2^2 + q_1^2 + \omega^2 q_2^2) - \frac{a_1}{3}q_1^3 - a_2 q_1 q_2^2.$$

Fig. 1. Periodic solutions obtained from the normal form to cubic terms of Braun's family of discrete-symmetric Hamiltonians. The horizontal lines correspond with isolated periodic solutions on the energy manifold, dots at $-1/3$ (the Hénon-Heiles case) and at $1/3$ correspond with continuous families of periodic solutions.

The analysis is given in [8] and summarized in [5]; consider for instance $\omega = 1$, a_1 and $a_2 \neq 0$ are parameters. The normal form to cubic terms produces two normal modes and, depending on the parameters, two families of in-phase periodic solutions, two families of out-phase periodic solutions and for specific parameter values two continuous families of periodic solutions on the energy manifold; see fig. 1. Normalizing to quartic terms the continuous family at $a_1/(3a_2) = -1/3$ (the Hénon-Heiles Hamiltonian) breaks up into separate periodic solutions; the continuous family at $a_1/(3a_2) = 1/3$ persists, this Hamiltonian before normalization is already integrable.

4   Three degrees of freedom

Genuine first-order resonances are characterized by its normal form. Apart from the three actions, this contains at least two independent combination angles. We have for three DOF:

- $1 : 2 : 1$ resonance
- $1 : 2 : 2$ resonance
- $1 : 2 : 3$ resonance
- $1 : 2 : 4$ resonance

A basic analysis of the normal forms to cubic order $\bar{H} = H_2 + \bar{H}_3$ yields short-periodic solutions and integrals. The use of integrals gives insight in the geometry of the flow, enables possible application of the KAM-theorem and may produce measure-theoretic restrictions on chaos.

5   Integrability of normal forms

The normal form has two integrals, H_2 and $\bar{H}$ (or $\bar{H}_3$). Is there a third integral? To establish (non-)integrability we have:

- Ingenious inspection of the normal form or obvious signs of integrability, see van der Aa and F.V. [7].
- Extension into the complex domain and analysis of singularities, see Duistermaat [2].
- Applying Shilnikov-Devaney theory to establish the existence of a transverse homoclinic orbit on the energy manifold, see Hoveijn and F.V. [3].
- Using Ziglin-Morales-Ramis theory to study the monodromy group of a particular nontrivial solution; this study may lead to non-integrability. This involves the variational equation and the characteristic exponents in the spirit of Poincaré. In an extension one introduces the differential Galois group associated with a particular solution; if it is non-commutative, the system is non-integrable. See Christov [1].

5.1 The genuine first-order resonances

A remarkable result is that the normal form to cubic terms of the $1:2:2$ resonance is integrable with quadratic third integral, see [7]. We have that $p_1 = q_1 = 0$ corresponds with an invariant manifold of the normal form; the manifold consists of a continuous set of periodic solutions and is a degeneration according to Poincaré with 4 characteristic exponents zero. The calculation of the normal form to quartic terms produces a break-up of this continuous set into six periodic solutions on the energy manifold.

It was shown in [2] that the normal form to cubic terms of the $1:2:1$ resonance is non-integrable. This was shown by singularity analysis in the complex domain. A different approach was used in [1] where it was shown that for a particular solution the monodromy group is not Abelian; this precludes that the normal form is integrable by meromorphic integrals.

Non-integrability was shown in [1] for the $1:2:4$ resonance in a similar way. One identifies a particular solution in the $(p_1, q_1) = (0,0)$ submanifold; the local monodromy group is not Abelian which precludes integrability.

The case of the $1:2:3$ resonance is different. The analysis in [3] shows that a complex unstable normal mode (p_2, q_2) is present. The normal form contains an invariant manifold N defined by $H_2 = E_0, \bar{H}_3 = 0$. N contains an invariant ellipsoid, also homoclinic and heteroclinic solutions. They are forming an organizing center producing a horseshoe map and chaos in $H_2 + \bar{H}_3 + \bar{H}_4$. So, the normal form contains only two integrals.

Later, Christov [1] showed by algebraic methods that $H_2 + \bar{H}_3$ is already non-integrable, but the consequences for the dynamics are not yet clear. Technically, this is his most complicated case.

6 Discussion and consequences

In two DOF the Hamiltonian normal form is integrable to any order; this restricts the chaos near stable equilibrium to exponentially small sets between the invariant tori.

For three and more DOF, the situation is more complicated. If the normal form is integrable, chaos is restricted to sets that are algebraically small with respect to the small parameter that scales the energy with respect to stable equilibrium. We would like to distinguish between various kinds of non-integrability near equilibrium. The chaos is usually localized near homoclinic intersections of stable and unstable manifolds.

The phenomenon is most striking after a Hamiltonian-Hopf bifurcation of a periodic solution has taken place, see for the bifurcation diagram fig. 2.
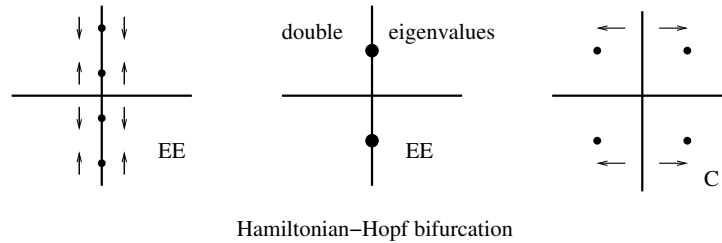

Hamiltonian−Hopf bifurcation

Fig. 2. As a parameter varies, eigenvalues on the imaginary axis become coincident and then move into the complex plane.

Consider the following explicit examples of the $1:2:3$ resonance:

$$H(p,q) = \frac{1}{2}(p_1^2 + q_1^2) + (p_2^2 + q_2^2) + \frac{3}{2}(p_3^2 + q_3^2) + H_3(p,q),$$

$$H_3(p,q) = -q_1^2(a_2 q_2 + a_3 q_3) - q_2^2(c_1 q_1 + c_3 q_3) - b q_1 q_2 q_3.$$

We will consider two cases. If $a_2 > b$, analysis of the normal form shows that the (p_2, q_2) normal mode is unstable of type HH (hyperbolic-hyperbolic or 4 real eigenvalues). If $a_2 < b$ the (p_2, q_2) normal mode is unstable of type C (complex eigenvalues). The $H_2(p,q)(t)$ time series is shown in figs. 3 and fig 4. Both time series display chaotic behavior, but the case of instability C involves the Devaney-Shilnikov bifurcation producing strong chaotic behaviour; for more information see [3].

References

1. O. Christov, *Non-integrability of first order resonances in Hamiltonian systems in three degrees of freedom*, Celest. Mech. Dyn. Astron. 112 pp. 149-167, (2012).
2. J.J. Duistermaat, *Non-integrability of the $1:2:1$ resoannce*, Ergod. Theory Dyn. Syst. 4 pp. 553-568, (1984).
3. I. Hoveijn and F. Verhulst, *Chaos in the $1:2:3$ Hamiltonian normal form*, Physica D 44 pp. 397-406, (1990).
4. Henri Poincaré, *Les Méthodes Nouvelles de la Mécanique Céèste*, 3 vols., Gauthier-Villars, Paris (1892, 1893, 1899).
5. j.A. Sanders, F.Verhulst and J.Murdock, *Averaging Methods in Nonlinear Dynamical Systems*, Springer (2007), 2nd ed.
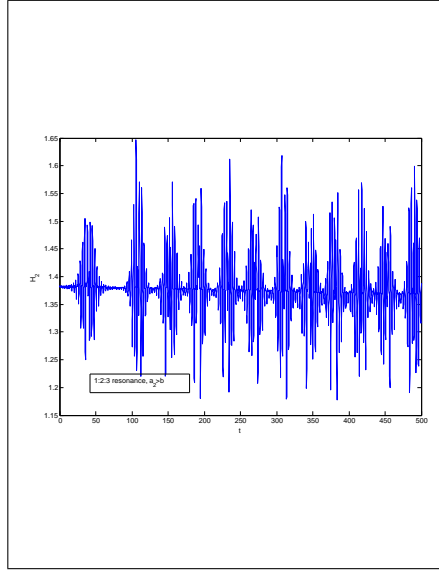
Fig. 3. The $H_2(p,q)(t)$ time series in the case of normal mode instability HH.
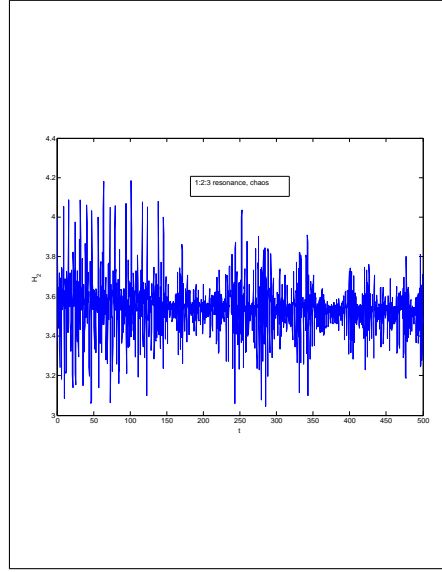
Fig. 4. The $H_2(p,q)(t)$ time series in the case of normal mode instability C.

6. J.M. Tuwankotta and F. Verhulst, *Symmetry and resonance in Hamiltonian systems*, SIAM J. Appl. Math. 61 pp. 1369-1385, (2000).

7. E. van der Aa and F. Verhulst, *Asymptotic integrability and periodic solutions of a Hamiltonian system in* $1:2:2$ *resonance*, SIAM J. Math. Anal. 15 pp. 890-911, (1984).

8. Ferdinand Verhulst, *Discrete symmetric dynamical systems at the main resonances with applications to axi-symmetric galaxies*, Trans. roy. Soc. London 290, pp. 435-465 (1979).

9. Ferdinand Verhulst, *Integrability and non-integrability of Hamiltonian normal forms*, Acta Applicandae Mathematicae 137, pp. 253-272 (2015), DOI 10.1007/s10440-014-9998-5.

Nonlinear Impacting Oscillations of a Simply Supported Pipe Conveying Pulsating Fluid Subjected to Distributed Motion Constraints

Yikun Wang[1,2], Qiao Ni[1,2], Min Tang[1,2], Yangyang Luo[1,2], Hao Yan[1,2], Lin Wang[1,2]

1. Department of Mechanics, Huazhong University of Science and Technology, Wuhan 430074, China
2. Hubei Key Laboratory for Engineering Structural Analysis and Safety Assessment, Wuhan 430074, China
(Email: wykfang1053@hust.edu.cn; niqiao@hust.edu.cn; tangminnx@gmail.com; 123443887@qq.com; 824174017@qq.com; wanglinfliping@sohu.com)

Abstract

In this paper, the nonlinear dynamics of simply supported pipe conveying pulsating fluid is investigated, by introducing the effect of distributed motion constraint along the pipe axis modeled as trilinear springs. The internal fluid is assumed to be a harmonic component of flow velocity superposed on a constant mean value. Attention is concentrated on the possible motions of the system with various mean values of flow velocity, pulsating amplitude and frequency. As for the impact force term, the damping effect during impacting process is considered in analyzing. The partial differential equations are then transformed into a set of ordinary differential equations (ODEs) using the Galerkin's method. The nonlinear dynamical responses are presented in the form of bifurcation diagrams, time histories, phase portraits and power spectrums. Some interesting results have been observed with different parameters.

Keywords

Nonlinear dynamics; chaotic motion; pipe conveying pulsating fluid; distributed motion constraints; bifurcation

1. Introduction

The dynamics of pipes conveying fluid is an important academic topic with broad industrial application, e.g., pump discharge lines, oil pipelines, propellant lines, reactor system components and so forth. They were also the most troublesome elements in these fields. These industries utilize high thermal efficiency shell and heat exchanger designs to avoid failure. Performance requirements often require the devices to be able to work under high coolant velocities and to be flexible tubes, which in turn would cause pipes to experience excessive flow-induced vibrations. A large number of studies have been made on flow-induced vibrations due to the corresponding significance [1-4]. Focuses of flow-induced vibrations were put on these fields in understanding the mechanisms of pipes conveying fluid. Works on this topic appear to have started in the 1960s. Many studies have investigated the stabilities and nonlinear dynamics of pipes conveying fluid both theoretically and experimentally. A very comprehensive introduction to vibrations induced by fluid flow and the associated linear stability problems can be found in the work of Chen [5]. The nonlinear behavior of slender structures subjected to axial fluid flows was discussed in detail in the monograph by Paidoussis [6]. The system exhibits a wide range of interesting dynamical behavior under different boundary conditions and motion constraints. These conditions cover a number of factors, such as parametric excitation in the form of flow fluctuation, external excitations, various support conditions, articulated or continuous

configuration, additional system configurations like lumped mass, attached nozzles, elastic foundations, elastic constraints, and different forms of nonlinearities in the system arising from various sources.

In a survey of this subject, many researches were conducted either with pulsating fluid flow or motion constraint on one or finite number of locations on the pipe. Paidoussis and Sundararajan [7] explored the dynamics of a pipe conveying fluid when the flow velocity is harmonically perturbed about a mean value. Cantilevered pipe and clamped-clamped pipe models are investigated and parametric and combination resonances are analyzed. Namchchivaya [8] and Chen S S [9] examined the nonlinear dynamics of supported pipes conveying pulsating fluid in the vicinity of subharmonic resonances using the method of averaging. Some other detailed investigations based on linear analytical models of these parametric instability problems for simply supported pipes were conducted [10, 11, 12]. They have studied the parametric and combination resonances and evaluated instability regions using Bolotin's method and numerical Floquet analysis. Various other authors considered nonlinear pipes conveying pulsating fluid referring to Sri Namchchivaya N et al. [13], Jayaraman et al. [14], Chang et al. [15], YOSHIZAWA et al. [16]. From these and several other studies, it is clear that the basic system of a pipe conveying pulsating fluid can lose stability when flow velocity becomes sufficiently high. Thus, the analysis of subharmonic and combination resonances was the main interest for simply supported pipes conveying pulsating fluid, yielding the stability boundaries in the parameter space. For a perspective on the whole field of pipes conveying pulsating fluid, the reader is referred to the book by Paidoussis [6].

In several recent papers, a simply supported pipe conveying pulsating fluid were analyzed, in which a non-linear force considered is associated with the axial extension of the pipe [17, 18]. The combination and principal parametric and internal resonances of a supported pipe were investigated. Paidoussis et al. [19] conducted a nonlinear analysis of a cantilevered pipe conveying fluid with a motion constraint on the pipe under steady flow velocity. Two contact models, cubic springs and trilinear springs, were introduced in the nonlinear equations of motion and results were obtained numerically. Another study performed by Hassan et al. [20] provided a means of representing contact as a combination of edge and segmental contact. The contact segment was unknown and determined artificially according to the researcher's interests. The selection of the location of the segment could affect the performance of the system. Wang L. [21] further studied the nonlinear dynamics of a simply supported pipe conveying pulsating fluid by considering the effect of motion constraints modeled as cubic springs. Quasi-periodic and chaotic motions are obtained by using the Galerkin method with N=2. W. Xia et al. [22] developed an improved model with the consideration of the nonlinearity associated with the mean axial extension of the tube array. Cross flow and motion constraints are the main points of this study. The restraining forces were modeled cubic and trilinear springs too. Tang M. et al. [23] developed an improved model aimed at analyzing the fluidelastic vibration of a single flexible curved pipe that is surrounded by rigid cylinders and subjected to cross-flow and loose support.

In this study, it is investigated with both internal pulsating fluid flow and motion constraints imposed on the fluid conveying simply supported pipe systems. The simply supported pipe would impact the constraints once the motion becomes sufficiently large. The constraints are modeled as trilinear springs and further improved as distributed constraints acting on the pipe along its axis. Damping effects during impacting process are considered. The internal flow has a time-dependent harmonic component superposed on steady flow, such that $u = u_0(1+\sigma\sin\omega\tau)$, where σ is generally small and u_0 is called the mean flow velocity; ω is defined as the pulsating frequency of the pulsating fluid flow. Attention is concentrated on the possible behaviors of the system with various values of

pulsating amplitude and frequency associated with the unsteady internal fluid. Some interesting results will be represented. Thus, bifurcation diagram, phase portraits and power spectral density diagrams will be constructed to represent the dynamical motions of the pipe system.

2. Equations of Motion

In the current work, the simply supported pipe conveying pulsating fluid interacting with distributed motion constraints is of length L, cross section of the pipe wall A, flexural rigidity EI, density ρ_p, mass per unit length m and coefficient of viscoelastic damping E^*. The internal flowing fluid is of density ρ_f and mass per unit length M, with flow velocity U. The impacting component is modeled as trilinear springs distributed along the pipe axis, as depicted in Fig. 1. The equation for unconstrained motions without taking into account the effect of motion constraints has been obtained before [17, 18, 24]. The equation of motions without motion constraints are modified here to describe this impacting oscillation with pulsating fluid. The equation of motion is given by
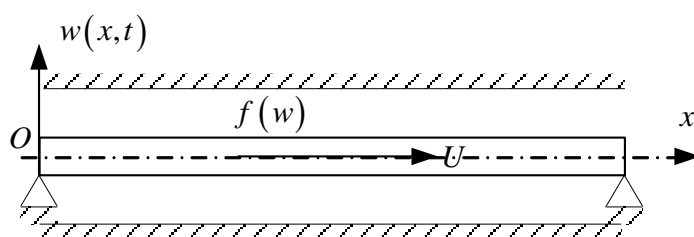

Fig. 1 Schematic of the simply supported pipe conveying pulsating fluid with distributed motion constraints.

$$EI\frac{\partial^4 w}{\partial x^4} + E^* I \frac{\partial^5 w}{\partial t \partial x^4} + 2MU\frac{\partial^2 w}{\partial t \partial x} + \left(M+m\right)\frac{\partial^2 w}{\partial t^2}$$
$$+\left[MU^2 + M\frac{\partial U}{\partial t}\left(l-x\right) - \left(E+E^*\frac{\partial}{\partial t}\right)\frac{A}{2l}\int_0^l \left(\frac{\partial w}{\partial x}\right)^2 dx\right]\frac{\partial^2 w}{\partial x^2} + F\left(w\right) = 0 \tag{1}$$

in which, $F(\omega)$ represents the effect of the nonlinear motion constraint on the pipe. Here in this paper, impacting force F_{spr} and damping force F_{dmp} are included in calculation. Description of the nonlinear force is depicted by [19, 25]

$$F\left(w\right) = F_{spr} + F_{dmp} \tag{2}$$

Where,

$$F_{spr} = K_{spr}\left[w - \frac{1}{2}\left(\left|w+w_0\right| - \left|w-w_0\right|\right)\right]^3 \tag{3}$$

$$F_{dam} = 1.5C_{dmp}F_{spr}\frac{\partial w}{\partial t} = 1.5C_{dmp}K_{spr}\frac{\partial w}{\partial t}\left[w - \frac{1}{2}\left(\left|w+w_0\right| - \left|w-w_0\right|\right)\right]^3 \tag{4}$$

In which, w_0 is the gap between the pipe axis and the edge of the motion constraints; K_{spr} and C_{dmp} are the trilinear spring stiffness and material damping coefficient, respectively. The nonlinear spring force F_{spr} agrees with experimental test well according to Paidoussis et al. [19]. The damping force F_{dmp} illustrated the opposite direction of the force and velocity. Introducing next the non-dimensional quantities

$$\eta = \frac{w}{L}, \xi = \frac{x}{L}, d = \frac{w_0}{L}, \tau = \sqrt{\frac{EI}{m+M}} \frac{t}{L^2}, u = \sqrt{\frac{M}{EI}} LU, k = \frac{K_{spr} L^5}{EI}, c = \frac{C_{dmp} L^2}{EI}$$

$$\alpha = \sqrt{\frac{EI}{m+M}} \frac{E^*}{L^2}, \beta = \frac{M}{m+M}, \kappa = \frac{AL^2}{2I}$$

Eq. (1) can be rewritten in a dimensionless form as follows:

$$\alpha \frac{\partial^5 \eta}{\partial \tau \partial \xi^4} + \frac{\partial^4 \eta}{\partial \xi^4} + \left[u^2 + \sqrt{\beta} \dot{u} (1-\xi) \right] \frac{\partial^2 \eta}{\partial \xi^2} + 2\sqrt{\beta} u \frac{\partial^2 \eta}{\partial \tau \partial \xi} + \frac{\partial^2 \eta}{\partial \tau^2}$$
$$- \kappa \frac{\partial^2 \eta}{\partial \xi^2} \int_0^1 \left(\frac{\partial \eta}{\partial \xi} \right)^2 d\xi - 2\alpha \kappa \frac{\partial^2 \eta}{\partial \xi^2} \int_0^1 \frac{\partial \eta}{\partial \xi} \frac{\partial^2 \eta}{\partial \tau \partial \xi} d\xi + f(\eta) = 0 \tag{5}$$

Nondimensional impact force is expressed as follows:

$$f(\eta) = k \left[\eta - \frac{1}{2} (|\eta + d| - |\eta - d|) \right]^3 + \frac{3}{2} ck \frac{\partial \eta}{\partial \tau} \left[\eta - \frac{1}{2} (|\eta + d| - |\eta - d|) \right]^3 \tag{6}$$

The non-dimensional pulsating fluid velocity is described by a sinusoidal fluctuation depend on τ,

$$u = u_0 (1 + \sigma \sin \omega \tau) \tag{7}$$

In Eq. (7), u_0 is the mean flow velocity and σ and ω is the pulsating magnitude and pulsating frequency, respectively.

The infinite dimensional modal can be discretized by the Galerkin's technique, with the simply supported beam eigenfunctions $\varphi_j(\xi)$. These eigenfunctions are used as a suitable set of base functions with $q_j(\tau)$ being the corresponding generalized coordinates; thus,

$$\eta(\xi, \tau) = \sum_{j=1}^{N} \varphi_j(\xi) q_j(\tau) \tag{8}$$

where, N is the number of modes taken into calculations. Substituting Eq. (8) into Eq. (5), multiplying by $\varphi_i(\xi)$ and integrating from 0 to 1 leads to

$$\{\ddot{q}\} + [C]\{\dot{q}\} + [K]\{q\} + \{f(q)\} + \{g(q, \dot{q})\} = \{0\} \tag{9}$$

$[C]$, $[K]$, $\{f(q)\}$ and $\{g(q, \dot{q})\}$ represent the stationary damping, stiffness matrices, nonlinear constraint force vector and nonlinear vector, respectively. The elements of $[C]$, $[K]$, $\{f(q)\}$ and $\{g(q, \dot{q})\}$ are given by

$$C_{ij} = \alpha c_{ij}^1 + 2\sqrt{\beta} u_0 (1 + \sigma \sin \omega \tau) c_{ij}^2$$

$$K_{ij} = k_{ij}^1 + u_0^2 (1 + \sigma \sin \omega \tau)^2 k_{ij}^2 + \sqrt{\beta} u_0 \sigma \omega \cos \omega \tau k_{ij}^3$$

$$f_i = \int_0^1 \varphi_i(\xi) f\left(\sum_{j=1}^{N} \varphi_j(\xi) q_j \right) d\xi$$

$$g_i = g_{ijkl}^1 q_j q_k q_l + g_{ijkl}^2 q_j q_k \dot{q}_l \tag{10}$$

Where, the coefficients in these quantities can be written in the following form:

$$c_{ij}^1 = \lambda_i^4 \delta_{ij}, \quad c_{ij}^2 = \int_0^1 \varphi_i \varphi_j' d\xi$$

$$k_{ij}^1 = \lambda_i \delta_{ij}, \quad k_{ij}^2 = -\lambda_i^2 \delta_{ij}, \quad k_{ij}^3 = \int_0^1 (1-\xi) \varphi_i \varphi_j'' d\xi$$

$$g_{ijkl}^1 = g_{ijkl}^2 = \int_0^1 \varphi_i \varphi_j'' \int_0^1 \varphi_k' \varphi_l' d\xi d\xi \tag{11}$$

For the purpose of numerical computation, define $\{p\} = \{\dot{q}\}$ and $\{z\} = [\{q\}; \{p\}]$; Eq. (9) is then reduced to its first-order form:

$$\{\dot{z}\} = [A]\{z\} + \{F(z)\} + \{G(z)\} \tag{12}$$

Where,

$$[A] = \begin{bmatrix} [0] & [I] \\ -[K] & -[C] \end{bmatrix}, \quad \{G\} = \begin{bmatrix} \{0\} \\ -\{g\} \end{bmatrix}, \{F\} = \begin{bmatrix} \{0\} \\ -\{f\} \end{bmatrix}$$

They are $2N \square 2N$, $2N \square 1$ and $2N \square 1$ matrixes, respectively. Solutions of $\{q\}$ and $\{p\}$ consist of the displacement and velocity at any point ξ along the pipe.

3. Results and Discussion

In the current work, the dynamical behaviors of the simply supported pipe conveying pulsating fluid with distributed motion constraints will be investigated numerically. To the author's knowledge, it is found that the non-linear responses in supported pipes conveying pulsating fluid with reasonably high mean flow velocity and for the case with distributed motion constraints have not yet been explored so far. Therefore, we analyze the non-linear vibrations of hinged–hinged pipes conveying fluid on the two topics. As it is well known that, for a simply-supported pipe conveying fluid with steady flow velocity, divergence in the first mode occurs at a dimensionless critical flow velocity $u_c = \pi$ [6]. The main aim of this paper is to explore the effect of the pulsating amplitude σ and frequency ω with higher mean flow velocity u_0 and distributed motion constraints on the dynamics of this pipe system. For that reason, solutions of Eq. (10) are obtained by using the fourth order Runge-Kutta method, with the following initial conditions employed, $z(1) = \cdots = z(N) = -0.001$ and $z(N+1) = \cdots = z(2N) = 0$.

In this project, the results to be presented have been obtained with $N = 4$ since reasonably converged frequencies are accomplished and identical to the theoretical results presented by Ni Q et al. [26], when $N = 4$. Some of the physical parameters are chosen to be

$$\alpha = 0.005, \quad \beta = 0.2, \quad \kappa = 5000, \quad k = 5.6 \times 10^6, \quad c = 0.2, \quad d = 0.044 \tag{13}$$

3.1 Responses for various mean flow velocity

In this subsection, we consider the case of $u_0 = 6$ and $u_0 = 8$, respectively. The purpose is to explore how the responses of the pipe conveying pulsating fluid with distributed motion constraints would appear under low, middle and high mean flow velocities. In the calculations to construct the bifurcation diagram, whenever the midpoint velocity was zero, the midpoint displacement $\eta(0.5, \tau)$ was recorded. The bifurcation diagrams for the midpoint displacement of the pipe are shown in Fig. 2, as forcing frequency ω is varied.

It is obviously found that a great change takes place on the dynamical behavior of the simply supported pipe when mean flow velocity is under consideration, as seen in Figs. 2-6. As shown in Fig 2 (a) and (b), for mean flow velocity is at $u_0 = 8$, a large region of chaotic motion exists for $33.6 < \omega < 70$. However, when the pulsating frequency is in this region at $u_0 = 6$, the pipe exhibits chaotic motions and periodic motions, respectively. At the case of low pulsating frequencies ($0 < \omega < 12.2$ for $u_0 = 6$ and $0 < \omega < 18.3$ for $u_0 = 8$), dynamical behaviors of the two cases present periodic oscillations. As the forcing frequency increases, the pipe undergoes periodic motions, quasi periodic motions and chaotic motions. From Fig. 2 (a) and (b), both of the two systems exhibit chaotic motions and regain stability oscillating periodically. For example, for system of $u_0 = 6$, in the regions of $0 < \omega < 7.7$, $9 < \omega < 11.8$ and $20.8 < \omega < 27.9$, period-1 motion occurs; in the region of $7.8 < \omega < 8.9$, period-3 motion occurs; in the regions of $12 < \omega < 14.3$, $17.7 < \omega < 20.7$ and $28 < \omega < 34$, the system exhibits chaotic motions and transitions to chaotic motions. The system undergoes loosing stability and regaining stability as the forcing frequency increases.
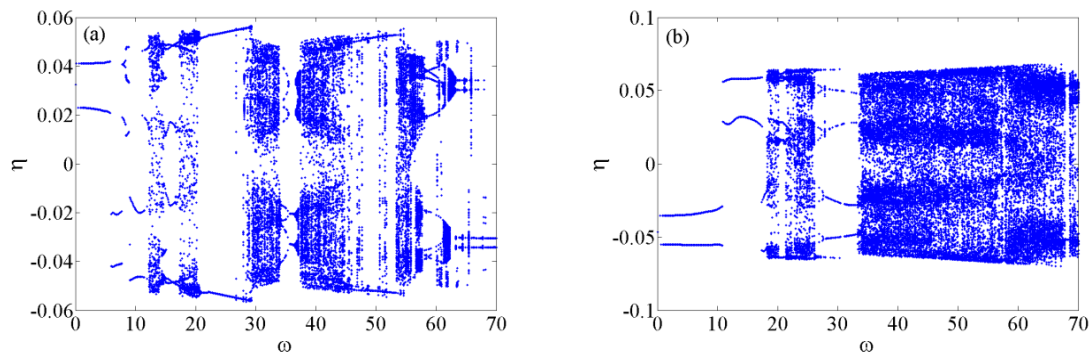

Fig. 2 Bifurcation diagrams of the midpoint displacement of the pipe. (a) $u_0 = 6$; (b) $u_0 = 8$
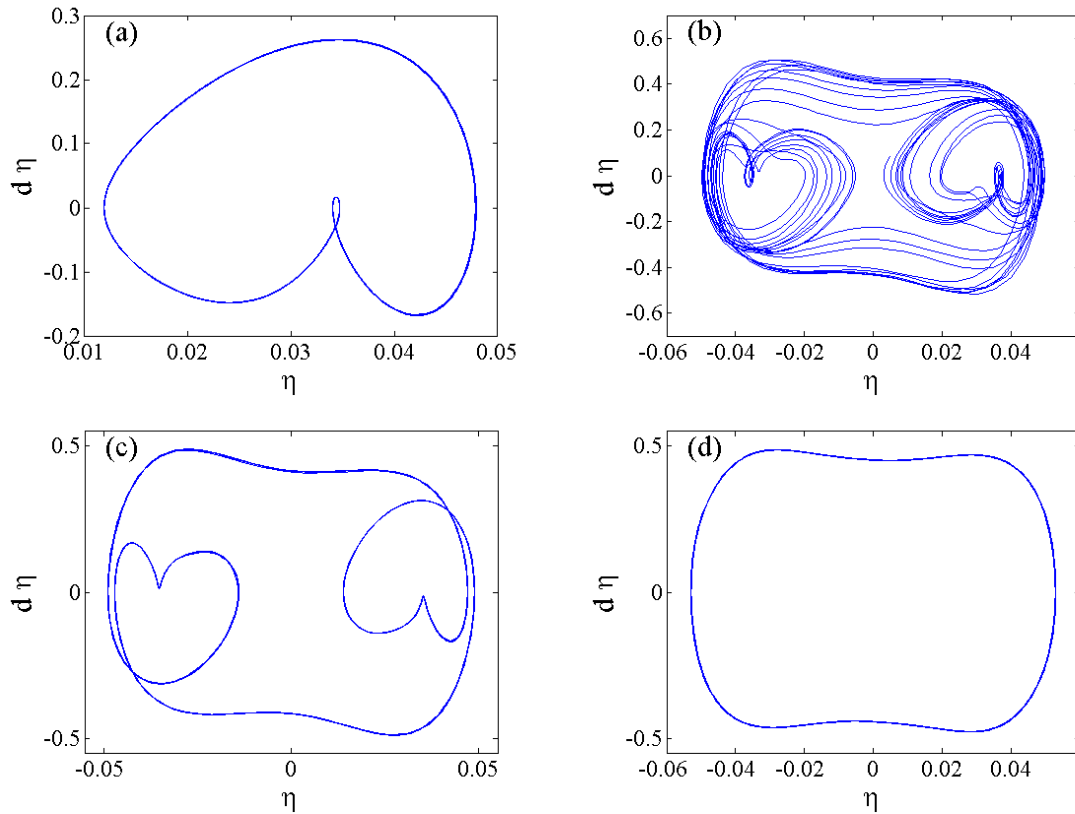

Fig. 3 Phase portraits of the motions of the midpoint of the simply supported system at $u_0 = 6$;

924

(a) ω = 8.6 (period-2 motion); (b) ω = 14.5 (phase transition);

(c) ω = 15.3 (period-3 motion); (d) ω = 23 (period-1 motion);

Changing our view to the system of $u_0 = 8$, the pipe oscillates periodically at low pulsating frequencies and experiences chaotic motions and regains stability as the frequency takes a proper range of values. The regaining stability process is similar to a Hopf bifurcation to some extent.

Phase portraits and power spectral diagrams for $u_0 = 6$ and $u_0 = 8$ with several pulsating frequencies are shown in Figs. 3-6. It can be seen from the power spectral diagrams that period oscillations present several peaks and is a smooth curve. For transitions to chaotic motion, the PSD curve exhibits broadband characteristics with several peaks in it. While for chaotic motions, the PSD curve displays broadband characteristics only.
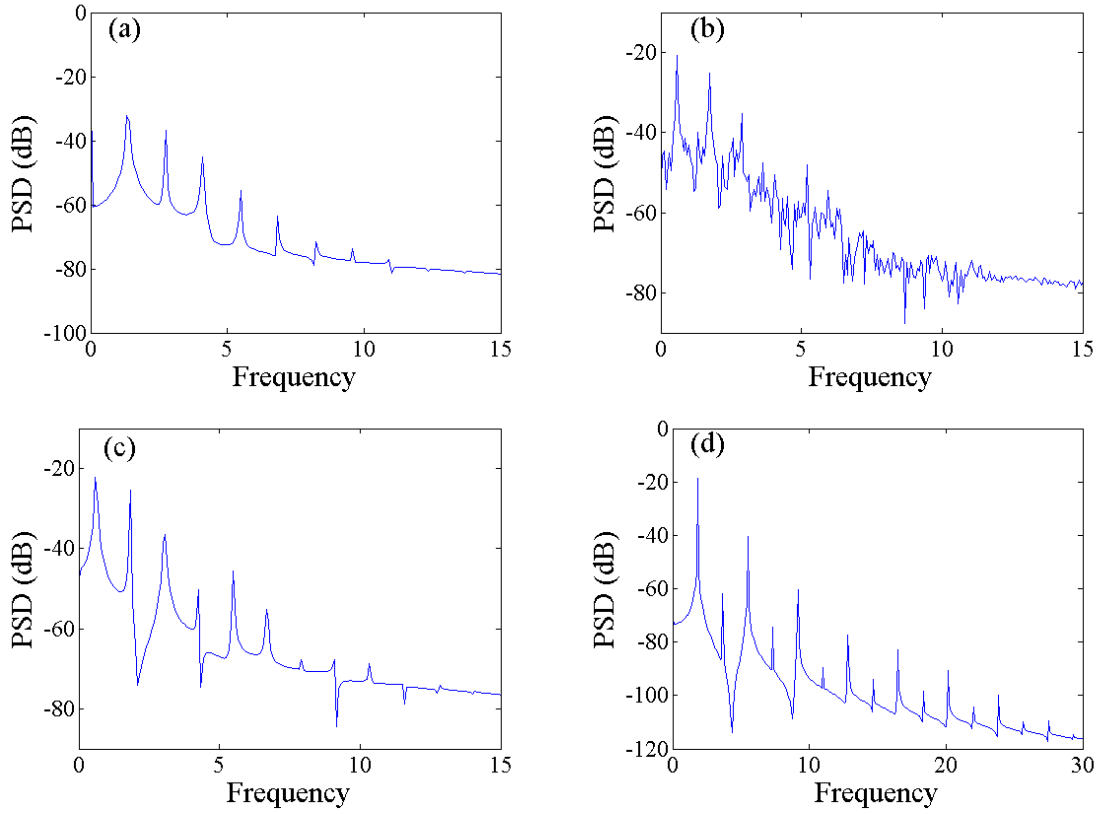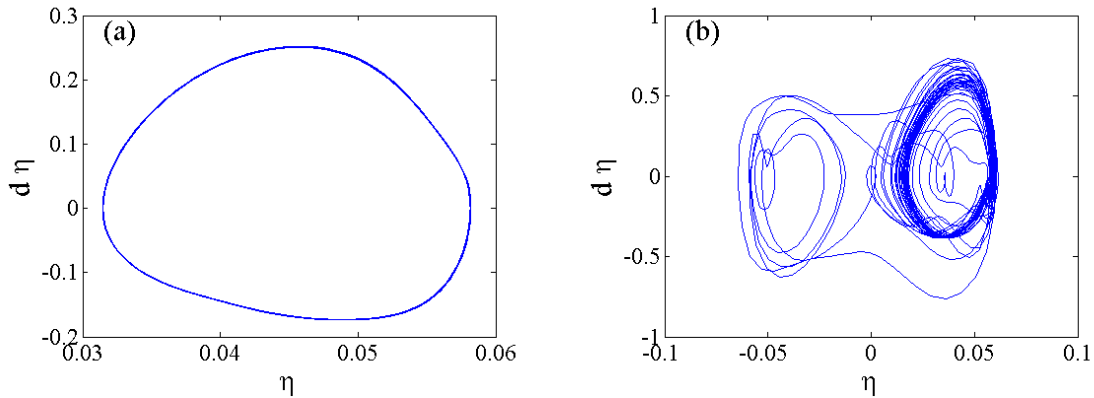

Fig. 4 Power spectral diagram of the midpoint of the simply supported system at $u_0 = 6$;

(a) ω = 8.6 (period-2 motion); (b) ω = 14.5 (phase transition);

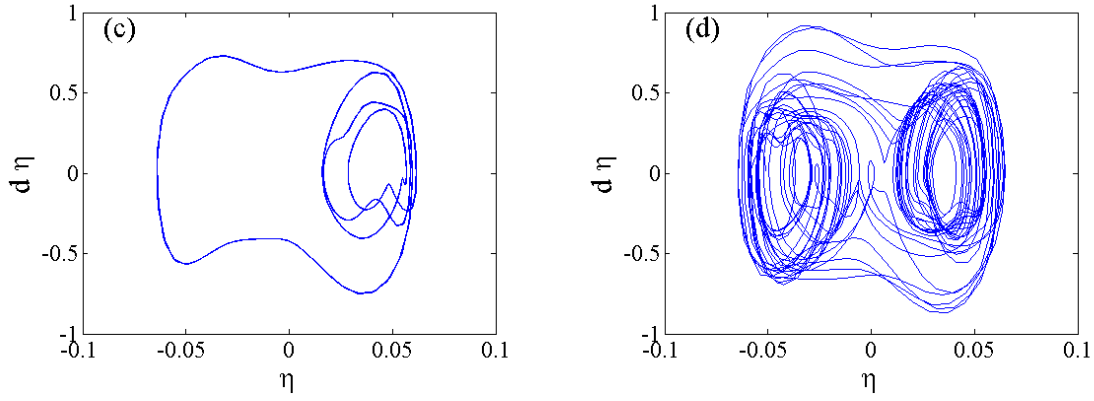(c) ω = 15.3 (period-3 motion); (d) ω = 23 (period-1 motion);

Fig. 5 Phase portraits of the motions of the midpoint of the simply supported system at $u_0 = 8$;
(a) $\omega = 15$ (period-1 motion); (b) $\omega = 18.3$ (phase transition);
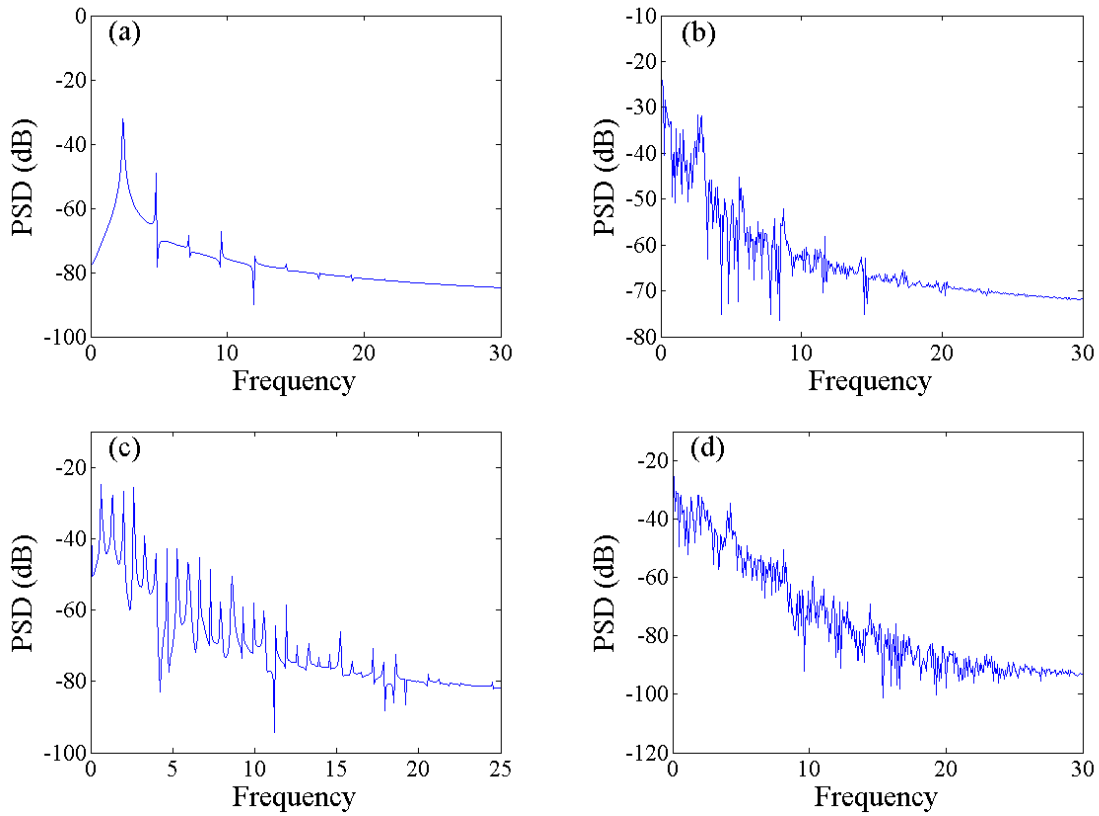(c) $\omega = 20.8$ (multi-period motion); (d) $\omega = 25.8$ (chaotic motion);

Fig. 6 Power spectral diagram of the midpoint of the simply supported system at $u_0 = 8$;
(a) $\omega = 15$ (period-1 motion); (b) $\omega = 18.3$ (phase transition);
(c) $\omega = 20.8$ (multi-period motion); (d) $\omega = 25.8$ (chaotic motion);

3.2 Responses for various pulsating amplitude

In this subsection, the effects of the pulsating amplitude to the dynamic behavior of the simply supported pipe with distributed motion constraints are studied. The pulsating amplitude is chosen to be $\sigma = 0.4$, compared to that in last subsection used as $\sigma = 0.2$. Interesting results have come out in this project. The bifurcation diagrams for the midpoint displacement of the pipe are shown in Fig. 7, as forcing frequency ω is varied. Compared to the bifurcations in Fig. 2, it can be seen from Fig. 7 (a) that the pipe become more stable for the case of $\sigma = 0.4$ when the mean flow velocity takes the value of u_0

926

= 6, and regions of periodic motion is enlarged to a wide range of $0<\omega<44.2$. From Fig. 7 (b), we can see that $\sigma = 0.4$ also expands the stable region of the system of $u_0 = 8$. This may be explained by the fact that, with large pulsating amplitude, the flowing fluid plays an important role of exciting to the system. The pulsating effect becomes more remarkable during the oscillating.
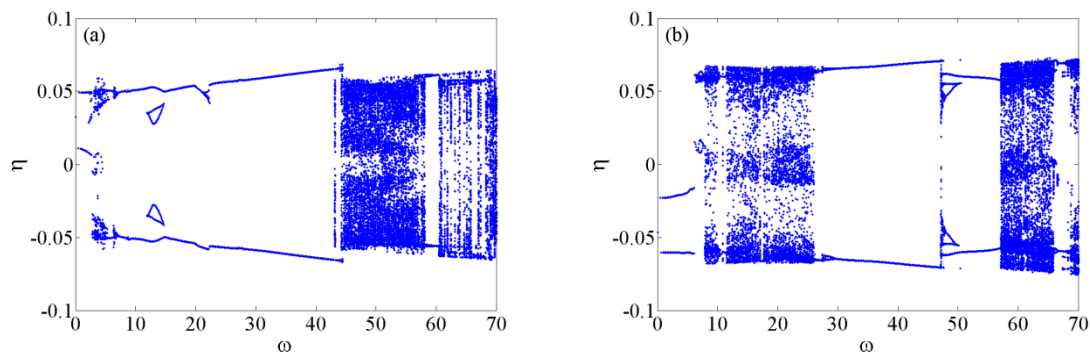

Fig. 7 Bifurcation diagrams of the midpoint displacement of the pipe. (a) $u_0 = 6$; (b) $u_0 = 8$

4. Conclusions

In this paper, the nonlinear dynamics of simply supported pipe conveying pulsating fluid is investigated numerically, by introducing the effect of distributed motion constraint along the pipe axis modeled as trilinear springs. The distributed motion constraint's parameters adopted here are in agreement with experiments. The internal pulsating fluid is assumed to be a harmonic component of flow velocity superposed on a constant mean value. The effects of the pulsating amplitude, forcing frequency and mean flow velocity to the dynamical behavior of the pipe are studied in this project. Interesting results have been obtained by exploring these parameters. It has been shown that the pipe is capable of displaying chaotic motions with various pulsating amplitudes and frequencies under the existing of distributed motion constraints. It ought to be remarked that, all the results obtained in the foregoing are based on the Galerkin method with $N = 4$. It has been proved effective for relatively low pulsating frequencies by Ni Q et al. [26]. However, it is expected that some such results for higher flow velocities and pulsating frequencies, especially for chaos, would also exist in different ranges of the parameter space if higher values of N had been used.

References

1 Paidoussis, M. P. A review of flow-induced vibrations in reactors and reactor components. *Nuclear Engineering and Design*, *74*(1), 31-60 (1983)

2 Chen, S. S. A review of dynamic tube-support interaction in heat exchanger tubes. *Proc. Inst. Mech. Eng., Flow Induced Vibration C*, *416*, 20-22 (1991)

3 Weaver, D. S., Ziada, S., Au-Yang, M. K., Chen, S. S., Paıdoussis, M. P., & Pettigrew, M. J. Flow-induced vibrations in power and process plant components—progress and prospects. *Journal of Pressure Vessel Technology*, *122*(3), 339-348 (2000)

4 Pettigrew, M. J., Sylvestre, Y., & Campagna, A. O. Vibration analysis of heat exchanger and steam generator designs. *Nuclear Engineering and Design*, *48*(1), 97-115 (1978)

5 Chen, S. S. Flow-induced vibration of circular cylindrical structures. *Washington, DC, Hemisphere Publishing Corp., 1987, 487 p. Research supported by AEC, ERDA, and DOE.*, *1* (1987)

6 Paidoussis, M. P. *Fluid-structure interactions: slender structures and axial flow* (Vol. 1). Academic press (1998)

7 Paidoussis, M. P., & Sundararajan, C. Parametric and combination resonances of a pipe conveying pulsating

fluid. *Journal of Applied Mechanics*,*42*(4), 780-784 (1975)

8 Sri Namchchivaya, N. Non-linear dynamics of supported pipe conveying pulsating fluid—I. Subharmonic resonance. *International Journal of Non-Linear Mechanics*, *24*(3), 185-196 (1989)

9 Chen, S. S. Dynamic stability of tube conveying fluid. *Journal of the Engineering Mechanics Division*, *97*(5), 1469-1485 (1971)

10 Paidoussis, M. P., & Issid, N. T. Dynamic stability of pipes conveying fluid. *Journal of sound and vibration*, *33*(3), 267-294 (1974)

11 Ginsberg, J. H. The dynamic stability of a pipe conveying a pulsatile flow. *International Journal of Engineering Science*, *11*(9), 1013-1024 (1973)

12 Ariaratnam, S. T., & Sri Namachchivaya, N. Dynamic stability of pipes conveying pulsating fluid. *Journal of Sound and Vibration*, *107*(2), 215-230 (1986)

13 Sri Namchchivaya, N., & Tien, W. M. Non-linear dynamics of supported pipe conveying pulsating fluid—II. Combination resonance. *International Journal of Non-Linear Mechanics*, *24*(3), 197-208 (1989)

14 Jayaraman, K., & Narayanan, S. Chaotic oscillations in pipes conveying pulsating fluid. *Nonlinear Dynamics*, *10*(4), 333-357 (1996)

15 Chang, C. O., & Chen, K. C. Dynamics and stability of pipes conveying fluid. *Journal of pressure vessel technology*, *116*(1), 57-66 (1994)

16 YOSHIZAWA, M., NAO, H., HASEGAWA, E., & TSUJIOKA, Y. Lateral vibration of a flexible pipe conveying fluid with pulsating flow. *Bulletin of JSME*, *29*(253), 2243-2250 (1986)

17 Panda, L. N., & Kar, R. C. Nonlinear dynamics of a pipe conveying pulsating fluid with parametric and internal resonances. *Nonlinear Dynamics*,*49*(1-2), 9-30 (2007)

18 Panda, L. N., & Kar, R. C. Nonlinear dynamics of a pipe conveying pulsating fluid with combination, principal parametric and internal resonances. *Journal of Sound and Vibration*, *309*(3), 375-406 (2008)

19 Païdoussis, M. P., & Semler, C. Nonlinear and chaotic oscillations of a constrained cantilevered pipe conveying fluid: a full nonlinear analysis. *Nonlinear Dynamics*, *4*(6), 655-670 (1993)

20 Hassan, M. A., Weaver, D. S., & Dokainish, M. A. A new tube/support impact model for heat exchanger tubes. *Journal of fluids and structures*, *21*(5), 561-577 (2005)

21 Wang, L. A further study on the non-linear dynamics of simply supported pipes conveying pulsating fluid. *International Journal of Non-Linear Mechanics*, *44*(1), 115-121 (2009)

22 Xia, W., & Wang, L. The effect of axial extension on the fluidelastic vibration of an array of cylinders in cross-flow. *Nuclear Engineering and Design*, *240*(7), 1707-1713 (2010)

23 Tang, M., Ni, Q., Luo, Y., Wang, Y., & Wang, L. Flow-induced vibration of curved cylinder arrays subject to loose support. *Nonlinear Dynamics*, 1-13 (2014)

24 Jin J D, Song Z Y. Parametric resonances of supported pipes conveying pulsating fluid[J]. *Journal of Fluids and Structures*, 20(6): 763-783 (2005)

25 Hassan, M. A., Weaver, D. S., & Dokainish, M. A. A simulation of the turbulence response of heat exchanger tubes in lattice-bar supports. *Journal of Fluids and Structures*, *16*(8), 1145-1176 (2002)

26 Ni, Q., Zhang, Z., Wang, L., Qian, Q., & Tang, M. Nonlinear dynamics and synchronization of two coupled pipes conveying pulsating fluid. *Acta Mechanica Solida Sinica*, *27*(2), 162-171 (2014)

First observation of Quasi-Chaos in Erbium doped fiber ring laser

S. Zafar Ali

Department of Electrical Engineering, Air University, E-9 Islamabad, Pakistan
email *zafarali@mail.au.edu.pk*

Abstract

This work reports the first numerical evidence of existence of pseudo or quasi-chaos in a loss modulated EDFRL true Additive Chaos Modulation (ACM) scheme, thus possibly adding fifth region of operation in non-autonomous nonlinear systems. Quasi-chaos apparently looks like chaos but actually converges to same time and physical phase space trajectory, even with widely separated initial conditions, behaviour exactly opposite to the basic essence of chaos i.e. sensitive dependence on initial conditions (SDIC). Subject quasi-chaos was earlier believed to be pure chaos since the output passed qualitative visual tests of chaos like aperiodicity in time domain, rich spectral content in frequency domain, direct observation test in phase space, and fast decreasing autocorrelation function. Even quasi-chaos gives positive Lyapunov Exponent (LE), using TISEAN, in time delayed pseudo phase space built by time delaying lasing E field. Thus a complete knowledge of numerical model and driving conditions is a must to validate existence of a pure or quasi-chaos. EDFRL Chaos Message Masking(CMS) configuration is also shown here producing a pure chaos, for comparison, with desired sensitivity to initial conditions, besides passing all above mentioned visual tests of chaos and a positive LE spectrum. Emergence of quasi-chaos will have far reaching implications in chaos applications.

I   Introduction

Chaos is the third most important discovery of 21st century being actively researched in multiple disciplines in theoretical and applied contexts and new aspects of chaos are still forthcoming [1]. An improved knowledge of chaos will help better understanding of various important phenomenon including heartbeat and neuron signals which are inherently chaotic. Optical chaos produced by different types of lasers is a well-researched field which met successful experimental demonstration in Athens [2]. EDFRL shows rich dynamical behaviour and have proven to be a useful platform to study nonlinear dynamics and chaos [3-10] in addition to other practical applications. There are three main schemes for generation of chaos in EDFRL i.e. loop nonlinearities [3], cavity loss modulation [4-9] and pump modulation [10]. The detailed study of chaos generation dynamics of EDFRL with five key parameters i.e. cavity loss, cavity gain, modulation index, pump power and modulating frequency variation was done earlier [4,6], showing how EDFRL switches, with the change of above mentioned control parameters, between four possible regions of operation i.e. periodic, quasi-periodic, stable and chaotic. It was next shown [7] that using square and other complex loss modulating signals the LE of EDFRL chaos increases thereby raising the degree of unpredictability and security. Later [8] it was found that pulsed chaos gives better LE than non-pulsed chaotic oscillations in EDFRL. It was pointed out later [9] that the original EDFRL model with chaos message masking (CMA/CMS) as proposed by Luo [4] and later studied in detail [6] has message signal also being added into the loop which makes it true ACM scheme instead of reported CMA / CMS. The detailed study of effect of message

---

parameters i.e. message frequency, amplitude and phase on EDFRL chaos dynamics therefore became necessary which was carried out in next work [9]. It was shown there [9] that chaos is produced only once the modulating and message frequencies are not integral multiple of each other which shows that the two frequencies interplay with each other to give shown results.

The detailed study carried out in this work was triggered by an unusual observation during simulations that different initial conditions did not produce different chaos as expected but all chaos seemed to be forced to single trajectory. This is a violation of SDIC which is main defining attribute of chaos and therefore this output needs to be termed as something other than chaos, say quasi-chaos, because apparently it behaves like chaos unless numerically subjected to different initial conditions. Negating SDIC in turn negates long term unpredictability. Previously, it was believed and reported [4-9] to be pure chaos because it mimicked all behaviour of chaos and qualifies qualitative tests as well as LE test in time delayed pseudo phase space using TISEAN routines [11]. Once message signal is removed from the loop, EDFRL starts producing pure chaos for same set of parameters and modulating signal.

The paper is organised as follows. Section I is introduction and literature review, followed by Section II which gives mathematical models and optical circuits of both configurations studied in this paper. Section III on simulations shows convergence of quasi-chaos of ACM to same trajectory irrespective of IC and divergence of trajectories in CMS configuration even for small IC deviations. Section IV discusses these simulation results and Section V concludes the results and indicates their implications.

II   Mathematical model

In this section the optical circuits and corresponding mathematical models of loss modulated EDFRL true ACM and true CMA/CMS schemes respectively in Fig.1 and Eq. (1) and (2), 'true' emphasizing their corrected versions [9]. It is obvious from figures and equations that ACM has message sine wave being added into the loop modifying chaos dynamics, as studied in detail [6,9] while CMS is devoid of message and its effects on chaos dynamics.

$$\dot{E}_{LA} = -k_a(E_{LA} - c_a S_{in}) + g_a E_{LA} D_A + \xi_{LA} \qquad (1a)$$

$$\dot{D}_A = -\frac{1}{\tau}[(1 + I_{PA} + E_{LA}^2)D_A - I_{PA} + 1] \qquad (1b)$$

$$k_a = k_{a0}(1 + m_a \sin(\omega_a t)) \qquad (1c)$$

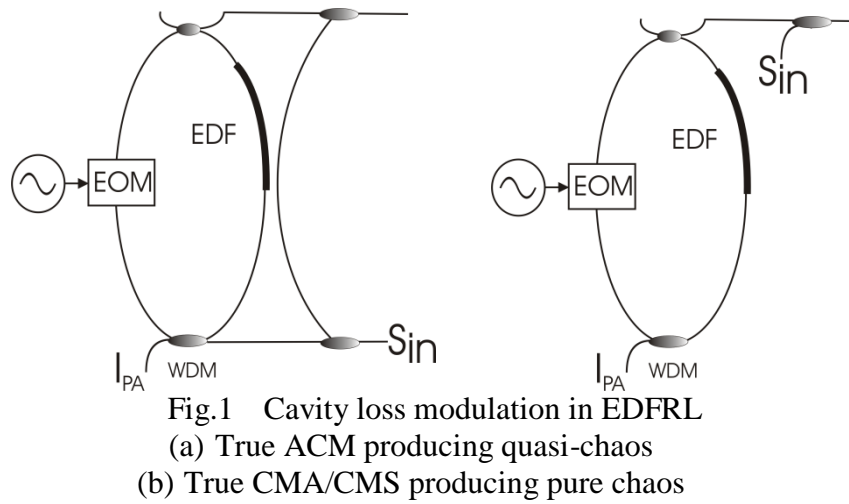$$S_{in} = S_0(1 - m_s \sin(\omega_s t)) \qquad (1d)$$

$$\dot{E}_{LA} = -k_a E_{LA} + g_a E_{LA} D_A + \xi_{LA} \qquad (2a)$$

$$\dot{D}_A = -\frac{1}{\tau}[(1 + I_{PA} + E_{LA}^2)D_A - I_{PA} + 1] \qquad (2b)$$

$$k_a = k_{a0}(1 + m_a \sin(\omega_a t)) \qquad (2c)$$

where "." denotes time derivative, E_{LA} is the lasing field strength, D_A is population inversion density, τ is the of Erbium meta-stable state decay time, ξ_{LA} is the spontaneous emission factor, I_{PA} is the pump power, k_{a0} is the cavity loss (decay rate), g_a is the cavity gain, m_a is the modulation index, ω_a is the angular loss modulating frequency, S_0 is the

message amplitude and ω_s is the message frequency. The various sets of parameters for which chaos is produced is extensively discussed earlier [6].

Fig.1   Cavity loss modulation in EDFRL
(a) True ACM producing quasi-chaos
(b) True CMA/CMS producing pure chaos

The values of model parameters used in simulations in following section are same as early [6] and given in Table.1 below. The only difference is there is no message S_0 in CMS model.

Table 1 EDFRL parameters-default values and range of variation

Parameter	Symbol	Value
Pump power	I_{PA}	10 mw
Modulation index	m_a	0.03
Decay rate	k_{a0}	3.3×10^7
Gain	g_a	6.6×10^7
Message amplitude	S_0	1
Modulating frequency	ω_a	3.5×10^5
Message frequency	ω_s	3.14×10^5
Message Coupling strength	c_a	0.01

III   Simulations results

Fig.2 shows the convergence to same trajectory of differently starting chaotic trajectories in time and phase plots for same set of EDFRL parameters as given in Table.1 as well as driving conditions in loss modulated ACM model. It may be noted that one set of initial conditions i.e. $E_{LA0}=0$ and $D_{A0}=0.47$ is taken as a reference to compare the convergence time of other initial conditions to the reference trajectory. It can be observed in time domain plots of Fig. 2(a) where the initial conditions are $E_{LA0}=12$ and $D_{A0}=0.496$ that it converges to the defined reference trajectory in approx. 0.75 msec. The arrows in time domain mark significantly different amplitudes in the chaotic pulses initially. However, it can be observed that amplitude difference is very small in next pulses after which the two chaotic trajectories converge to same value exactly overlapping in time and phase plots. In Fig. 2(b) once the initial conditions are $E_{LA0}=5$ and $D_{A0}=0.496$, resulting chaos converge to the reference trajectory in about 1.75 msec. It is to be noted that the distance of initial conditions from reference initial conditions is more in Fig. 2(a) than in Fig. 2(b), yet convergence time is

smaller in first figure than the second. Thus the convergence time is not proportional to the distance of initial conditions from the reference initial condition. The arrows in phase plots indicate that the initial conditions for the two waveforms are taken far away from each other yet the red phase plot converges to the green one after few turns in phase plot.
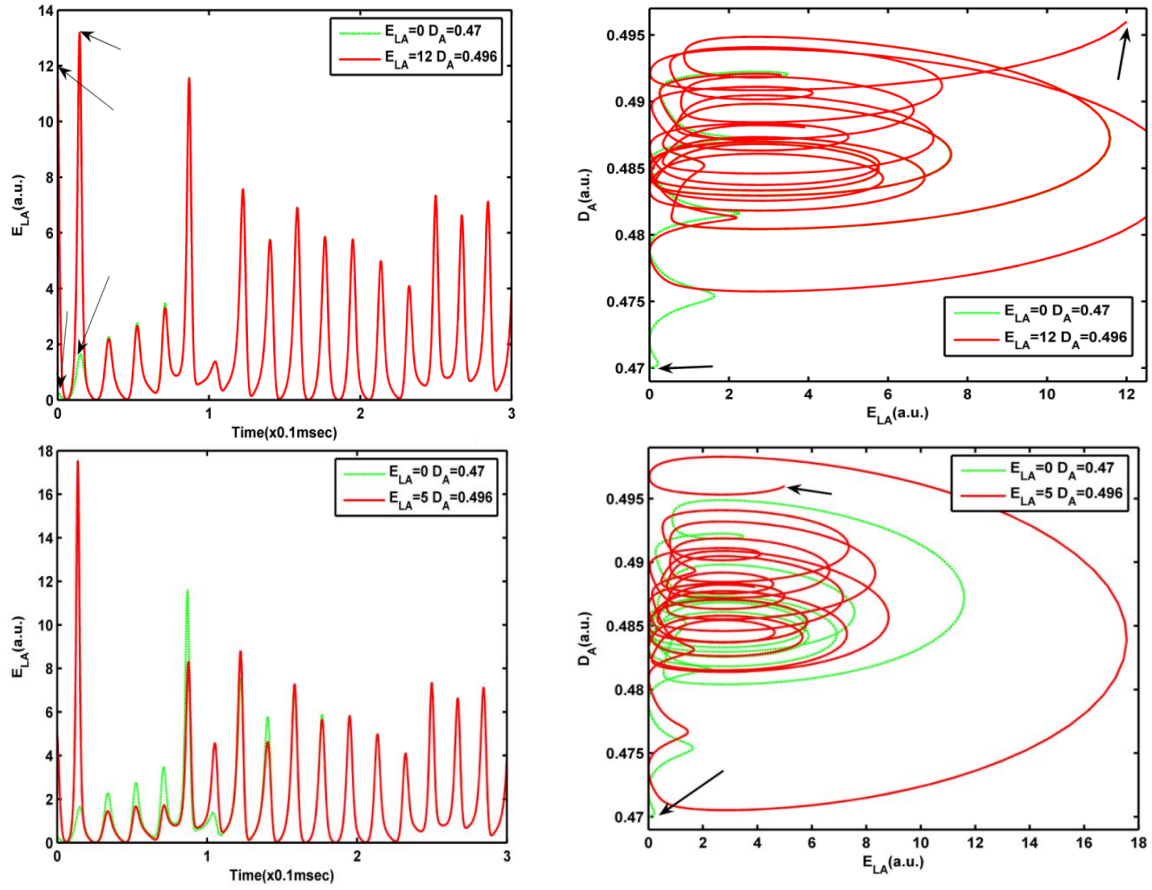

Fig.2   ACM Quasi-chaos convergence for different initial conditions.
(a) $E_{LA}=0$, $D_A=0.47$ (green) and $E_{LA}=12$, $D_A=0.496$ (red)
(b) $E_{LA}=0$, $D_A=0.47$ (green) and $E_{LA}=5$, $D_A=0.496$ (red)

Once convergence of quasi-chaos to same trajectory is established above simulations of the ACM model, the CMS model is simulated next, using Table.1 parameter values again, with different initial conditions to dig for either converging or diverging behaviour with different initial conditions but same parameters eliminating message sine wave. It is found that even slightly varying initial conditions as labelled in Fig.3 time domain plots make the pure chaos diverge in longer run. Also the time of start of divergence of trajectories as marked by arrow in Fig.3 increases with the decrease in difference in initial conditions. The later behaviour is quite as expected for a pure chaos which is SDIC as well as long-term unpredictable.
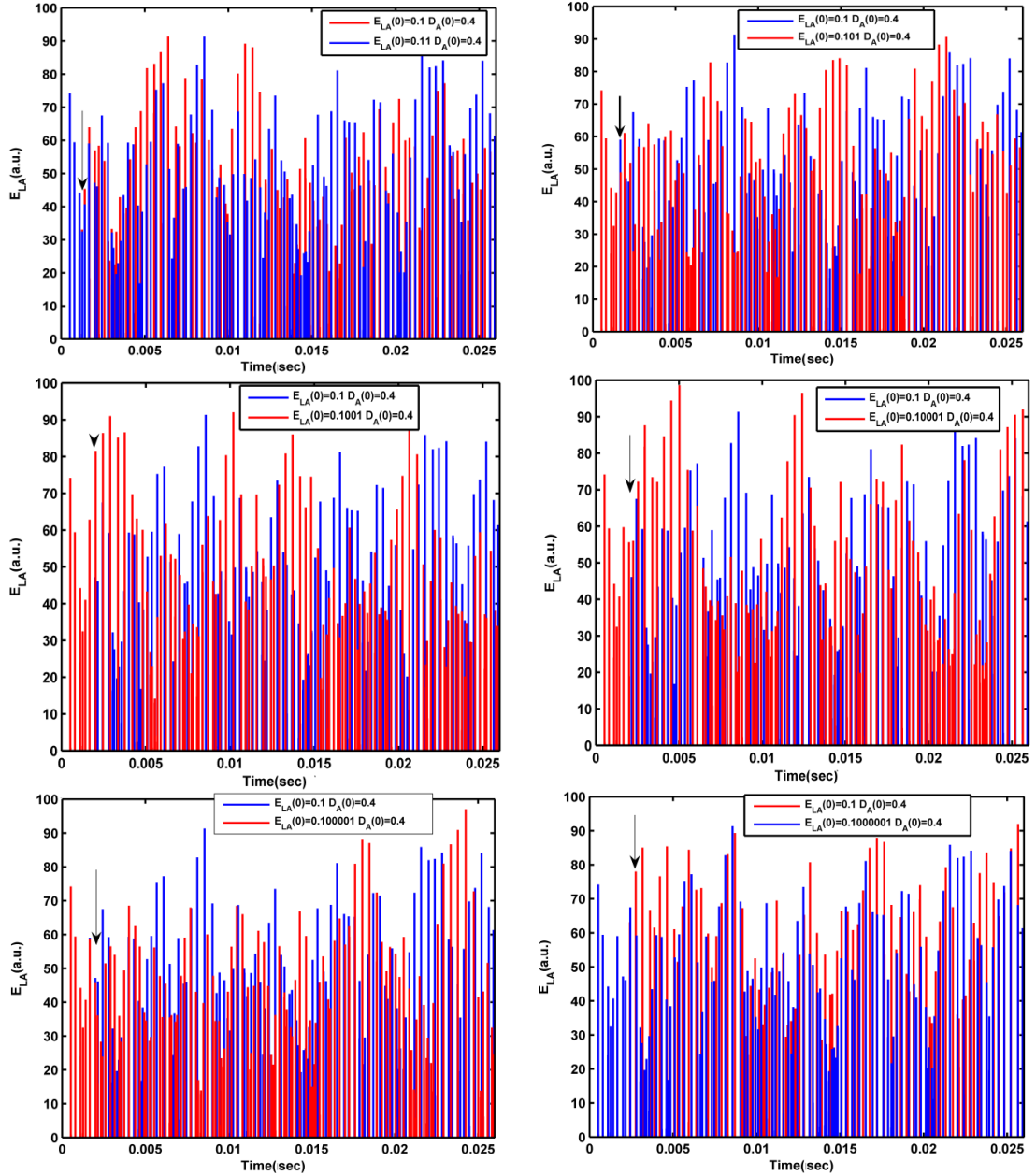

Fig.3   CMS Pure chaos showing SDIC for different initial conditions.
(a) $E_{LA0}=0.1$, $D_{A0}=0.4$ (red) and $E_{LA0}=0.11$, $D_{A0}=0.4$ (blue)
(b) $E_{LA0}=0.1$, $D_{A0}=0.4$ (blue) and $E_{LA0}=0.101$, $D_{A0}=0.4$ (red)
(c) $E_{LA0}=0.1$, $D_{A0}=0.4$ (blue) and $E_{LA0}=0.1001$, $D_{A0}=0.4$ (red)
(d) $E_{LA0}=0.1$, $D_{A0}=0.4$ (blue) and $E_{LA0}=0.10001$, $D_{A0}=0.4$ (red)
(e) $E_{LA0}=0.1$, $D_{A0}=0.4$ (blue) and $E_{LA0}=0.100001$, $D_{A0}=0.4$ (red)

(f) E_{LA0}=0.1, D_{A0}=0.4 (red) and E_{LA0}=0.1000001, D_{A0}=0.4 (blue)

The various plots (time, phase space, frequency, and autocorrelation) are shown in Fig.4 to compare quasi and pure chaos, in left and right coloums, as produced by ACM and CMS configurations respectively with system parameters kept same except elimination of messge in later. The quasi-chaos time plots in Fig.4(a) (left) has pulse time period equal to time period of modulating sine wave while pure chaos plot (on right) is chaotic in time interval as well as pulses amplitude. The pulses in quasi-chaos are bunched while pure chaos has no bunching, while the dynamic range of pure chaos appears better than its counterpart. Fig.4(b) shows the phase space of both chaos and it can be seen that both phase space plots are strange attractors indicating chaos as per direct observation method [6]. The apparent crossing of phase space lines will not be there if time is added as third dimension because the third assumed differential eqaution will be simply t'=1. It can be seen in Fig4.(c) that the phase space of quasi-chaos is less fractal as compared to that of pure chaos. Also quasi-chaos is denser at lower pulse amplitudes while pure chaos is denser at higher pulse amplitudes making phase space plots denser on inner and outer sides respectively. Fig.4(c) shows frequency spectrum of quasi and pure chaos with latter being richer and more random in spectral lines as compared to former. Also the modulating frequency and its harmonics are visible only in the case of quasi-chaos frequecny spectrum because here the pulse repetition time is being decided by modulating signal itself as reported earlier [6] also.The autocorrelation diagrams of both chaos are compared in Fig.4(d) and it is found that pure chaos has a sharper decay of autocorrelation than its counterpart while the autocorrelation function has nonzero lower values in quasi-chaos due to humps beneath pulses in time domain. But above all the most important observation is that quasi-chaos is in fact difficult to detect from the diagrams as shown in Fig.4 till it is discovered by actually testing initial conditions as in this work. Now once it is discovered the clues of quasi-chaos can be outlined, the most important being the fixed time period instead of chaotic time period and visibility of modulating frequency and harmonics in frequency domain.
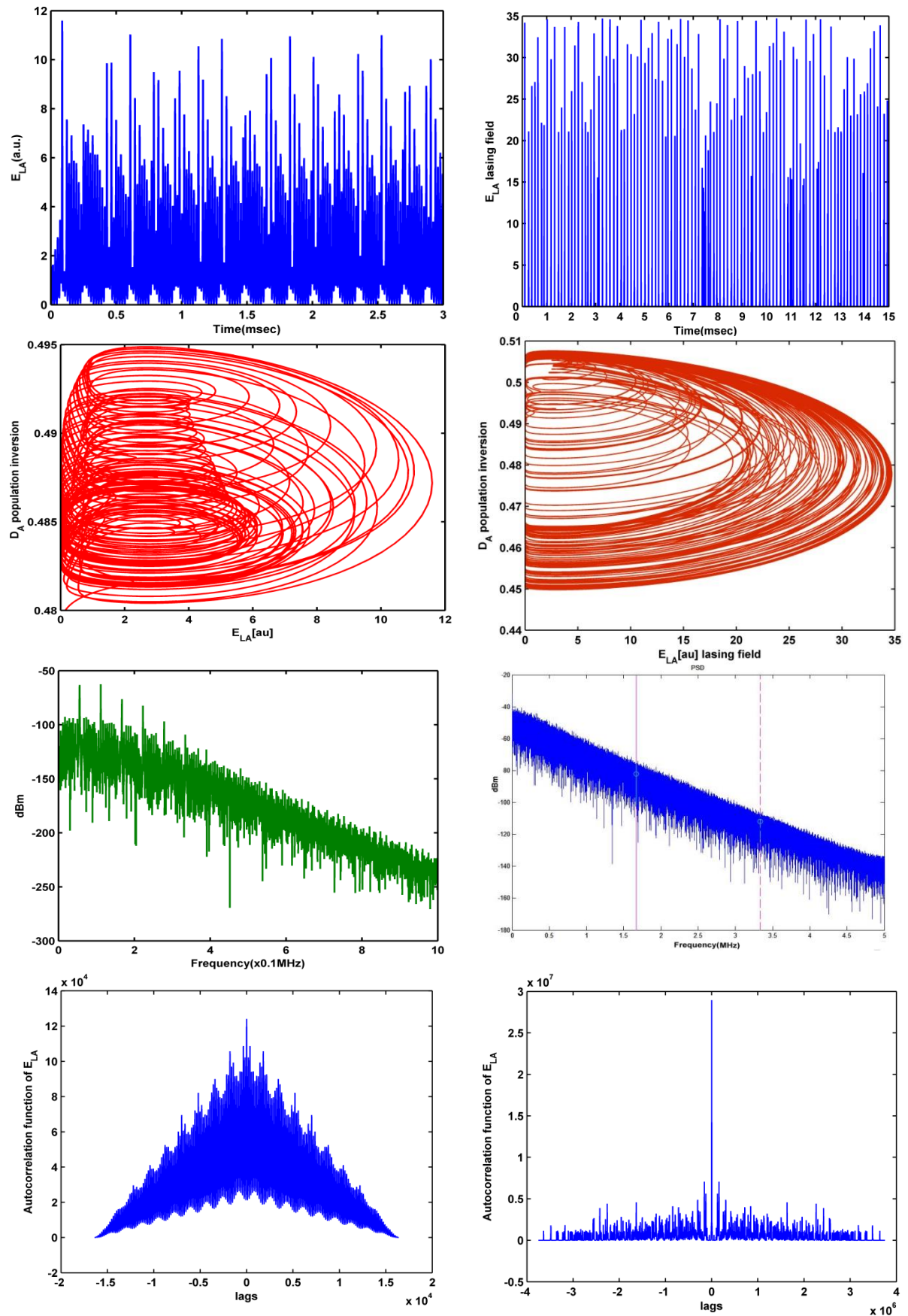
Fig.4　Comparison of quasi-chaos(left) with pure chaos(right) for loss modulation EDFRL
(a) Time domain　　　(b) Phase space (c)　　　Frequency domain (d) Autocorrelation

935

The LE spectrums of quasi chaos generated from ACM and reported earlier for sine[6] and square [7] modulating signals were based on time series analysis of pseudo phase space generated by time delaying E_{LA} lasing. The reason why quasi-chaos also showed positive LE there, is that SDIC is not violated in pseudo time delayed phase space of lasing field. This fact is shown here in Fig. 5 for two such values of time delay (in samples) i.e. tau=2 and tau=5 samples, that these attractors are fractal in nature. Fractal nature of phase space means a strange attractor which shall give positive LE result with TISEAN. It implies that LE calculation using TISEAN is not a sufficient test to differentiate pure chaos from quasi-chaos and subjecting the system to different initial conditions numerically or experimentally is a must.

(a)   **(b)**

Fig.5   Time delayed (tau) pseudo phase plots of quasi-chaos
(a) tau=2   (b) tau=5
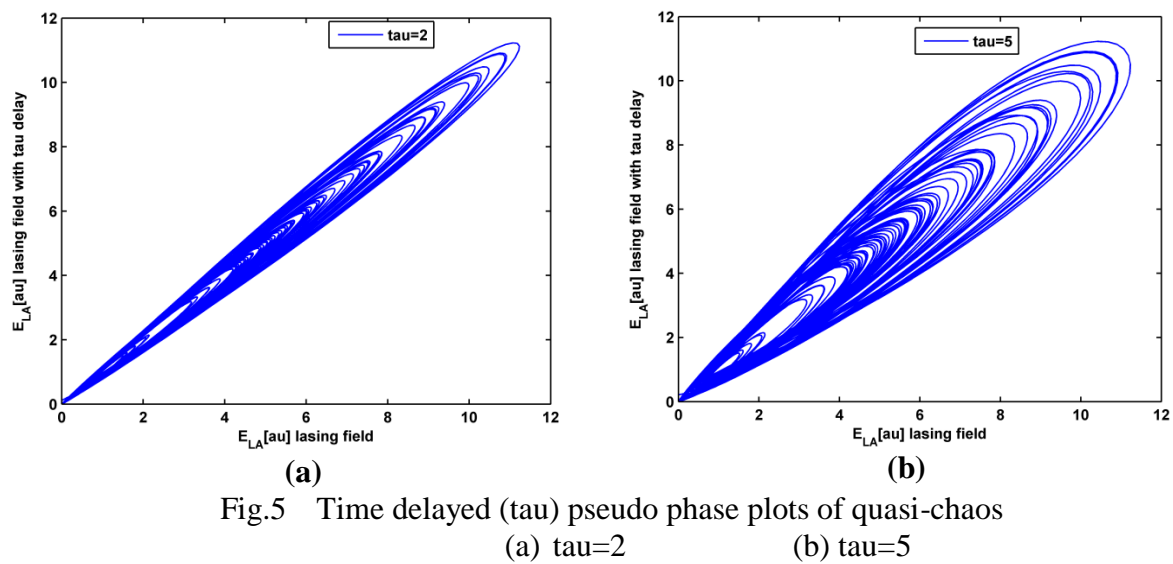
IV.   Discussion

The simulations were carried out to establish the presence of quasi-chaos in ACM and pure chaos in CMS. First it is shown that ACM loss modulated EDFRL produces an apparent chaos which converges to single trajectory making it a quasi- instead of a pure chaos. It is also observed for quasi-chaos that convergence time is not strictly dependent on deviation of initial conditions. As soon as the message is removed to reconfigure it as CMS, keeping all other parameters same including loss modulating sine wave, the convergence is immediately replaced by divergence of pure chaos trajectories. This divergence of trajectories is observed even for very small deviations in initial conditions as is expected for a pure chaos. It is noted that the time for the start of this divergence decreases with the increase in deviation of initial conditions, also as expected. Hence it is indicated that message signal is adding an extra periodic perturbation in the cavity which is interacting with the multiplicative perturbation of loss modulating sine wave, thus producing quasi instead of pure chaos. Next the LE spectrums of quasi and pure chaos are calculated using time series analysis with well-known TISEAN routines and plotted side by side. Most surprisingly, quasi-chaos gives positive LE since TISEAN uses time delayed pseudo phase space of lasing E field. The time delayed phase space is found fractal for two time delays. Thus LE calculation using time series analysis by TISEAN is not a sufficient test to identify pure chaos as shown in this study, because it misjudges quasi-chaos in EDFRL also as pure chaos. The most valid test of chaos is physically subjecting the system or its numerical model to different initial conditions and look for either convergence or divergence of trajectories for quasi and pure chaos respectively. This observation of pseudo or quasi chaos adds fifth region of operation in

nonlinear systems; the other well-known four regions being periodic, quasi-periodic, stable and chaotic already reported and studied in detail for loss modulated EDFRL [6].

V. Conclusions

This work was motivated by an unusual observation of converging behaviour in temporal and physical phase space of apparently chaotic trajectories, for different initial conditions, in ACM loss modulated EDFRL. Such behaviour is totally new and cannot be categorised as any of four known modes of operation in nonlinear systems i.e. periodic, quasi-periodic, stable and chaos. Therefore, it is termed as quasi-chaos, as it looks like chaos, but violates the basic definition of chaos i.e. sensitive dependence on initial conditions. The findings here confirm the presence of convergence to same quasi-chaotic trajectories even for very widely separated initial conditions. Previously, this output from this EDFRL configuration was considered to be pure chaos since the output passed all qualitative visual tests of chaos; like aperiodicity in time domain, rich spectral content in frequency domain, direct observation test in phase space, and fast decreasing autocorrelation function. In this work all above plots are placed side by side for making comparisons between pure and quasi-chaos. However, EDFRL quasi-chaos surprisingly gives positive lyapunov exponents with TISEAN; as TISEAN routines are based on time delayed pseudo phase space of observed time series data, which is found fractal in this work, for the lasing E field. At the same time, it in no case implies that loss modulation scheme in EDFRL is not capable of producing a pure chaos. For comparison purposes, EDFRL is also shown to be able to produce a pure chaos, just by eliminating the message from the loop (CMS scheme), exhibiting desired sensitivity to minute changes in initial conditions. Pure chaos, as expected, passes all above mentioned visual tests of chaos and also giving positive LE using TISEAN. The only main test of quasi-chaos is thus numerically subjecting the system model to different initial conditions.

This is an important discovery which has five main implications on chaos theory and its engineering applications. Firstly, a complete knowledge of numerical model and driving conditions is a must to validate existence of either pure or quasi-chaos. Secondly, finding quasi-chaos would not be possible in an experimental work on EDFRL, because of inaccessibility of population inversion initial condition. Secondly, fractal nature of time delayed pseudo phase space is responsible for positive lyapunov exponent calculations, using TISEAN, misinterpreting quasi-chaos as pure chaos in earlier works. Fourth, chaos synchronisation of quasi-chaotic systems is also artificial i.e. ACM EDFRL receiver is in fact not synchronised to corresponding transmitter because of any seed being fed, since both outputs readily get converged to same trajectory, independent of their initial conditions, in reality, due to their quasi-chaotic nature. Fifth, pure chaos will always prove as chaos in qualitative and quantitative tests, but quasi-chaos will spoof itself as pure chaos until complete model is available for trying different initial conditions; output time series shall not be the only thing available. Other possible implications of this discovery are presently under study and will be reported shortly.

VI. References

1. M. Virte, K. Panajotov, H. Thienpont and M. Sciamanna, "Deterministic polarization chaos from a laser diode" Nat. Photonics, **7**(1) ,60-65 (2013).

2. A. Argyris, D. Syvridis, L. Larger, V. A. Lodi, P. Colet, I. Fischer, J. G. Ojalvo, C. R. Mirasso, L. Pesquera and K. A. Shore, "Chaos-based communications at high bit rates using commercial fibre-optic links", Nature, **438** (17),343-346(2005).

3. H. D. I. Abarbanel, M. B. Kennel, M. Buhl and C. T. Lewis, "Chaotic Dynamics in Erbium-doped fiber ring lasers", Phy. Rev. A, **6**(3), 2360-2374(1999).

4. L. G. Luo and P. L. Chu , "Optical secure communications with chaotic Erbium doped fiber lasers", J. Opt. Soc. Am. B, **15**(10), 2524-2530 (1998).

5. Y. Imai, H. Murakawa and T. Imoto, "Chaos synchronisation characteristics in Erbium-doped fiber laser systems", Opt. Commun., **217**(1-6), 415-420 (2003).

6. S. Z. Ali, M. K. Islam and M. Zafrullah "Effect of Parametric variation on generation and enhancement of chaos in erbium-doped fiber-ring lasers" Opt. Engg., **49**(10), 105002-1-12(2010).

7. S. Z. Ali, M. K. Islam and M. Zafrullah "Generation of higher degree Chaos by controlling harmonics of the modulating signal in EDFRL", Optik **122**(21) , 1903-1909 (2011).

8. S. Z. Ali, M. K. Islam and M. Zafrullah "Comparative Analysis of Chaotic Properties of Optical Chaos Generators", Optik **123**(11), 950-955 (2012).

9. S. Z. Ali, M. K. Islam and M. Zafrullah, "Effect of message parameters in additive chaos modulation in Erbium Doped Fiber Ring Laser ", Optik **124**(18), 3746-3750 (2013).

10. A. N. Pisarchik, A. V. Kir'yanov and Y. O. Barmenkov "Dynamics of an Erbium-doped fiber laser with pump modulation : theory and experiment" J. Opt. Soc. Am., **22**(10), 2107- 2114 (2005).

11. R. Hegger, H. Kantz, and T. Schreiber*, "Practical implementation of nonlinear time series methods: The TISEAN package "*, Chaos **9**(2), 413-435(1999).

Second Observation of Quasi-Chaos in Erbium doped fiber ring laser

S. Zafar Ali

Department of Electrical Engineering, Air University, E-9 Islamabad, Pakistan
email zafarali@mail.au.edu.pk

Abstract

This numerical investigation is motivated by the exciting recent discovery of quasi-chaos, in loss modulated erbium doped fiber ring laser (EDFRL), which looks like chaos but converges to single trajectory for widely separate initial conditions in physical phase space. Both pure and quasi-chaos are generated in pump modulated EDFRL using chaos message masking and additive chaos modulation configurations respectively, for comparison in different domains. Quasi-chaos has chaotic amplitude in time domain, rich spectral content in frequency domain, fractal physical phase space, and fast decreasing autocorrelation function. Sensitive dependence on initial conditions is numerically tested for both these chaos, with pure chaos diverging even for minute deviations while quasi-chaos converging even for extreme values of initial conditions. Lyapunov exponent of quasi-chaos, calculated with TISEAN, however, are still positive, as TISEAN works on time delay embedded phase space of single variable, which is shown fractal here. Quasi-chaotic pulses are periodic in time and chaotic in amplitude, with bunching of sub-pulses into super pulses with respective fixed periods. Quasi-chaos cannot be used for secure communication and experimental outputs in forced chaotic oscillators under noisy conditions need careful analysis. This evidence marks the confirmation of existence of fifth region of operation in nonlinear systems.

Keywords:
    Quasi-chaos, Nonlinear dynamics of fiber laser, Pump modulation.

I   Introduction

Chaos, quantum mechanics and theory of relativity are widely accepted as the three most important discoveries of 21st century. Chaos, which is mainly identified by its sensitive dependence on initial conditions, is a ubiquitous phenomenon in many nonlinear systems fulfilling Poincare Bendixon's criteria. The application of optical chaos in secure optical communication has reached successful results in Athens experiment [1] and yet new exciting aspects of optical chaos are being discovered [2, 3]. Optical chaos in EDFRL can be produced both in autonomous manner [4] and by periodic perturbations as in loss modulation [5-6] and pump modulation [7-14]. Recently quasi-chaos was discovered [3] in loss modulated EDFRL, which looked like chaos in time, frequency, phase space and autocorrelation signatures but violated the basic criteria of chaos i.e. sensitive dependence on initial conditions (SDIC) once the system, is numerically subjected to different initial conditions. Until first discovery [3] of quasi-chaos, nonlinear systems were earlier known to exhibit only four regions of operation i.e. chaos, periodic, stable and quasi-periodic with switching of regions being determined by the tuning of parameters and driving conditions.

There are three message encoding configurations possible in each of three mentioned schemes in EDFRL i.e. additive chaos modulation (ACM) where message gets entered into

laser rate equations, chaos message masking (CMS) where message is not part of rate equations and is added in the last and chaos shift keying (CSK) where one parameter is switched with data. The message encoding scheme of loss modulated EDFRL reported earlier [5] as chaos message masking (CMS) was latter [6] corrected to be additive chaos modulation (ACM) scheme. The effect of message parameters (message frequency, amplitude and phase) on EDFRL chaos dynamics was studied in detail [6] and it was shown that one necessary condition of chaos generation is that message and modulating sine waves frequencies are not integral multiples of each other. However, the recent paper [3] has proven that the behaviour earlier identified as pure chaos in EDFRL ACM scheme [5,6], was in fact quasi-chaos, because it straightaway violates sensitive dependence on initial conditions. However, surprisingly it still looks like chaos in several domains and even renders positive lyapunov exponent using TISEAN [15]. The reason for this anomaly was identified [3] was the fractal nature of time-delayed embedded phase space of lasing field intensity. It was also shown [3] that in order to produce pure chaos, message had to be completely eliminated from EDFRL. Therefore, the factor responsible for generation of quasi chaos was the interplay of message and loss modulating frequencies within the laser cavity.

EDFRL pump modulation scheme shall be the next logical candidate for tracing the signs of quasi-chaos, because it is the next forced configuration of EDFRL which produces chaos. We will investigate both message encoding schemes i.e. chaos message masking and additive chaos modulation for generation of pure and quasi-chaos respectively, in the same stepwise manner as done earlier [3] in loss modulation scheme. We will specifically inspect the convergence of trajectories to same path in quasi-chaos for widely separated initial conditions. We shall also carry out all qualitative tests and quantitative test of lyapunov exponent calculation on both chaos and evaluate the results. Once quasi-chaos is proven discovered second time here, it will be safe to assume that it is a ubiquitous phenomenon in all forced chaotic generators under similar conditions as identified earlier [3] and revalidated here. The paper is organised as follows. Section I provides introduction and literature review, followed by Section II mentioning the mathematical models and optical circuits of both configurations studied in this paper. Section III shows simulations and section IV discusses these results. Section V concludes the results and indicates their implications in research.

II   Mathematical model

In this section the optical circuits and corresponding mathematical models of pump modulated EDFRL CMS and ACM schemes in Fig.1 (a)-(b) and Eq. 1(a)-(c) and Eq. 2 (a)-(d) respectively, the basic model adapted from Luo[14]. It is obvious from Fig.1 (a) and Eq.(1) that message is not part of loop dynamics and is added in the last to the chaos generated by loop in CMS. However, it can be seen in Fig. 1(a) and Eq.(2) that ACM has message sine wave is being added into the loop thus modifying chaos dynamics.

$$\dot{E}_{LA} = -k_{a0}E_{LA} + g_a E_{LA} D_A + \xi_{LA} \qquad (1a)$$

$$\dot{D}_A = -\frac{1}{\tau}[(1 + I_{PA} + E_{LA}^2)D_A - I_{PA} + 1] \qquad (1b)$$

$$I_{PA} = I_{PA0}(1 + m_a \sin(\omega_a t_a)) \qquad (1c)$$

$$\dot{E}_{LA} = -k_a(E_{LA} - c_a S_{in}) + g_a E_{LA} D_A + \xi_{LA} \qquad (2a)$$

$$\dot{D}_A = -\frac{1}{\tau}[(1 + I_{PA} + E_{LA}^2)D_A - I_{PA} + 1] \qquad (2b)$$

$$I_{PA} = I_{PA0}(1 + m_a \sin(\omega_a t_a)) \qquad (2c)$$

$$S_{in} = S_0(1 - m_s \sin(\omega_s t)) \qquad (2d)$$

where "." denotes time derivative, E_{LA} is the lasing field strength, D_A is population inversion density, τ is the of Erbium meta-stable state decay time, ξ_{LA} is the spontaneous emission factor, I_{PA} is the pump power, k_{a0} is the cavity loss (decay rate), g_a is the cavity gain, m_a is the modulation index, ω_a is the angular loss modulating frequency, S_0 is the message amplitude, c_a is the coupling strength of message and ω_s is the message frequency.
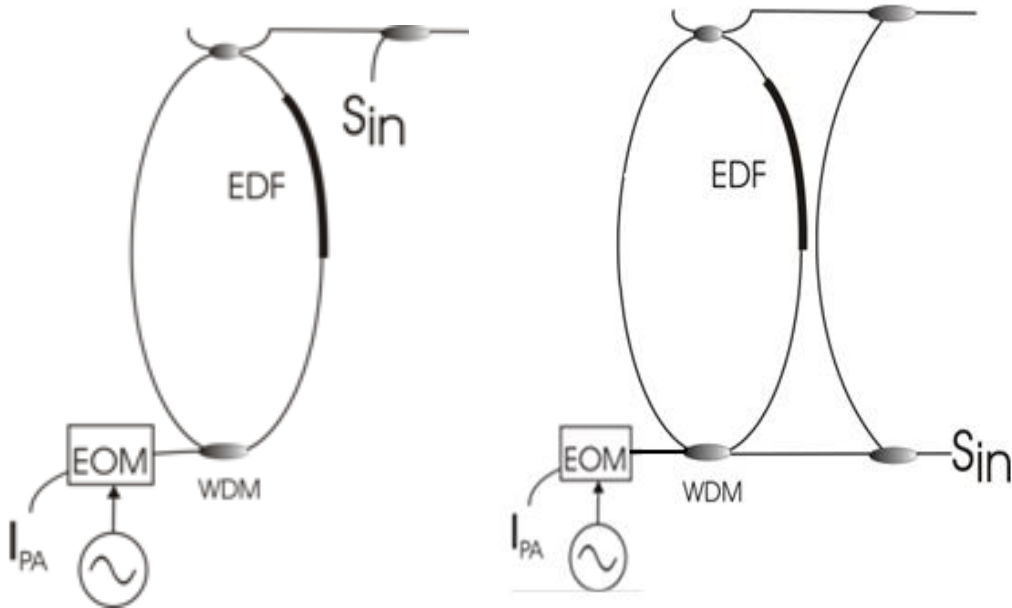

Fig.1   Pump modulation in EDFRL
(a) Chaos message Masking
(b) Additive Chaos Modulation

The values of model parameters used in simulations in following section are given in Table.1 below are same for CMS and ACM configurations except the last two are present in latter only. The numerical integration is performed using fourth order Runge-Kutta method with a step size of 10 nsec, in all simulations here, to ensure best accuracy of results. It may also be mentioned here that E_{LA0} and D_{A0} are the initial conditions for lasing field intensity and population inversion density here. The dynamic range is 0 to 150 a.u. for E_{LA0} and -1 to 1 for $D_{A0.}$

Table 1 Pump modulated EDFRL parameters for ACM and CMS

Parameter	Symbol	Value
Decay time metastable state	T	10 ms
Spontaneous emission factor	ξ_{LA}	10^{-4}
Pump power	I_{PA0}	20 mW
Modulation index	m_a	0.94
Cavity loss / Decay rate	k_{a0}	6.46×10^6
Pump Modulation frequency	ω_a	$2\pi \times 9 \times 10^3$
Message frequency	ω_s	$2\pi \times 3.1919 \times 10^3$
Message Amplitude	S_0	1
Coupling ratio	c_a	0.02

III   Simulations results

Initially the CMS model of Eq.1(a)-(c) is simulated using parameters as given in Table.1. The results are plotted in Fig. 2 for minutely varying initial conditions with Fig.2 (a) taken as reference i.e. E_{LA0}=0 and D_{A0}=0.47. E_{LA0} is kept at zero and D_{A0} is varied to 0.470001, 0.47001 and 0.4701 in Fig.2 (b)-(d) and the point of change in chaos signature with reference to Fig.2 (a) is marked by an arrow in last three diagrams. There are two important observations made here Firstly, the chaos outputs are different in all figures, even for the smallest change of 10^{-6} in D_{A0} in Fig.2 (b) which is quite in line with SDIC and is as expected for a pure chaos. Secondly, the starting time of change in chaos as marked by arrow shifts to right with the gradual increase in difference of D_{A0} from value of 0.47 which is again as expected. Both of these observations are well known for a pure chaos and are responsible for its long-term unpredictability.
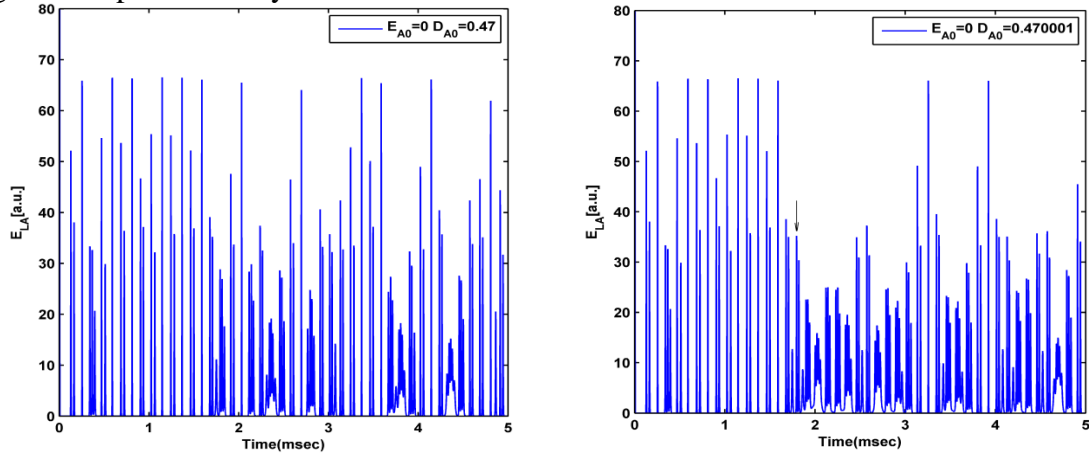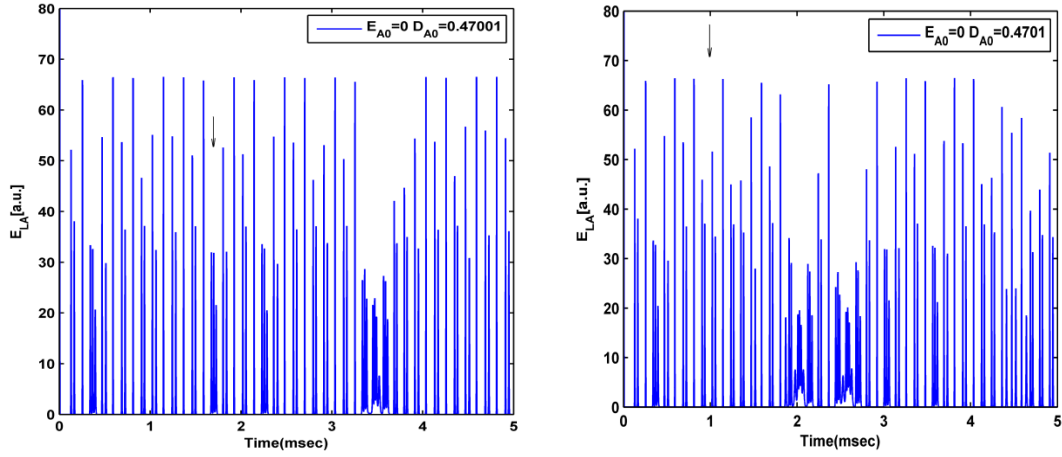
Fig.2   Pure chaos sensitivity to initial conditions.
(a) E_{LA0}=0, D_{A0}=0.47
(b) E_{LA0}=0, D_{A0}=0.470001
(c) E_{LA0}=0, D_{A0}=0.47001
(d) E_{LA0}=0, D_{A0}=0.4701

The ACM model as given in Eq.2(a)-(d) is simulated using same parameters as for CMS except for the addition of message signal in the loop as per Table.1 Quasi-chaos is observed this time with different chaos like time domain plots converging to single trajectory for largely varied values of both E_{LA0} and D_{A0}. D_{A0} is kept at 0.5 and E_{LA0} is changed at four different values i.e. 0, 40, 80 and 120 and result plotted at two time scales in Fig.3 (a) and (b). E_{LA0} is kept at 0 and D_{A0} is changed at four different values i.e. 0.5, 1,-0.5 and -1 and results plotted at two time scales in Fig.3 (c) and (d). It can be observed in all these four figures that the output converges to same trajectory for all these values which is exactly opposite to pure chaos behaviour, which is well known and just seen in CMS simulation. It is to be noted here that chaos outputs are observed here to be more sensitive to D_{A0} changes as compared to E_{LA0} because latter has a smaller scale of variation. However, the output still converges despite using extreme possible values of both E_{LA0} and D_{A0} which proves convergence for all smaller values of initial conditions. Moreover, the results are shown till 2msec only for clarity of diagrams but the convergence is tested to persist till 20 msec once it is achieved. It is believed that convergence will persist forever once achieved. The time of convergence is maximum for E_{LA0} = 80 in Fig. 2(a) and (b) ; not for E_{LA0} = 120 as could be speculated. However, it increases with absolute increase in deviation of D_{A0} from reference D_{A0}=0.5, with D_{A0}=-1 taking longest convergence time of 0.55 msec in Fig. 2(c) and (d).
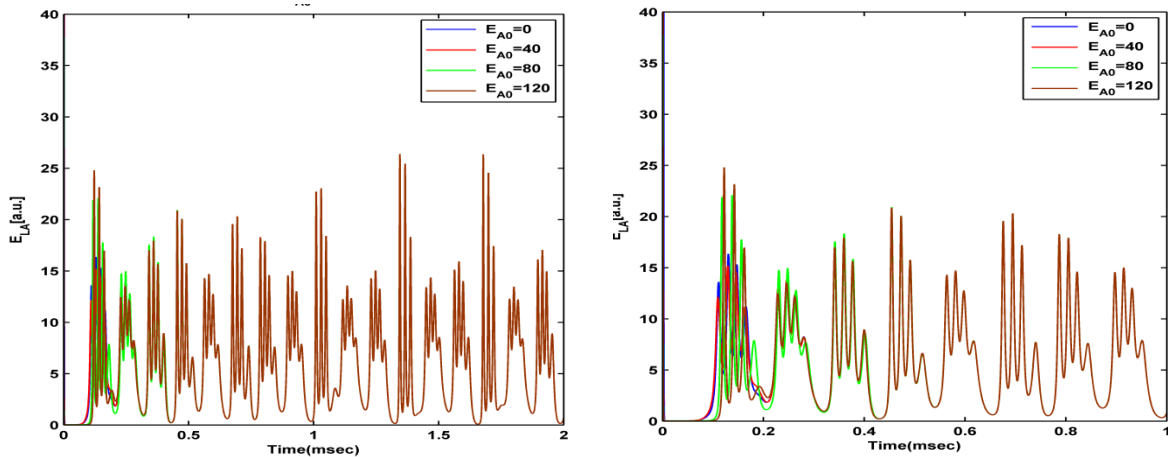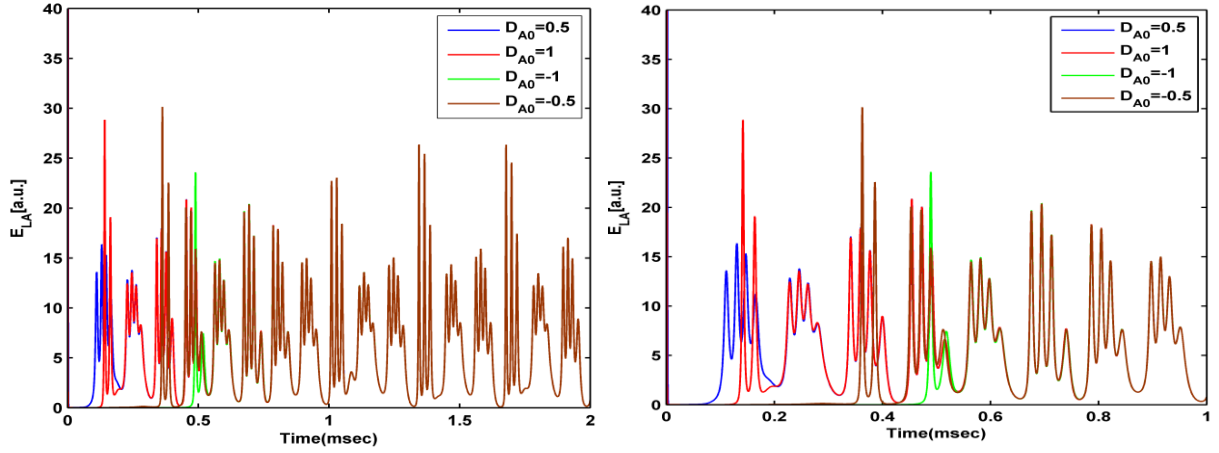
Fig.3   Convergence of quasi-chaos trajectories for different initial conditions.
(a) E_{LA0}=0, E_{LA0}=40, E_{LA0}=80, E_{LA0}=120 and D_{A0}=0.5 (2msec)
(b) E_{LA0}=0, E_{LA0}=40, E_{LA0}=80, E_{LA0}=120 and D_{A0}=0.5 (1msec)
(c) D_{A0}=0.5, D_{A0}=1 D_{A0}=-1 D_{A0}=-0.5 and E_{LA0}=0 (2msec)
(d) D_{A0}=0.5, D_{A0}=1 D_{A0}=-1 D_{A0}=-0.5 and E_{LA0}=0 (1msec)

The time, phase space, frequency, and autocorrelation plots are shown in Fig.4 (a) to (d) for quasi and pure chaos, with system parameters kept same in ACM and CMS, except addition of messge in former. The time domain plot of quasi-chaos here is having super pulses with bunches of sub pulses, both being Gaussian, with super pulses being periodic in time but chaotic in amplitude. The time period of sub-pulses is decided by the pump modulating frequency i.e. 9 kHz and there are three to four sub-pulses in every super pulse. Another way of looking at this chaos is considering them as periodic bunches of chaotic Gaussian pulses with humps underneath as reported earlier for loss modulation [5]. The pure chaos has independent Gaussian pulses with no humps underneath and sometimes two or three pulses seem getting merged together due to chaotic timing of pulses themselves. One important indicator of pure pulsed chaos is that it is chaotic in time as well as amplitude while quasi-chaos is chaotic in amplitude only and super and sub pulses are not chaotic in their respective time periods. Each loop in phase space corresponds to a gaussian pulse in time domain. The phase space of quasi-chaos is almost uniformly distributed as the pulses amplitude spreads over a bigger dynamic range. The phase space of pure chaos is spread uniformly on lower amplitudes and then on higher apmplitudes with a gap owing to its tiemporal signature. Also the DC component and the modulating frequency of 9 kHz are prominent lines in both frequency spectrums, but harmonics of 9kHz are more prominent in quasi-chaos frequecny spectrum, since the pulse repetition time of quasi-chaos sub-pulses is fixed and is being determined by modulating signal as reported earlier also [6]. The frequency of super pulse and its harmonics is also visble in quasi-chaos spectrum. The pure chaos spectrum is otherwise relatively flatter and richer due to variable chaotic time of pulses. The pure chaos autocorrelation diagrams of both chaos are has a sharper decay like early while the quasi-chaos autocorrelation function has nonzero lower values in due time domain. The fixed time period of chaotic pulses, super and subpulses or bunching and humps and visibility of modulating frequency harmonics in frequency domain are some clues of quasi-chaos revalidated here. There is no fixed linear relationship between delta of initial conditions and time of convergence of trajectories to same trajectory in quasi-chaos.
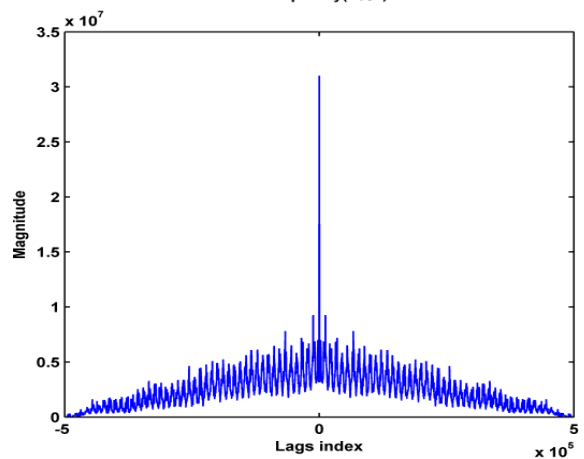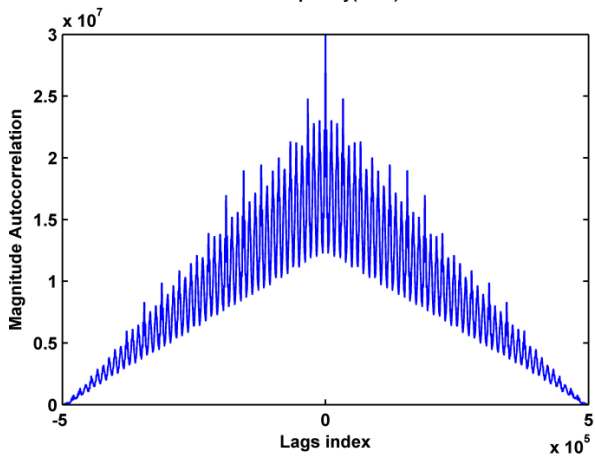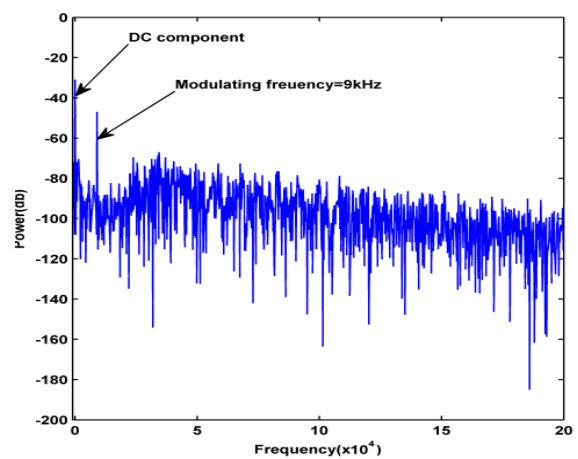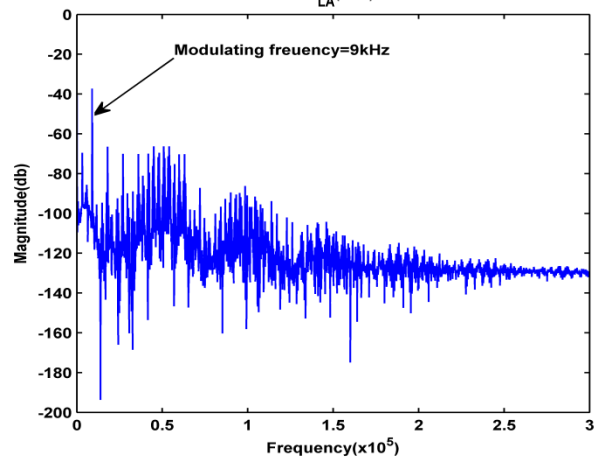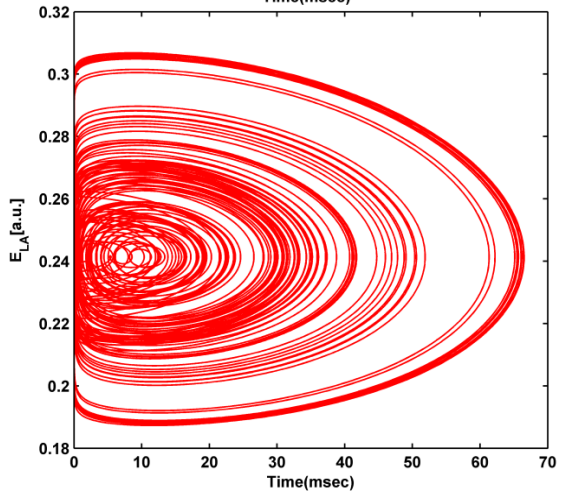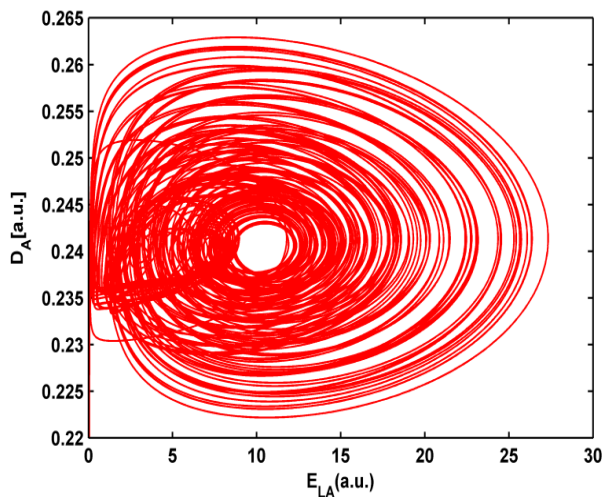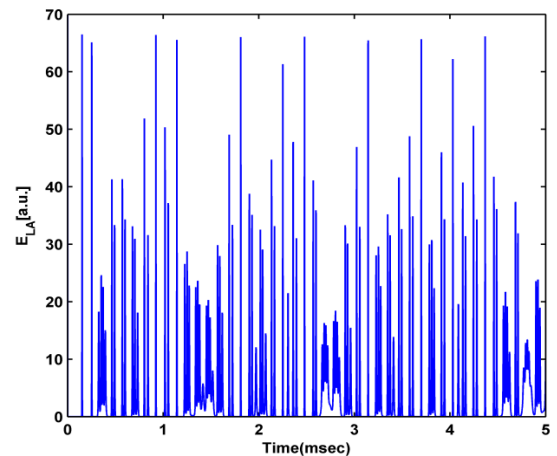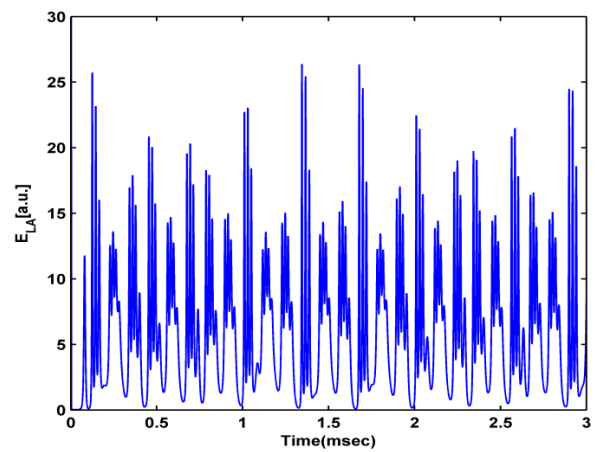
The time delayed embedded plots of $E_{LA}(t)$ vs $E_{LA}(t-\tau)$ are shown for different values of time delay τ for quasi-chaos and pure chaos in Fig.5 and 6 respectively with two important observations to be made. Firstly, both of these plots are fractal in nature and the degree of correlation between $E_{LA}(t)$ and $E_{LA}(t-\tau)$ decreases with the increase in τ in both figures. Secondly, the degree of correlation is lesser in pure chaos as compared to quasi-chaos for corresponding values of τ because randomness and degree of unpredictability is higher in pure chaos. The latter observation is further validated by LE spectrum calculation of both chaos using TISEAN, a well-known routines pack available. We get positive LE for both these types of chaos as shown in Fig.7 (a) and (b) with LE for pure chaos being significantly higher than quasi-chaos which is as expected. This proves that time delayed method of LE calculation will not differentiate between quasi and pure chaos. The only way to identify quasi-chaos is numerically simulating the system with different initial conditions and seeing the time domain plots or physical phase space or physically subjecting the system to different initial conditions if these are accessible in experimental works.

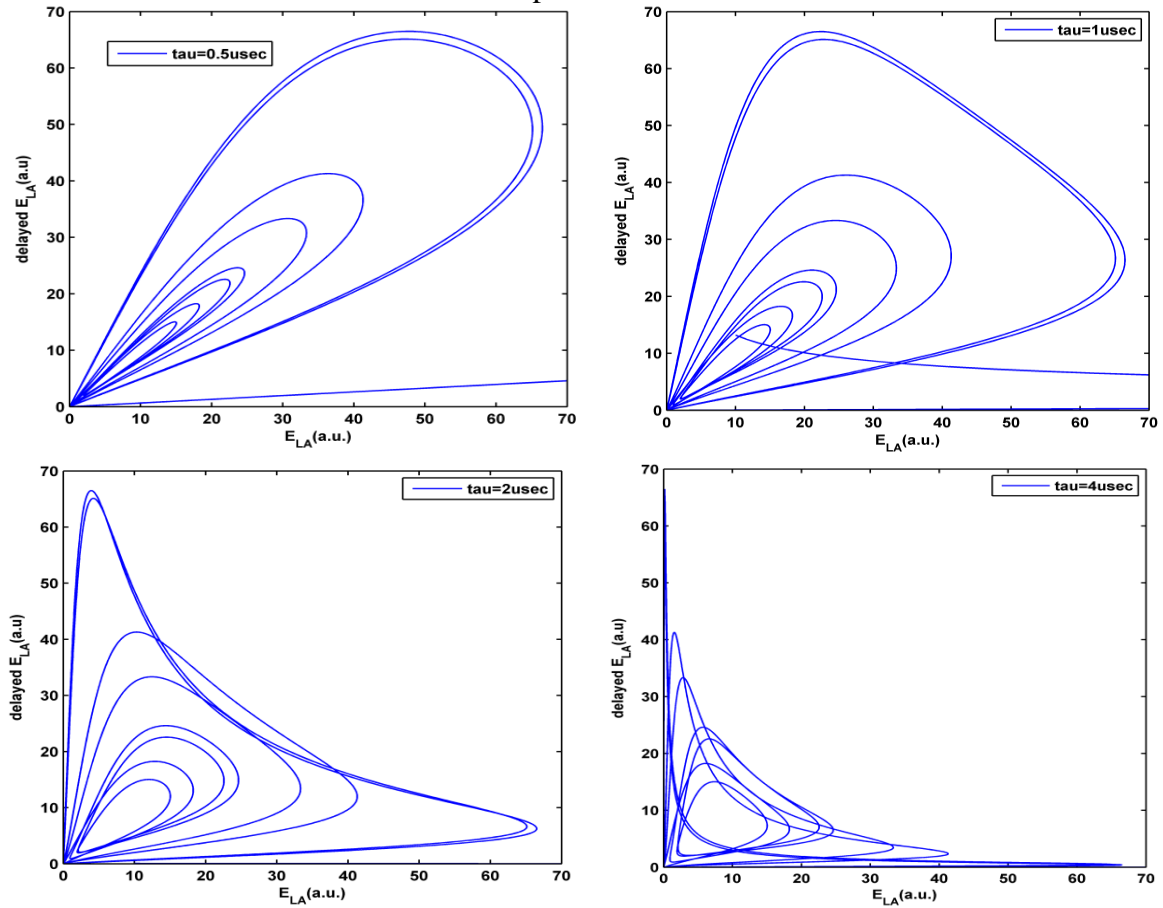

Fig.5   Pure chaos time delayed phase plots
(a) $\tau = 0.5$ usec   (b) $\tau = 1$ usec (c) $\tau = 2$ usec   (d) $\tau = 4$ usec
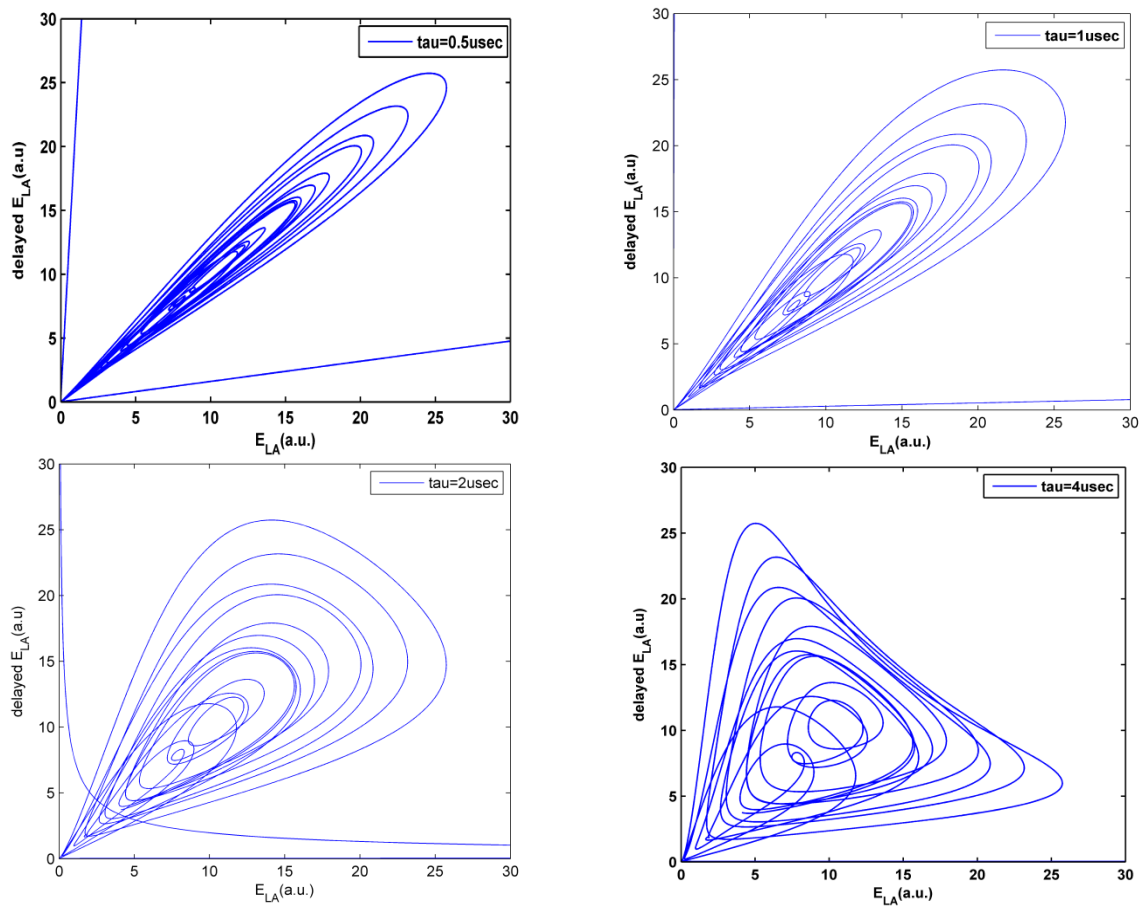
Fig.6   Quasi-chaos time delayed phase plots

(a) $\tau = 0.5$ usec   (b) $\tau = 1$ usec   (c) $\tau = 2$ usec   (d) $\tau = 4$ usec
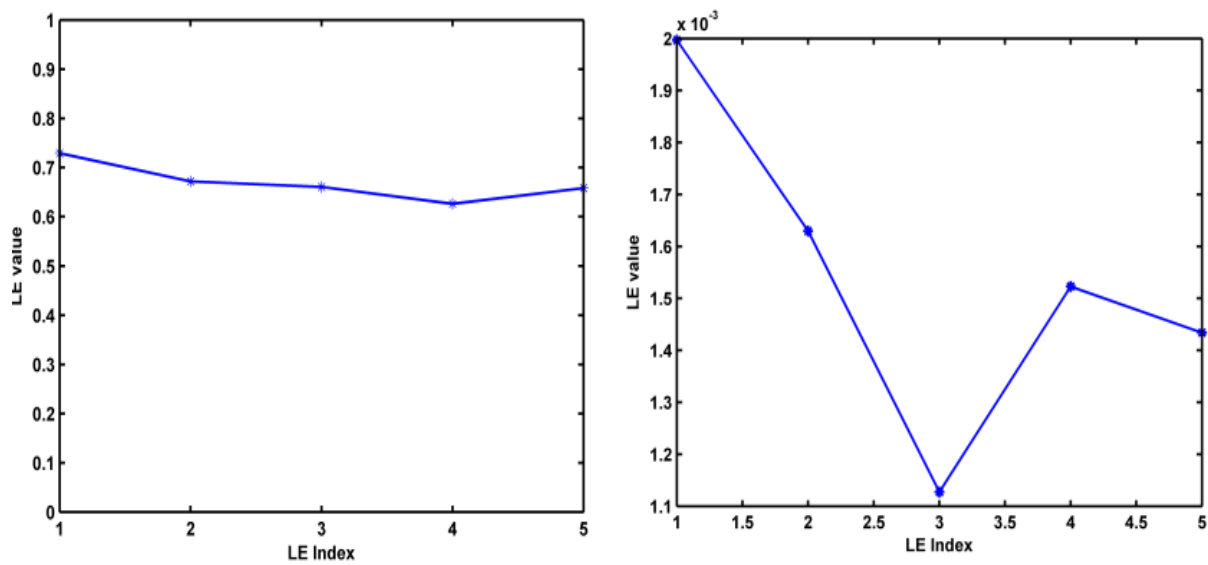

Fig.7   Lyapunov exponent spectrum   (a)   Pure chaos   (b)   Quasi-chaos

IV.   Discussion

This numerical investigation is done step-wise on same lines as done earlier [3] for loss modulation scheme and the results are also corresponding, proving the second appearance of quasi-chaos. In order to test the SDIC of pure chaos, the initial condition D_{A0} is varied by very minute differences and the output is still found to diverge even for the slightest of the difference as expected for pure chaos. However, the time of start of divergence of trajectories increases with decrease in difference of D_{A0} which is also anticipated behaviour. On the other hand, quasi-chaos proclaimed to converge instead of diverging, is tested with E_{LA0} and D_{A0} taken to their extreme limits. However, the differently starting trajectories still converge to same single trajectory instead of diverging with the time of convergence increasing this time with the deviation of initial conditions. The message signal adds an extra perturbation in the cavity which is interacting with the loss modulating sine wave, thus producing quasi instead of pure chaos.

The time, frequency, phase space and autocorrelation plots of quasi-chaos once seen independently give an impression of chaos. However, once pure and quasi-chaos plots are observed critically, some differences are observed in respective domains. One major difference is that quasi-chaos has periodic bunches of super pulses while pure chaos pulses, however, are chaotic both in time and in amplitude. Each super pulse has further four sub pulses and the frequency of sub-pulses is fixed at 9 kHz i.e. the modulating frequency. The frequency spectrum of quasi-chaos has all harmonics of both sub and super pulse frequencies while pure chaos spectrum is flatter and richer with better message masking capabilities. The pump modulating frequency is visible in both the spectrums but its harmonics are more vivid in quasi-chaos. The autocorrelation diagram of pure chaos is depicting more randomness due to chaotic timing of pulses. The LE of quasi-chaos calculated using TISEAN are still positive although the physical phase space converges to single trajectory. The reason of this anomaly is the fact that TISEAN calculates LE by creating a pseudo phase space by time delayed embedding of time series data of one physical variable i.e. $E_{LA(t)}$ and $E_{LA(t-\tau)}$ in this case. This pseudo phase space gives positive LE if it is fractal in nature; and it has been found to be fractal in this work not only for pure chaos but also for quasi-chaos. However, the LE values of pure chaos are order of magnitude higher than quasi-chaos. $E_{LA(t)}$ vs $E_{LA(t-\tau)}$ plotted for different values of τ i.e. 0.5 to 4 usec, give fractal plots whose correlation decreases with the increase of τ. The correlation is however, higher in quasi-chaos than pure chaos as the pulses timing is chaotic in latter only.

V.   Conclusions

Rediscovery of quasi-chaos in pump modulation scheme in this research, after its first discovery in loss modulation of EDFRL proves that quasi-chaos is also a ubiquitous phenomenon and is the fifth region of operation in nonlinear systems. This work proves that this phenomenon can be traced in all forced chaotic oscillators once the requisite conditions shown here are tuned i.e. one additional sine wave perturbation with frequency not integral multiple of forcing sine wave is added into the system dynamics. Quasi-chaos in this work spoofs itself as a pure chaos by passing all qualitative and visual tests i.e. it has rich spectral content and fast decreasing autocorrelation function and a strange attractor in pseudo phase space. The only visual indicator observed in this work is that pulses are chaotic in amplitude and not in time for quasi-chaos with bunching of pulses into super pulses. The most surprising result in this work is that quasi-chaos gives positive LEs' spectrum using time delayed pseudo phase space analysis of lasing field intensity using TISEAN, a well-known package of LE calculation. Therefore, qualitative visual tests and LE calculations on time delayed series have proven to be a weak test of pure chaos and we need to find stronger quantitative measures of distinguishing pure chaos from quasi-chaos and be cautious with experimental results in forced chaotic systems. The strangely deceptive behaviour of quasi-chaos observed in this work raises many questions from application point of view e.g can quasi-chaos be used for secure chaotic communication and whether to believe experimental data from forced chaotic systems to be pure chaos. Briefly, pure chaos is sensitively dependent on initial conditions both in physical phase space of all dynamic variables and time delayed pseudo phase space of any one physical variable while quasi-chaos is converging in physical phase space and sensitively dependent on initial conditions only in time delayed pseudo phase space.

VI. References

1.   A. Argyris, D. Syvridis, L. Larger, V. A. Lodi, P. Colet, I. Fischer, J. G. Ojalvo, C. R. Mirasso, L. Pesquera and K. A. Shore, "Chaos-based communications at high bit rates using commercial fibre-optic links",* Nature, Vol. 438, No. 17, pp. 343-346, November 2005.

2.   M. Virte, K. Panajotov, H. Thienpont and M. Sciamanna, "Deterministic polarization chaos from a laser diode" Nature Photonics 2013.

3.   S. Z. Ali, "First observation of Quasi-Chaos in Erbium doped fiber ring laser", Applied Optics, co-submitted to Chaos Modelling and Simulation CMSIM conference,2015.
-
4.   H. D. I. Abarbanel, M. B. Kennel, M. Buhl and C. T. Lewis, "Chaotic Dynamics in Erbium-doped fiber ring lasers", Physical Review A, Vol. 60 No. 3, pp. 2360-2374, Sep. 1999.

5.   S. Z. Ali, M. K. Islam and M. Zafrullah "Effect of Parametric variation on generation and enhancement of chaos in erbium-doped fiber-ring lasers" Optical Engineering Vol. 49 No.10, October 2010.

6.   S. Z. Ali, M. K. Islam and M. Zafrullah, "Effect of message parameters in additive chaos modulation in Erbium Doped Fiber Ring Laser ", Optik 124(18), September 2013, pp. 3746-3750.

7.   D. Derozier, S. Bielawski and P. Glorieu, "Dynamical behaviour of a doped fiber laser under pump modulation", Optics Communication, Vol. 83 No. 1,2, pp.97-102, 1991.

8.   A. N. Pisarchik , Y. O. Barmenkov, "Locking of self-oscillation frequency by pump modulation in an erbium-doped fiber laser" Optics Communications 254 (2005) 128–137.

9.   A. N. Pisarchik, Y. O. Barmenkov and A. V. Kir'yanov , "Experimental Characterization of the Bifurcation structure in an Erbium-Doped Fiber laser with Pump modulation", IEEE journal of Quantum Electronics, Vol. 39, No. 12, pp. 1567-1571, December 2003.

10.   A. N. Pisarchik, A. V. Kir'yanov and Y. O. Barmenkov "Dynamics of an Erbium-doped fiber laser with pump modulation : theory and experiment" Journal of Optical Society of America, Vol. 22, No. 10, pp. 2107- 2114, October 2005.

11.   I. J. Sola, J. C. Martin, J. M. Alvarez, "Analytical treatment for the study of an erbium-doped fiber ring laser fed by a sinusoidally modulated pump power", Optics Communications 258 (2006) 59–66.

12.   I. J. Sola, J. C. Martin and J. M. Alvarez, "Nonlinear response of a unidirectional Erbium-doped fiber ring laser to a sinusoidally modulated pump power", Optics Communication, Vol. 12 , No. 4-6, pp. 359-369, November 2002.

13.   A. N. Pisarchik, A. V. Kir'yanov and Y. O. Barmenkov "Dynamics of an Erbium-doped fiber laser with pump modulation : theory and experiment" Journal of Optical Society of America, Vol. 22, No. 10, pp. 2107- 2114, October 2005.

14.   L. G. Luo, T. J. Tee and P. L. Chu, "Bistability of Erbium-Doped Fiber Laser", Optics Communication, Vol. 146 No.1-6, pp. 151-157, 1998.

15.   R. Hegger, H. Kantz, and T. Schreiber, *"Practical implementation of nonlinear time series methods: The TISEAN package"*, C**http://ojps.aip.org/journals/doc/CHAOEH-home/top.html**haos Vol. 9, pp.413-435,1999.

Striation model of the population growth of the Earth

Vladimir G. Zhulego[1] , Artem A. Balyakin[2]

[1] Department of analysis and forecast, NRC "Kurchatov Institute", Moscow, Russia, (E-mail: zhulego@mail.ru)

[2] Department of scientific and technical programs and projects, NRC "Kurchatov Institute", Moscow, Russia, (E-mail: Balyakin_AA@nrcki.ru)

Abstract. On a base of a previous two-component model of population growth for one country the new striation model of population growth of the entire Earth is proposed. The obvious advantages compared with other models are studied. The methodological rules for finding the parameters included in the model are discussed as well as the possible application of the proposed model to international organizations such as UNESCO or the United Nations. Some results of numerical simulation are presented, socio-economic aspects of the model are discussed: the ability to control population size by adjusting the flow of people from the city to the countryside, and the trends in the urban and rural population

Keywords: population growth, chaotic simulation, modeling of socio-economic processes, striation model.

In this work we discuss several related problems: the problem of constructing a model of population growth, the problem of predicting population growth, and the problem of numerical simulation of population dynamics. Those issues attract a lot of attention in both natural and social sciences. Initially it was caused by simplest modeling of such dynamics when constant increase of population was inevitably shown as leading to overpopulation of the planet (Malthusian crisis). Later, a precise date of overpopulation was esteemed as 2004. By now a number of theoretical works arose, clarifying model representation of such dynamics. Along with Malthus classic work, one should mention Verhulst model [1], Kapitsa model [2], Forrester world-system model [3] and many others. As it turned out, the rate of population growth crucially determines the growth rate of GDP, and this fact has largely spurred interest in the subject [4,5]. The most interesting dynamics is connected with so called "demographic transition point" when population growth sharply decreases and number of people achieves stable value. However, at the same time, all proposed model are unlikely to describe the entire dynamics of the population: the explosive growth of the initial time, saturation stage (demographic transition point) and almost stable behavior on later stage.

In our previous work [6] we proposed new approach to modeling the dynamics of population growth. We consider the population dynamics from the

physical viewpoint: in particular, we believe that the population should be considered as two-phase system – "rural population" and "urban population", with each phase to behave under its own laws of growth, with having, however, a flow between two phases. This view of the population dynamics growth can decrease the number of arbitrary parameters in the model, and also give additional arguments and levers to control the pace of population growth that is important for countries experiencing problems with overcrowding and/or depopulation challenges. In our current work we outline the contours of the model of population growth throughout the Earth.

We assume that the entire population can be divided into two relatively independent groups (phases), focused respectively on the intensive and extensive ways of development - urban and rural areas. Note that these concepts are not geographical, and probably reflect the attitude of the population to the production of wealth and investing in future generations and lifestyles. The most important characteristic that allows extracting these two groups, apparently, is the population density per square kilometer. The problem to calculate/evaluate this value would be another interesting task that we will not consider in our work.

On a base of a previous two-component model of population growth for one country the new striation model of population growth of the entire Earth is proposed.

$$\frac{dx_i}{dt} = -a_i x_i(t) + \beta_i \frac{x_i(t-\tau_i)y_i(t-\tau_i)}{x_i^2(t)+\alpha_i^2} + \sum_k \gamma_{ik} \frac{x_i(t-\tau_i)x_k(t-\tau_k)}{x_i^2(t)+x_k^2(t)+\alpha_i^2+\alpha_k^2}$$

$$\frac{dy_i}{dt} = b_i y_i(t) - c_i y_i^2(t) - \beta_i \frac{x_i(t-\tau_i)y_i(t-\tau_i)}{x_i^2(t)+\alpha_i^2}$$

Here i = 1,2,3, ... N denotes the total number of countries in the world and x_i denote urban population, y_i denotes the rural population in the country *i*. Totally this system consists of 2N differential equations. The Earth's population will be calculated as a simple sum of all ($x_i + y_i$). Analysis of the system can be carried out numerically in the same way as it was done for the analysis of the model for a single country (see [6]).

We should mention that in our model there can be the difference in the behavior of various parts of the planet, and the whole planet is not considered as one large country. This approach could also work for a vast territories and/or countries.

In our opinion the socio-economic consequences of proposed strata model are of great interest. This mostly refers to GDP growth (so-called world-dynamics or the world-system dynamics). It is known that in such models economic growth is critically dependent on the rate of population growth. For example, in the Solow-Swan model [5,7] economy enters the steady growth of the national income at a constant rate equal to the rate of growth of the labor force. The stratification (or "splitting") of the population into two phases allows us to explain the economic growth in the country, even in the case where the

total population growth is missing or insufficient. The most striking examples of this growth is an economic growth in the USSR in the period of industrialization and economic growth of China under strict birth control nowadays. Thus in such models the economic growth becomes endogenous. Modelling of growth of the Russian economy on the basis of population stratification in eight groups was undertaken in [8,9], but it was done without reference to the modeling of population growth, which, of course, reduces the value of this approach.

The proposed model of the Earth's population growth has obvious advantages compared with other models and can be a good basis for the calculation of the realistic medium-term and long-term forecast population growth of the Earth, which is important to many international organizations such as UNESCO or the United Nations. It should be understood, however, that work on compiling such a forecast is very labor-intensive because of the need to analyze a large amount of statistical data on population growth in the countries and on this basis to determine the model parameters, such as the rate of flow of the villagers in the city and residents of one country to another. However, we hope that this work can be very useful and will provide, along with the forecast population growth, and long-term economic growth forecasts.

Acknowledgements

References

1. Verhulst P.F. Notice sur la loi que la population poursuit dans son accroisment. Correspondence mathematique et physique. 1838. N 10, P. 113-121.
2. Kapitsa S.P. Global population blow-up and after. The demographic revolution and information society. Moscow, 2006.
3. Forrester J.W. World Dynamics. Wright-Allen Press. 1971.
4. Solow R.M. (1956). A Contribution to the Theory of Economic Growth. Quarterly Journal of Economics 70 (1): 65–94.
5. Akaev A, Sadovnichy V and Korotayev A. On the dynamics of the world demographic transition and financial-economic crises forecasts. Eur. Phys. J. Special Topics 205, 355-373 (2012).
6. Zhulego V.G., Balyakin A.A. 2-Phase model for population growth. Chaotic modeling and Simulation (CMSIM), 2015, 1 (to be published)
7. Swan T. Economic Growth and Capital Accumulation. Economic Record.1956. Vol. 32.
8. Romanovsky M. Yu., Romanosky Yu.M. Introduction to econophysics. Moscow 2007. (in Russian).
9. Chernavski D.S., Starkov N.I, Sherbakov A.V. On some problems of physical economics Phys. Usp. 45 977–997 (2002)